Moments Based Analysis of Intermodulation Distortion in Radio Frequency Circuits

Dani A. Tannir

Department of Electrical & Computer Engineering
McGill University
Montreal, Canada

July 2010

A thesis submitted to McGill University in partial fulfillment of the requirements for the degree of Doctor of Philosophy.

Abstract

One of the key design requirements of communication circuits is that of linearity, and one of the main figures of merit for measuring the amount of nonlinear distortion at the output of Radio Frequency (RF) circuits is the third order intercept point (IP3). There are two general classes of methods for calculating the IP3 of a circuit. The first is analytical and is usually based on Volterra series. This approach is cumbersome and is difficult to automate for arbitrary circuits with arbitrary non-linearities. The second class of methods is based on multi-tone simulations and is general and flexible but requires significant computational cost due to the large number of variables present in the circuit equations and due to the need to perform a steady-state simulation. In this thesis, a new simulation based approach is presented for efficiently computing the value of IP3 and its sensitivity in RF circuits. The approach relies on the numerical computation of the Volterra series terms from the circuit moments by evaluating closed form expressions that link the distortion terms to the moments (The moments are defined as the Taylor series expansion of the system solution with respect to the RF input power). Obtaining the value of IP3 and its sensitivity therefore is reduced to solving a set of linear sparse equations. The new approach is simple to apply, fully automated and presents significant reduction in computational cost over existing simulation based approaches while being as accurate as Harmonic Balance based methods. The thesis consists of three main contributions. The first being the moments based approach for finding the IP3 of mixer circuits, which exhibit strong nonlinearities outside the signal path. The second contribution is a method for computing the value of IP3 using only single-tone inputs, which significantly reduces the size of the system of equations that need to be solved. The third contribution is the adjoint sensitivity computation of IP3 using moments. This adds insight to the numerical results of the moments based approach for computing IP3 which provides a critical advantage for optimization, design centering and yield analysis applications.

Résumé

Une des conditions essentielles dans la conception de circuits de communication est la linéarité. L'un des principaux facteurs de mérite pour mesurer la distorsion non linéaire des circuits de radiofréquence (RF) est le point d'interception du troisième ordre (IP3). Les méthodes de calcul de l'IP3 peuvent être divisées en deux categories: La première regroupe les méthodes analytiques généralement basées sure les séries Volterra. Cette méthode est difficile à automatiser d'une façon independante de la topologie des circuits et du type de la nonlinéarité. Les méthodes de la deuxième classe sont basées sur des simulations du type Harmonic Balance (HB). Ces méthodes necessitent un coût de calcul élevé en raison du grand nombre de variables dans les équations à resoudre. Dans cette thèse, on présente une approche nouvelle pour l'évaluation de l'IP3. Cette approche est basée sur les méthodes de simulation sans pour autant necessiter la solution des equations Harmonic Balance. Cette méthode repose sur le calcul numérique des termes de la série Volterra à partir des moments du circuit en évaluant les expressions de forme fermée qui relient les termes de distorsion aux moments (les moments sont définis comme l'expansion de la série de Taylor de la solution du système par rapport à la puissance d'entrée RF). L'obtention de la valeur de l'IP3 et sa sensibilité est donc réduite à résoudre un ensemble d'équations linéaires creuses. Cette nouvelle approche est simple à appliquer, entièrement automatisée et présente une grande réduction en calcul par rapport aux approches courrantes basées sur la simulation tout en étant aussi précises que les méthodes basées sur la balance harmonique. Cette thèse comprend trois contributions principales. La première est une approche basée sur les moments afin de trouver l'IP3 des circuits mélangeurs. La deuxième est une méthode de calcul de la valeur IP3 en utilisant une seule fréquence, ce qui réduit considérablement la taille du système d'équations qui doivent être résolu. La troisième contribution est le calcul de la sensibilité adjointe de l'IP3 à l'aide des moments. Cela ajoute un aperçu sur les résultats numériques provenant de l'approche basée sur les moments pour le calcul de l'IP3, ce qui offre un avantage déterminant pour l'optimisation, et l'analyse de rendement.

Acknowledgments

After several years of hard work and dedication, it is finally here, the moment at which I have completed my Ph.D. dissertation. I thank God for giving me the good health and all his blessings in life to be able to achieve this goal. Although this thesis marks the pinnacle of my academic achievements thus far, it is important to remember that this work could not have been completed without the assistance of a select group of people and organizations.

First and foremost, I would like to say that none of this would have been possible without the tremendous guidance, support and love that I have received from my family throughout my life. I would like to thank my elder brother Mustapha, who has been my best friend throughout my life, for all the advice and good times. I would especially like to thank my parents, Abdallah and Zouhar, who have provided me with the best possible upbringing and the highest of living standards under all circumstances. I want to thank them for all their care, sacrifice and patience through the many years and the difficult times. Without them I would not be the person that I am today and for this I am eternally grateful. This work is dedicated to them and I hope that I make them proud.

A very special word of gratitude goes to my research supervisor, Professor Roni Khazaka. I am very grateful for all his assistance, advice and contributions to my research and to the rest of my academic needs throughout my graduate studies at McGill. His insight and technical feedback have had a significant positive influence on this research. He has also provided me with a lot of support and advice on non-academic issues which I am truly grateful for. Above all, I would like to thank him for giving me the opportunity to come to McGill and to Canada back in 2004. For these reasons, I consider Professor Khazaka as a true mentor, colleague and friend. I would also like to say a special thanks to my Ph.D. committee which consists of Professor Milica Popovic and Professor Dennis Giannacopoulous. I always stated that I believe I had the best Ph.D. committee as I really enjoyed doing research, coursework and TA work with them. I would also like to thank them for all the letters of reference that I have requested.

For the duration of my Ph.D. studies, I have been very fortunate to receive financial support for my research work through several prestigious scholarships and research awards. In particular, I would like to thank the National Science and Engineering Research Council of Canada (NSERC) for the Canada Graduate Scholarship, and also the McGill Faculty of Engineering for the Doctoral Award.

Finally, I would like to mention that the years that I have spent as a graduate student have also been my first in Canada, which is really a wonderful country that is full of opportunities and great people. Montreal is a fantastic place to live and McGill University in particular is a top-level school. During this time, I have been fortunate to meet several friends and colleagues that have helped me settle in and make it a memorable experience. There would be too many people to list individually here, but I know for sure that I will always be grateful to them for their support and that I will always stay in contact. In particular, I want to thank Mr. Simon Hong for his contribution to the French Abstract of this thesis. Last but not least, I want to thank all the people that have had a positive influence throughout my academic life, including friends, relatives and professors, from back home in Lebanon and also from the early high school days in Jeddah.

Contents

1 Introduction **1**

1.1 Background and Motivation 1

1.2 Contributions of the Thesis 7

1.3 Organization 9

2 Review of Intermodulation Distortion Analysis Techniques **10**

2.1 Introduction 10

2.2 Importance of Nonlinear Distortion 11

2.3 Terminology and Figures of Merit 12

2.3.1 Weakly Nonlinear System Behavior 12

2.3.2 Gain Compression and the 1 dB Compression Point 12

2.3.3 Intercept Points 14

2.3.4 Other Figures of Merit 14

2.4 Simulation Based Distortion Analysis Methods 14

2.4.1 Distortion Analysis Using Harmonic Balance 15

2.4.2 Distortion Analysis Using the Simplified Newton Method 16

2.4.3 Fast IP3 Using Periodic Steady State Analysis 17

2.4.4 Linear Centric Distortion Analysis 18

2.4.5 Weakly Nonlinear RF Circuit Reduction and Other Simulation Enhancement Methods 19

2.5 Analytical Techniques for Distortion Analysis 20

2.5.1 Volterra Series Formulation 20

2.5.2 IP3 Computation Using Volterra Kernels 22

2.5.3 Distortion Analysis Using Time-Varying Volterra Series 25

2.5.4 Sensitivity Analysis Using Volterra Series 25
2.5.5 Rapid Estimation of IP3 Using the Three-Point Method 26
2.6 Moments Based Technique for the Distortion Analysis of Amplifier Circuits . . . 27
2.6.1 Moments Computation Algorithm 28
2.6.2 Computation of IP3 From the Moments 28
2.7 Conclusion 31

3 Circuit Simulation Using Harmonic Balance 32
3.1 Introduction 32
3.2 Modified Nodal Analysis Formulation 34
3.3 Harmonic Balance Formulation 36
3.4 Solution of the Harmonic Balance Equations 39
3.4.1 Direct Fourier Transform 41
3.4.2 Evaluation of the Nonlinear Vector $\boldsymbol{F}(\boldsymbol{X})$ 42
3.5 Harmonic Balance Jacobian 43
3.6 Harmonic Balance Difficulties and Improvements to the Harmonic Balance Method 44
3.6.1 Continuation Methods 45
3.6.2 Use of Preconditioning 45
3.7 Fourier Transform for Almost Periodic Input Signals 46
3.7.1 Block Truncation 47
3.7.2 Diamond Truncation 48
3.7.3 Three Tone Truncation 49
3.8 Sensitivity Analysis Techniques 50
3.8.1 Sensitivity Analysis Formulation 50
3.8.2 Perturbation 51
3.8.3 Differentiation 52
3.8.4 Adjoint Sensitivity 52
3.9 Conclusion 54

4 Moments Based Computation of Intermodulation Distortion of Mixer Circuits 56
4.1 Introduction 56
4.2 Obtaining the IP3 From Series Expansion 58
4.3 Definition and Calculation of the Moments For Mixers 59

4.3.1 System Formulation . . . 60
4.3.2 Moments Computation Algorithm . . . 60
4.3.3 Sparsity of the Moments Computation Matrix . . . 63
4.4 Derivation of the Link Between the Moments and the IP3 Terms . . . 65
4.4.1 Memoryless Systems . . . 66
4.4.2 Systems With Memory Elements . . . 68
4.5 Computation of the IP3 From the Moments . . . 73
4.6 Numerical Example . . . 75
4.6.1 Detailed Analysis of a Doubly Balanced Mixer Circuit . . . 75
4.6.2 Computation Cost Comparison . . . 79
4.7 Conclusion . . . 79

5 Computation of IP3 Using Single-Tone Moments Analysis 82
5.1 Introduction . . . 82
5.2 Third Order Nonlinearity and IP3 Definitions . . . 84
5.2.1 Evaluation of IP3 From the 1-dB Compression Point . . . 87
5.2.2 Computing IP3 Using Volterra Series . . . 87
5.3 Computation of IP3 Using Single-Tone Moments . . . 89
5.3.1 IP3 Formulation Using Single-Tone Volterra Kernels . . . 90
5.3.2 Definition of Single-Tone Moments . . . 91
5.3.3 Relation Between IP3 and the Harmonic Balance Moments . . . 92
5.3.4 Summary of the New Algorithm . . . 101
5.4 Computational Cost Considerations . . . 103
5.5 Numerical Examples . . . 105
5.5.1 Example 1 . . . 105
5.5.2 Example 2 . . . 109
5.6 Conclusion . . . 114

6 Efficient Sensitivity Analysis of Nonlinear Intermodulation Distortion 115
6.1 Introduction . . . 115
6.2 Sensitivity Analysis Using Multi-Dimensional Moments . . . 116
6.2.1 Computation of the Multi-Dimensional Moments . . . 116
6.2.2 Sensitivity of IP3 . . . 119

6.2.3 Numerical Example 121
6.3 Adjoint Moments Sensitivity Method 125
6.4 Harmonic Balance Adjoint Sensitivity 126
6.5 Moments Based Sensitivity Computation 127
6.6 Adjoint Sensitivity Derivation Using Moments 129
6.6.1 Linear Parameter Sensitivity 131
6.6.2 Nonlinear Parameter Sensitivity 132
6.6.3 Extension to IP3 Sensitivity Using Single-tone Moments 133
6.7 Moments Computation Algorithms 133
6.7.1 Computation of the Harmonic Balance Moments 134
6.7.2 Computation of the Adjoint Moments 135
6.7.3 Computation of the Nonlinear Vector Moments 135
6.8 Numerical Examples 139
6.8.1 Circuit Descriptions 139
6.8.2 Methodology and Results 139
6.8.3 Computation Cost Analysis 141
6.9 Conclusion 143

7 Summary and Future Work **144**
7.1 Summary 144
7.2 Future Work 146

References **149**

List of Figures

1.1 Multiple simultaneous wireless activities on a smartphone 2
1.2 General RF transceiver circuit [1] 3
1.3 Breakdown of wireless standards and specifications 3
1.4 Output spectra of linear and nonlinear time invariant circuits (a)-(d) and linear and non-linear periodically time varying circuits (e)-(h) [2]. 6

2.1 Output spectrum of narrow-band circuit driven by two closely spaced sinusoidal tones 11
2.2 Harmonic levels at the output of a nonlinear circuit [3] 13
2.3 Definition of the input and output third order intercept points (IIP3 and OIP3, respectively) 15
2.4 Measurement of intermodulation distortion using periodic-steady-state / periodic AC analysis 18
2.5 Overall linear-centric circuit model showing how a nonlinear circuit can be viewed as a linearized one driven by external inputs in addition to chord current sources due to the nonlinearities [4] 19
2.6 Block diagram representation of a Volterra series 21

3.1 Simple nonlinear circuit 35
3.2 Sparsity pattern of the Harmonic Balance Jacobian matrix. White space shows location of zero entries, dark space shows location of non-zero entries. 44
3.3 Frequency mapping using block truncations [5] 48
3.4 Frequency mapping using diamond truncations [5] 49
3.5 Frequency mapping using three-tone truncation with $k_3 > 0$ 50

4.1 Sparsity pattern of a single block in the moments computation matrix of mixer circuits . . . 66
4.2 Summary of the moments based algorithm for computing IP3 in mixer circuits. . 75
4.3 Active doubly-balanced mixer (Gilbert Cell) circuit diagram. . . . 76
4.4 Output power of the fundamental and the 3^{rd} order intermodulation (IM3) frequency tones using Harmonic Balance. . . . 77
4.5 Output voltage spectrum at the IF frequencies using Harmonic Balance. . . . 77
4.6 Sparsity pattern of the Harmonic Balance Jacobian for the doubly balanced mixer circuit example. . . . 78
4.7 Sparsity pattern of the dense blocks of the Harmonic Balance Jacobian matrix. . . 78
4.8 Sparsity pattern of the moments computation matrix $\mathbf{\Phi}$ for the doubly balanced mixer circuit example. . . . 80
4.9 Sparsity pattern of the sparse blocks of the moments computation matrix. . . . 80

5.1 Definition of the 1-dB compression point . . . 85
5.2 Adjacent channel interference due to intermodulation distortion [1] . . . 86
5.3 Single-tone vs. two-tone third order nonlinearity and system bandwidth . . . 86
5.4 Location of distortion terms in the moments for amplifiers . . . 102
5.5 Location of distortion terms in the moments for mixers . . . 102
5.6 Summary of the algorithm for computing IP3 using single-tone moments analysis. 103
5.7 Circuit diagram example 1 . . . 105
5.8 Sparsity pattern of Harmonic Balance Jacobian for the circuit in example 1 . . . 107
5.9 Sparsity pattern of the moments computation matrix for the circuit in example 1 . 108
5.10 Differential bipolar Gilbert mixer circuit diagram. . . . 111
5.11 Sparsity pattern of the Harmonic Balance Jacobian for the mixer circuit in example 2 . . . 112
5.12 Sparsity pattern of the moments computation matrix for the mixer circuit in example 2 . . . 113

6.1 Location of sensitivity terms in the multi-dimensional moment vectors . . . 122
6.2 Summary of the algorithm for computing the sensitivity of IP3 using multi-dimensional moments. . . . 122
6.3 Example circuit diagram . . . 123
6.4 Location of sensitivity terms in the moment vectors for amplifier circuits . . . 128

6.5 Location of sensitivity terms in the moment vectors for mixer circuits 129
6.6 Summary of the algorithm for the adjoint sensitivity analysis of nonlinear distortion in RF circuits. 138

List of Tables

2.1 Summary of distortion components [6] 22

2.2 Distortion components described by Volterra kernels at the corresponding output frequencies [3] 24

3.1 Harmonic Balance adjoint sensitivity expressions for different elements [7] . . . 54

4.1 Summary of distortion components in mixer circuits 58

4.2 Comparison of computation times between the moments method and the Harmonic Balance solution 81

5.1 Comparison of IP3 values between traditional Harmonic Balance and the single-tone moments method 110

5.2 Comparison of computation times between the single-tone moments method and the Harmonic Balance solution 110

5.3 The effects of increasing harmonics on speedup of IP3 simulation of example 1 between the single-tone moments method and Harmonic Balance. 110

5.4 Comparison of moments computation matrix sizes between the single-tone and the two-tone moments methods. 114

6.1 Normalized sensitivity of IP3 with respect to circuit parameters for the example circuit 124

6.2 CPU cost comparison of finding IP3 and its sensitivity with respect to 2 parameters for the example circuit 124

6.3 Comparison of relative sensitivities of IP3 with respect to a linear and nonlinear parameter for the example circuits. 140

6.4 CPU cost comparison of finding the adjoint sensitivity of IP3 for the example circuits . . . 140
6.5 Computation cost comparison of finding both IP3 and its adjoint sensitivity for the example circuits . . . 142
6.6 Computation cost comparison of finding both IP3 and its adjoint sensitivity using single-tone moments analysis . . . 142

List of Acronyms

BVP	Boundary Value Problem
CAD	Computer Aided Design
CPU	Central processing unit
DAE	Differential Algebraic Equations
DFT	Direct Fourier Transform
EDA	Electronic design automation
FFT	Fast Fourier transform
GMRES	Generalized Minimal Residual
GPS	Global Positioning System
GSM	Global System for Mobile Communication
HB	Harmonic Balance
HD	Harmonic Distortion
HSDPA	High Speed Data Packet
IC	Integrated circuit
IDFT	Inverse Direct Fourier Transform
IF	Intermediate Frequency
IFFT	Inverse fast Fourier transform
IIP3	Input 3^{rd} Order Intercept Point
IM3	3^{rd} Order Intermodulation
IMFDR	Intermodulation Free Dynamic Range
IP3	3^{rd} Order Intercept Point
KCL	Kirchhoff's current law
LNA	Low Noise Amplifier
LO	Local Oscillator

LU	Lower/upper triangular decomposition
MEMS	Micro-Electro-Mechanical Systems
MNA	Modified nodal analysis
NR	Newton Raphson iteration
OIP3	Output 3^{rd} Order Intercept Point
RF	Radio Frequency
RFIC	Radio frequency Integrated Circuit
SNR	Signal to Noise Ratio
SPICE	Simulation Program with Integrated Circuits Emphasis
THD	Total Harmonic Distortion
VCCS	Voltage Controlled Current Source
WLAN	Wireless Local Area Network

Notation

$\boldsymbol{A}$	Matrix A
$\boldsymbol{A}^T$	Matrix A transposed
$\boldsymbol{A}^{-1}$	Matrix A inverted
$\mathbb{R}^n$	The set of real vectors of size n
$\mathbb{R}^{n\times n}$	The set of real matrices of size n $\times$ n
$\boldsymbol{\Gamma}$	Inverse DFT matrix
$\boldsymbol{x}(\mathsf{t})$	Vector of unknown voltages and currents in the time domain
$\boldsymbol{G}$	Matrix containing MNA stamps of linear memoryless elements
$\boldsymbol{C}$	Matrix containing MNA stamps of linear memory elements
$\boldsymbol{f}(x)$	Vector of nonlinear scalar functions in MNA equations
$\boldsymbol{b}(t)$	Vector of independent sources in MNA equations
T	Period of a signal
ω_k	Set of fundamental, harmonic and intermodulation frequencies
$\boldsymbol{X}$	Vector of sine and cosine components of unknown voltages and currents in frequency domain
$\boldsymbol{X}_a$	Harmonic Balance Adjoint solution vector
$\bar{\boldsymbol{G}}$	Block matrix containing stamps of linear memoryless elements in expanded HB format
$\bar{\boldsymbol{C}}$	Block matrix containing stamps of linear memory elements in expanded HB format
$\boldsymbol{F}(\boldsymbol{X})$	Vector containing sine and cosine components of scalar nonlinear functions
H	Highest order of harmonics considered
$\boldsymbol{d}$	Selection vector
N_b	Expanded number of variables for each original variable
N_h	Total number of variables for HB system of equations

$\boldsymbol{\Psi}(\boldsymbol{X})$	Objective function for HB solution
$\boldsymbol{J}_{HB}$	Harmonic Balance Jacobian matrix
$\boldsymbol{\Phi}$	Moments computation matrix
k_n	n^{th} order power series coefficient
$H_n[v(t)]$	n^{th} order Volterra operator
$h_n(\tau_1, \ldots, \tau_n)$	n^{th} order Volterra kernel
$H_n(j\omega_1, , j\omega_n)$	n^{th} order Volterra kernel in Frequency Domain
α	Small signal input amplitude
β	Amplitude of Local Oscillator
λ	Parameter of circuit element
$\boldsymbol{M}_n$	n^{th} moment vector
$\boldsymbol{N}_{m,n}$	m, n^{th} multi-dimensional moment vector
$\boldsymbol{D}_n$	n^{th} Taylor coefficient of $\boldsymbol{F}(\boldsymbol{X})$
$\boldsymbol{T}_n$	n^{th} Taylor coefficient of $\partial\boldsymbol{F}(\boldsymbol{X})/\partial\boldsymbol{X}$
$\boldsymbol{P}_n$	n^{th} Taylor coefficient of block matrices in $\boldsymbol{T}$
$\boldsymbol{g}_n$	n^{th} Taylor coefficient of vector of derivatives of nonlinear scalar functions

Chapter 1

Introduction

1.1 Background and Motivation

The market for wireless industrial and consumer electronics has experienced remarkable growth over the past decade. The demand for wireless technology continues to be fueled by the need to enable people to communicate and share all forms of media at anytime, anywhere and in an efficient cost-effective way. This has lead to the popularity of devices such as notebook computers and cellular smartphones, which are now considered to be staples of modern life. Increased competition in the marketplace and the need to rapidly introduce new technologies to replace outgoing products with ever decreasing life cycles has in turn led to the need to reduce design, testing and manufacturing time. This has to be accomplished while also simultaneously improving the performance of increasingly complex circuits and systems. As an example of how complex modern wireless systems have become, consider a common smartphone such as the one illustrated in Fig. 1.1. At any one instance in time, this device could be wirelessly connecting through any combination of methods simultaneously, including a Global System for Mobile Communication (GSM) connection for voice, an IEEE 802.11b/g connection to a Wireless Local Area Network (WLAN) for data, and a Global Positioning System (GPS) satellite connection for navigation, among others [8]. As a result of this complexity, a significant emphasis is now placed on better Electronic Design Automation (EDA) tools as a way to reduce time to market and bring down development costs. While the increased complications of modern designs has led to a growing reliance on Computer Aided Design (CAD) tools, these same complications have stretched the limits of these tools. In fact, for many applications the overall performance of the system is now limited by the capabilities of a CAD tool rather than by the actual technological limitations. Fig.

Fig. 1.1 Multiple simultaneous wireless activities on a smartphone

1.2 shows the RF section of a cellphone [1], and is a good illustration of the complexity of modern transceiver circuits.

Wireless industry standards, such as GSM and IEEE 802.11b/g/n, stipulate many stringent technical specifications which the RF circuit designers must meet. These specifications translate to overall requirements at the system level, at the building-block level and also at the circuit level as illustrated in Fig. 1.3. Therefore, it is of particular importance for circuit designers to have at their disposal tools that can measure specific performance figures of merit such as the Signal to Noise Ratio (SNR) or the Power Gain of common RF transceiver circuits in order to ensure they meet the standard specifications. One of the most important requirements is that of linearity, and more specifically the linearity of core RFIC building blocks such as Low Noise Amplifiers (LNAs) and mixers of RF circuits similar to that shown in Fig. 1.2. The design requirements of such circuits typically include stringent conditions on intermodulation distortion. The main figure of merit used by RF engineers to quantify the amount of intermodulation distortion has typically been that of the third order intercept point (IP3), which provides a measure of the third order nonlinearity in a circuit [6]. It is also very important for circuit designers to be able to perform an efficient sensitivity analysis of the circuit's intermodulation distortion without the need for inefficient brute-force perturbation of the system solution. This would give the designers insight into the numerical results of the circuit simulator by showing how much of an effect changes to

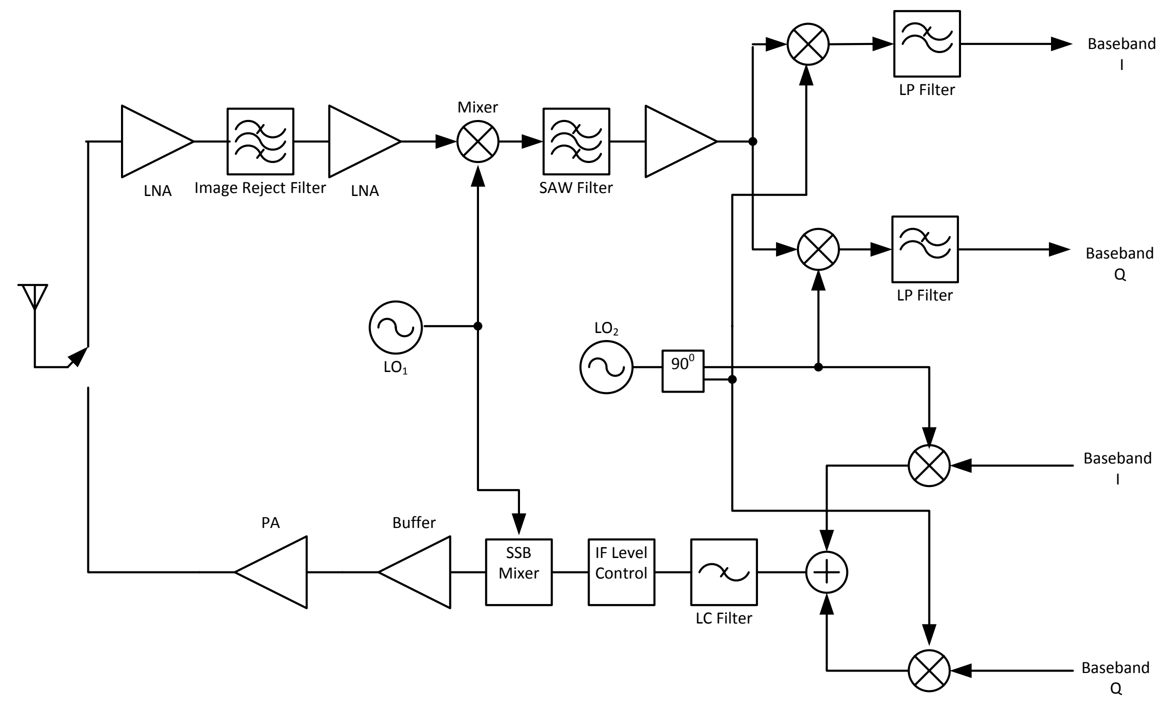

Fig. 1.2 General RF transceiver circuit [1]

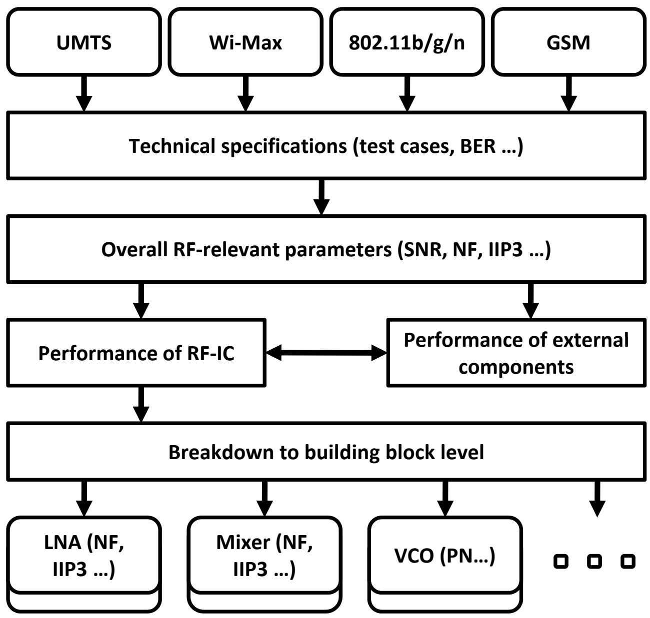

Fig. 1.3 Breakdown of wireless standards and specifications

certain circuit parameters or variables will have on the linearity of the output. This is particularly important for design centering, optimization and yield analysis applications among others [9].

Radio Frequency circuits are typically designed to be as linear as possible in order to reduce nonlinear distortion. Nonlinear distortion is due to the inherent nonlinearity of circuit components and results in the harmonics of input tones, as well as the intermodulation products, being present at the output. Of particular interest are third order intermodulation products because they mix back into the frequency band of operation and result in many undesirable effects such as gain compression and adjacent channel interference. In a communication system, nonlinear distortion along with noise and interference in the transmission channel can then affect the receiver side Bit Error Rate (BER) [10]. In a typical laboratory measurement setup on a workbench, the circuit hardware can be tested and the value of IP3 can be obtained by applying a 2-tone input and measuring the third order intermodulation product which mixes back into the passband of the circuit. Note that applying a single-tone input and attempting to characterize the third order nonlinearity by measuring the third harmonic is not a suitable approach because the third harmonic typically falls outside the passband of the circuit. This has lead to the popularity of obtaining IP3 based on the measurement of the third order intermodulation product of a two-tone input as a figure of merit for linearity. At the design and development stage of the process, most of the common and efficient methods for the distortion analysis of analog and RF circuits can be categorized under one of two general classes of techniques. The first class of methods is that of simulation based approaches and the second class is that of analytical techniques.

In a simulation environment, the most common approach for determining IP3 is to mimic the laboratory measurement by applying a two-tone input and performing a steady-state analysis using time-domain techniques such as the Shooting method [11], or frequency domain techniques such as the Harmonic Balance method [5], [12], [13]. These approaches are general and give very accurate results; however these methods are often very CPU expensive. For example, in the case of Harmonic Balance, the simulation requires a large CPU cost because of the large number of variables present due to the two-tone input. This concept is illustrated in Fig. 1.4 which shows the output spectra of a combination of linear and nonlinear time invariant (amplifier) and periodically time varying (mixer) systems excited by single-tone and two-tone inputs [2]. As can be seen from Fig. 1.4 (d) and (h), the nonlinear systems with multi-tone inputs exhibit a significantly larger number of distortion tones at the output even for a small number of harmonics (only 3 harmonics are considered in Fig. 1.4). This is particularly the case for mixer circuits which would, in this instance, have a three-tone input (the local oscillator tone in addition to the two RF tones).

Another factor which leads to a high CPU cost is that in order to obtain the steady-state solution of nonlinear systems, a set of nonlinear equations needs to be solved using iterative techniques such as Newton iteration [11], [14] which comes with its own set of limitations, including accuracy and convergence issues. Furthermore, most of the simulation based approaches provide little or no insight into the numerical results, which means that a sensitivity analysis algorithm must then be applied as a post-processing step in order obtain this insight. Many sensitivity analysis algorithms could also exhibit a high CPU cost. It is also possible to obtain the nonlinear steady-state response using a SPICE-like simulator by performing a long enough transient analysis until the transients die out. Such an approach is, however, extremely inefficient due to large deviations in the time constants of the circuit and also due to the input frequencies which result in a very large number of time steps being required before reaching steady-state [15].

Alternatively, the value of IP3 can be obtained analytically through the use of the Volterra functional series [3], [16]. This approach requires complex mathematical analysis for obtaining expressions for higher order Volterra kernels which can then be used to compute a whole range of distortion figures of merit such as IP3. The advantage of these approaches is that, once the analytical expressions are derived, the CPU cost of evaluating them is extremely low. Furthermore, these expressions provide considerable insight which help designers identify the key sources of nonlinearity in a given circuit. However, such approaches suffer from two main shortcomings. The first is due to the complex analytical manipulations that are required to obtain the closed form expressions for the Volterra kernels. These typically involve solving multi-dimensional convolution integrals which makes these analytical methods very difficult to automate in a general purpose simulator that must handle circuits with arbitrary topologies. The second shortcoming results from the fact that Volterra series are most suitable for weakly nonlinear circuits and are difficult to apply to circuits with inherent strong nonlinearities such as switching circuits and mixers.

In this thesis, a new approach is presented for analyzing the linearity of Radio Frequency circuits in an efficient and accurate manner. The new method does not attempt to mimic laboratory measurements by performing multi-tone steady-state analysis. Instead, the value of IP3 and its sensitivity are computed directly from the Harmonic Balance equations by applying efficient algorithms that compute the system moments [17], [18]. It is important to note that, in this case, the nonlinear Harmonic Balance equations do not need to be solved, and that the computational complexity of obtaining IP3 is reduced to that of computing the moments which is essentially the solution of a set of sparse linear equations. Furthermore, given that the new approach is based

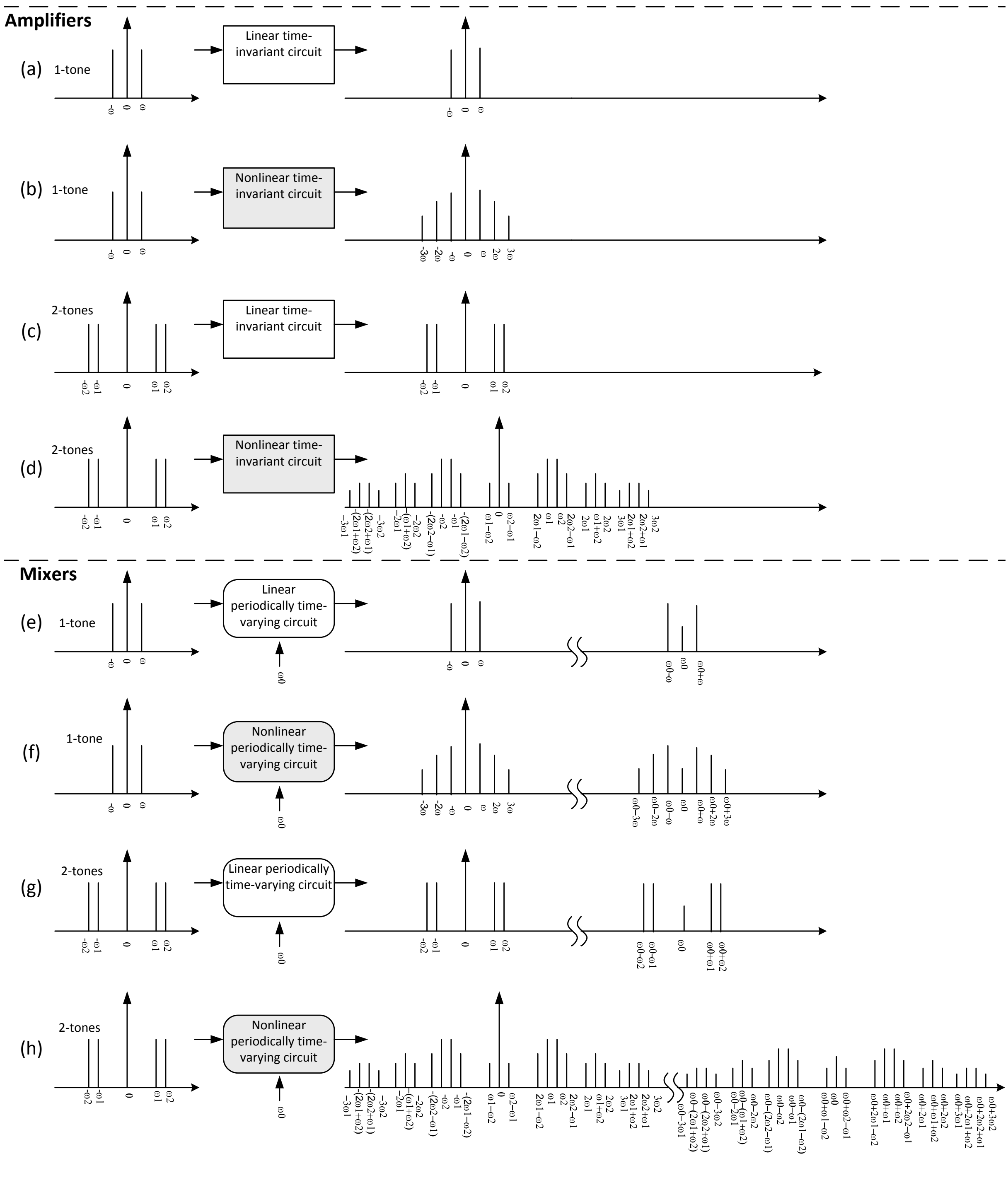

Fig. 1.4 Output spectra of linear and nonlinear time invariant circuits (a)-(d) and linear and non-linear periodically time varying circuits (e)-(h) [2].

on the Harmonic Balance formulation, it is general and can be applied to any arbitrary circuit topology, nonlinearity or model in a fully automated environment unlike Volterra series based methods. The scope of the new method presented in this thesis spans that of RF amplifier circuits in addition to mixers.

1.2 Contributions of the Thesis

In this thesis, a number of advanced novel simulation algorithms have been developed to efficiently analyze the effects of the third order intermodulation distortion on the linearity of RF building blocks such as Low Noise Amplifiers and Mixers. These new algorithms provide significant computational cost savings without sacrificing accuracy when compared to existing methods. More specifically, the main contributions of this thesis are listed as follows.

1. Moments based computation of intermodulation distortion in mixer circuits [19], [20] (see Chapter 4): In this thesis, a new method for the efficient computation of the value of IP3 in mixer circuits based on the system moments is presented. These circuits are designed to be highly linear in the signal path, but contain highly nonlinear internal switching due to the large signal Local Oscillator (LO) input. Using this new approach, the circuit moments expansion around the local oscillator power is used to compute the value of IP3. This method is shown to be equivalent to the numerical computation of the necessary Volterra series distortion terms. This approach does not require any analytical manipulation but is rather applied directly to the Harmonic Balance equations based on the Modified Nodal Analysis (MNA) [21] formulation of the circuit. It can therefore be applied to circuits of arbitrary topology and complexity. The moments computation is done numerically around a given LO input power (operating point) and with the input frequencies known, and thus produces very accurate results. Furthermore, the computation of all the moments requires only one LU decomposition of a moments computation matrix that is very sparse. The method for computing this moments matrix for mixers in addition to the proof of its sparsity is also presented in this contribution.

2. Single-tone computation of the third order intercept point [22], [23] (see Chapter 5): In this thesis, a novel approach for obtaining the IP3 of general RF circuits is presented where the number of variables is the same as a Harmonic Balance formulation with a single-tone input, thus making the size of the system of linear equations that need to be solved

considerably smaller than what is proposed in the literature. Furthermore, the computation complexity of this method is that of solving a set of linear equations and does not require the solution of the nonlinear Harmonic Balance equations which results in a considerable reduction in computation cost. In this contribution, the general framework of the method is presented that spans mixers in addition to amplifier circuits. The details of the mathematical derivations linking the single-tone moments to the IP3 of the circuit for both amplifiers and mixers are also provided. The new approach offers a fast alternative to the two-tone moments method with a considerably reduced CPU cost, as will be seen in the numerical examples section for this contribution. The speedup is mainly due to the significantly smaller size of the set of linear equations to be solved.

3. Sensitivity Analysis using multi-dimensional moments [24] (see Section 6.2): In this contribution, an analytical relationship is presented between the value of IP3 and the multi-dimensional Harmonic Balance moments (the moments with respect to the input RF power as well as the design parameters). This allows for the derivation of closed form expressions for the sensitivity of IP3 as a function of these multi-dimensional moments and thus provides insight into the numerical results of the moments based methods for computing IP3. The CPU cost of the operation is that of finding the multi-dimensional moments which is of the same order as solving a system of sparse linear equations.

4. Adjoint Sensitivity Analysis of nonlinear distortion [25], [26] (see Section 6.3): In this thesis, a new approach for computing the sensitivity of IP3 based on the adjoint sensitivity method is presented. The adjoint method has been a classical tool for the sensitivity analysis of linear circuits in addition to nonlinear circuits in the time-domain and DC [27], [28] and has also been extended to cover the sensitivity analysis of nonlinear circuits operating under large signal periodic and almost-periodic conditions as is the case with the Harmonic Balance method [7]. The new method presented in this contribution benefits from the same CPU cost advantage of the moments based techniques while providing the sensitivity of IP3 with respect to all circuit parameters. This would provide a critical advantage enabling circuit optimization, design space exploration and design centering. This method is general and easily automated for any arbitrary circuit topology. The method also shares the same properties of the adjoint approach, namely those of having low incremental CPU cost to the original algorithm, and the ability to find the sensitivity with respect to all circuit parameters.

1.3 Organization

This thesis is organized into seven chapters. Following this introduction, Chapter 2 provides a review of nonlinear intermodulation distortion analysis methods for RF circuits and some of the most common approaches in the literature for obtaining the value of the third order intercept point. This is then followed by Chapter 3, in which the formulation of the Harmonic Balance equations is presented in addition to an overview of nonlinear steady-state circuit simulation using Harmonic Balance. An overview of sensitivity analysis methods is also presented in Chapter 3. The first main contribution of this research work is presented in Chapter 4, which is that of computing the value of IP3 in mixer circuits using moments. The second main contribution is found in Chapter 5, which includes the definition of the single-tone IP3 formulation and the derivation of the link between the single-tone moments and the value of IP3. Chapter 6 presents the two moments based sensitivity analysis techniques that were developed. Finally a summary and the conclusions are presented in Chapter 7.

Chapter 2

Review of Intermodulation Distortion Analysis Techniques

2.1 Introduction

In general, distortion is defined to be simply the deviation of the output signal from the expected or desired waveform [3]. The distortion that is a result of the nonlinear behavior of circuit parameters is referred to as nonlinear distortion. One example of nonlinear distortion is crossover distortion at the output of a Class B output stage [3]. Linear distortion can also affect the behavior of linear circuits driven by signals with complex spectral distributions such as square waves. A good example of linear distortion is the response of an RC circuit to a square wave input, which could deviate quite considerably from a square wave depending on its time constant even though the circuit only contains linear elements. In Radio Frequency and microwave circuits, nonlinear distortion is of particular importance since it is an important and usually an undesired behavior that limits their performance. It is therefore very important to be able to measure the amount of nonlinear distortion efficiently using CAD tools and is thus the focus of this research work. In this chapter, an overview of nonlinear distortion is presented in addition to a review of some of the main methods described in the literature for quantifying the amount of nonlinear distortion in RF circuits.

2.2 Importance of Nonlinear Distortion

Nonlinear distortion presents several significant challenges to circuit designers. If a nonlinear circuit is driven by a single-tone sinusoidal source at a frequency of ω_1 with a sufficiently small amplitude, then the output spectrum will contain only one frequency component above the noise floor. This frequency is the same as that of the input and is referred to as the fundamental frequency. This represents the linear response of the circuit and in this case, the circuit can be analyzed using small signal models since it is basically considered to exhibit linear behavior. However, when a larger input amplitude is applied, the output signal spectrum will now also contain frequency components at multiples of the fundamental frequency, known as harmonics, which will distort the desired linear response and therefore the small signal models become no longer valid. A fundamentally similar analysis can be performed for a nonlinear circuit that is driven by a multi-tone sinusoidal input signal. For the case of a two-tone input signal of frequencies ω_1 and ω_2, the output spectrum will resemble that shown in Fig. 2.1.

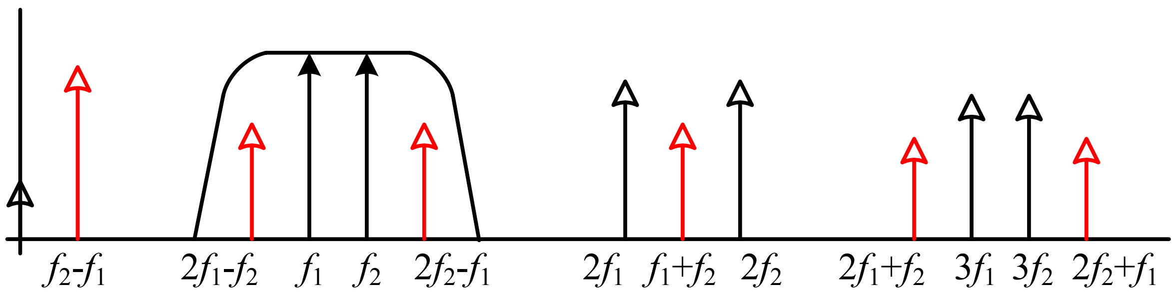

Fig. 2.1 Output spectrum of narrow-band circuit driven by two closely spaced sinusoidal tones

As illustrated in Fig. 2.1, the output not only contains the responses at the fundamental frequencies of ω_1 and ω_2 and their harmonics, but also additional intermodulation products at frequencies that result from the mixing of the fundamental frequency tones and their harmonics (i.e. $m\omega_1 + n\omega_2$). This is where some of the major problems associated with nonlinear intermodulation distortion start to become visible. First of all, the number of frequency tones at each node in the circuit becomes very large, even when only a small number of harmonics is considered. In addition, for a narrow-band circuit excited by two frequency tones that are narrowly separated in frequency, the third order intermodulation products located at $2\omega_{1,2} - \omega_{2,1}$ become of particular importance since they often mix back into the passband of the circuit and are thus extremely difficult to filter out as shown in Fig. 2.1. This leads to many undesirable effects such as adjacent channel interference.

2.3 Terminology and Figures of Merit

The nonlinear behavior and performance of analog integrated circuits is often characterized in terms of parameters and figures of merit measured in the frequency domain [3], [6]. There are many such figures of merit that are commonly used in the literature. In this section, only the main figures of merit and terminology used by RF circuit engineers to quantify nonlinear distortion in addition to those that are used extensively in this thesis are presented. In general, the definitions refer to the output variable of a nonlinear circuit that is excited with one or more input sinusoidal signals. The definitions below all refer to Fig. 2.2 which shows the output power levels of the fundamental tone in addition to the second and third harmonics as a function of the input power level.

2.3.1 Weakly Nonlinear System Behavior

Consider a nonlinear circuit that is excited with a small input signal. If the signal is small enough such that the energy of the output signal is mainly concentrated in the lower order harmonics, then this is referred to as weakly nonlinear behavior. This implies that the amplitude of the second harmonic will be much higher than the following higher order even harmonics, and the amplitude of the third harmonic will be much higher than the following higher order odd harmonics. A circuit excited by a small input signal that satisfies this criteria is referred to as a weakly nonlinear circuit. The amplifier circuits covered in this thesis fall under this category of circuits. For the case of mixer circuits, these exhibit strong nonlinear behavior outside the signal path due to the switching nature of the large Local Oscillator (LO) amplitude, but are still considered weakly nonlinear around the LO.

2.3.2 Gain Compression and the 1 dB Compression Point

The output of a nonlinear circuit that is excited by a single input frequency tone consists of the desired linear response at the fundamental frequency in addition to responses at the harmonics of the fundamental frequency. For input amplitudes that are sufficiently small, the circuit behaves in a weakly nonlinear fashion which implies that the fundamental response increases linearly

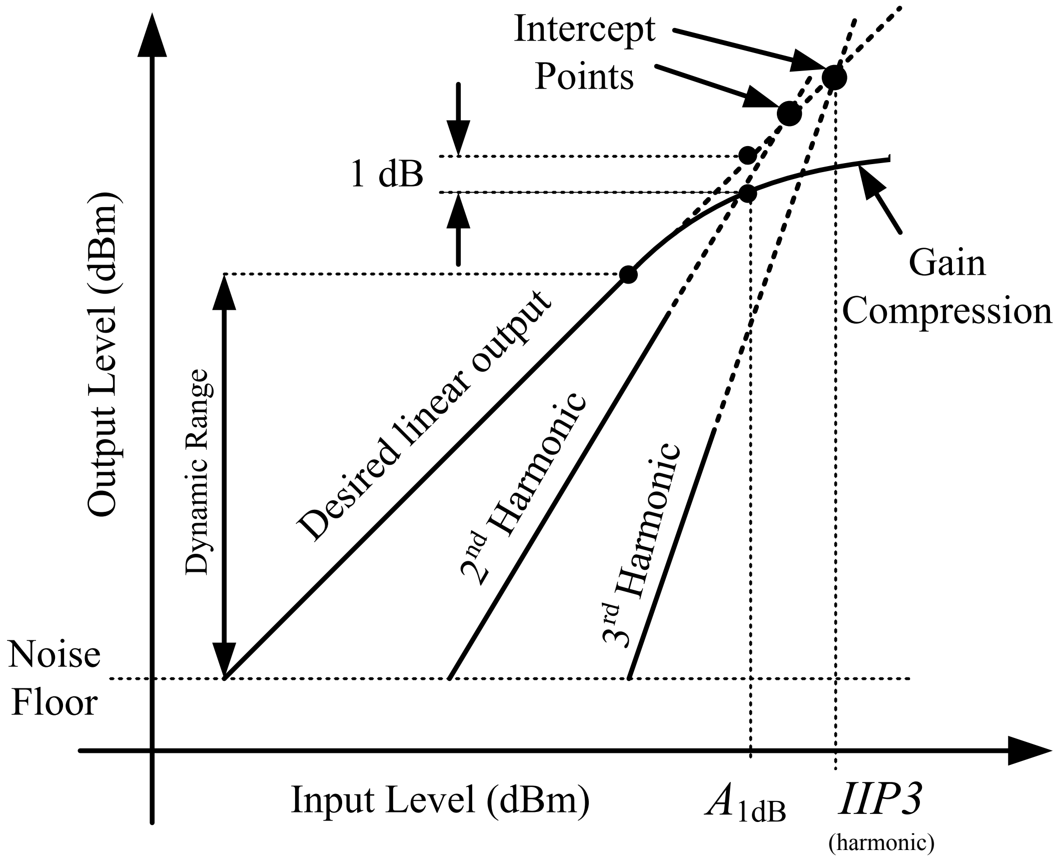

Fig. 2.2 Harmonic levels at the output of a nonlinear circuit [3]

with the input amplitude. However, there is a point at which higher input levels will lead to the fundamental response no longer increasing in a proportional manner. Instead, as is illustrated in Fig. 2.2, the gain starts to decrease due to the effects of higher order terms. This behavior is known as gain compression. Alternatively, gain expansion could occur depending on the sign of the higher order terms that influence the fundamental response. A popular way to quantify the amount of gain compression is by finding the 1-dB compression point which indicates the point at which the fundamental response deviates from the expected extrapolated linear response by 1 dB.

2.3.3 Intercept Points

As the input amplitude level is increased, the fundamental response increases linearly with the amplitude, as does the response at the second and third harmonics. However, the fundamental response increases with a slope of 1 on a dB scale, while the second and third harmonics increase with slopes of 2 and 3 on a dB scale, respectively. These linear increases will continue until the output begins to compress. However, if an extrapolation of the linear increases is made, the responses of the second and third harmonics will theoretically cross those of the fundamental response due to the difference in slope, as shown in Fig. 2.2. The points at which the harmonics meet the fundamental response are known as the intercept points and can be measured at either the corresponding input or output power levels. The 3rd order intercept point (IP3) can be defined in one of two ways. The first is the power level at which the third harmonic theoretically meets the fundamental as shown in Fig. 2.2. The second and more common definition is the power level at which the third order intermodulation tone would be equal to that of the fundamental, as shown in Fig. 2.3, in the presence of multi-tone inputs. The input IP3 power level is referred to as IIP3 while the output power level is referred to as OIP3. Other intercept points such as IP2 and IP5 can also be obtained if the appropriate harmonics are considered.

2.3.4 Other Figures of Merit

There are many other parameters that engineers use to quantify distortion in RF circuits. Total Harmonic Distortion for example measures the amount of energy in the harmonics relative to the energy in the fundamental and thus indicates how closely the output waveform resembles a pure sinusoidal wave. Intermodulation Free Dynamic Range is another commonly used term that shows the ratio of the largest and smallest signal levels the circuit can handle without the appearance of an intermodulation component. Fig. 2.2 shows the dynamic range relative to the 3rd order component. Other parameters in the literature include Harmonic Distortion, Cross-Modulation factor and 3-dB compression point among others [3], [6], [29].

2.4 Simulation Based Distortion Analysis Methods

In the literature, there are two general classes of methods for analyzing the distortion in RF circuits. The first class is that of simulation based methods. Typically, simulation based approaches aim to mimic a measurement environment using a workbench by finding the steady-state solution of the nonlinear circuit with multi-tone inputs. The intermodulation distortion is then obtained from the resulting output spectrum. Sensitivity analysis can then be performed on the results by applying a sensitivity analysis algorithm. Simulation based approaches are easy to automate. However, they typically suffer from a large CPU cost due to the presence of multi-tone inputs and the need to perform a steady-state solution. An excellent introduction to simulation methods for RF circuits is presented in [30]. In this section, an overview of the most common and state-of-the-art simulation based approaches for distortion analysis is presented.

2.4.1 Distortion Analysis Using Harmonic Balance

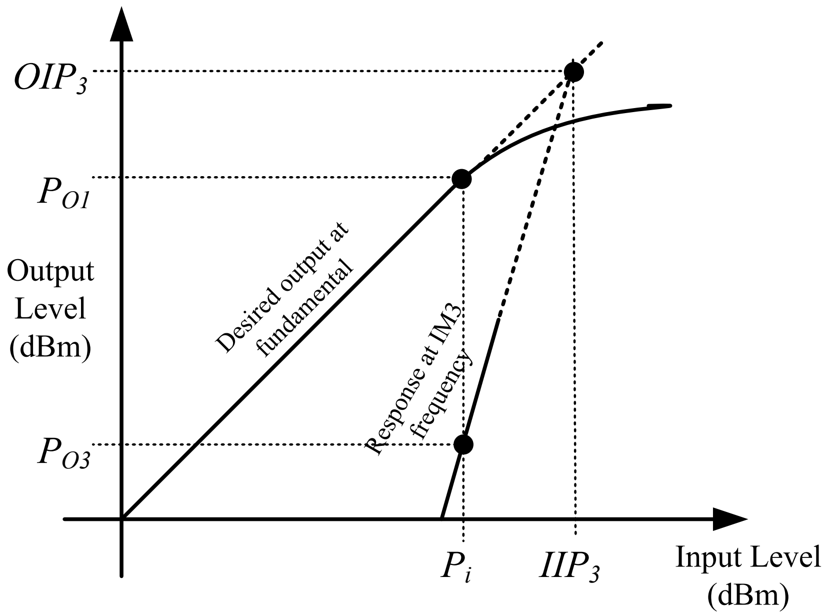

Fig. 2.3 Definition of the input and output third order intercept points (IIP3 and OIP3, respectively)

To determine the value of the third order intercept point using brute force simulation, the steady-state solution for a circuit due to a two tone input is obtained using the Harmonic Balance method (as will be described in Chapter 3). Then, noting the input power P_i, the output powers at the fundamental frequency P_{o1}, and at third order intermodulation product P_{o3}, and considering that the slope of P_1 as a function of P_i is 1 on a dB scale, and the slope of P_3 as a function of P_i is 3 on a dB scale, the graphs of P_1 and P_3 can be extrapolated as shown in Fig. 2.3 in order to obtain the values of the third order intercept points. This results in the following relations for the input third order intercept point ($IIP3$) and the output third order intercept point ($OIP3$) [6]

$$IIP3 = P_i + \frac{1}{2}[P_{o1} - P_{o3}] \tag{2.1}$$

$$OIP3 = IIP3 + G \tag{2.2}$$

where G is the linear power gain of the circuit. This approach is fully automated and applicable to general circuit types and topologies. The main disadvantage with this approach is that it is very CPU expensive. This is a result of the presence of a large number of frequency tones that are a product of the multi-tone input, in addition to the fact that a full steady-state simulation needs to be performed by solving a system of nonlinear equations using iterative techniques [31], [32]. A more detailed formulation and analysis of the Harmonic Balance method is presented in Chapter 3.

2.4.2 Distortion Analysis Using the Simplified Newton Method

The most CPU expensive task in performing a Harmonic Balance solution is solving the system of equations with a dense Jacobian matrix at each step of an iterative process. This CPU cost can be reduced through the application of the simplified Newton method [31] for distortion analysis purposes in communication circuits [33] [34]. In addition to being efficient, these methods are simple to apply as they do not require the computation of higher order derivatives of the device model nonlinearities.

The simplified Newton method, when applied to solving a nonlinear set of equations of the form $f(x) = 0$, results in the following iterative formula

$$\boldsymbol{J}(x^{(0)})\Delta x^{(i)} = -f(x^i); \quad x^{(i+1)} = x^{(i)} + \Delta x^{(i)} \tag{2.3}$$

where $\boldsymbol{J}$ is the Jacobian matrix that does not require updating under the simplified Newton method. After formulating the Harmonic Balance equations in the frequency domain, the periodic large signal solution is found using a single-tone input to determine a periodic steady state Jacobian matrix ($\boldsymbol{J}^{PSS}$), which is of a smaller order than the regular HB Jacobian matrix. The solution is then obtained by solving

$$\boldsymbol{J}^{PSS}(\omega)\Delta \boldsymbol{X}^{(j)}(\omega) = -F^{(j)}(\omega); \quad \boldsymbol{X}^{(j+1)} = \boldsymbol{X}^{(j)} + \Delta \boldsymbol{X}^{(j)} \tag{2.4}$$

twice, first to determine $X^{(1)}$ and then to determine $X^{(2)}$. To determine $X^{(1)}$, the right hand side vector of (2.4) contains contributions of small signal sources at the fundamental frequencies of ω_1 and ω_2. For determining IP3, it is sufficient to solve only one linear system at the IM3 frequency when determining the value of $X^{(2)}$. In these relations, $F(\omega)$ is the formulation of the function $f(x)$ of the system in the frequency domain. During the solution process, switching between the time and frequency domains occurs using the Direct Fourier Transform (DFT) and the Inverse Direct Fourier Transform (IDFT) to evaluate the nonlinear components of the system in order to compute the right-hand-side of equation (2.4), at each iteration.

Because distortion analysis typically requires computing only up to 3rd order nonlinearities, this method can only involve as little as two steps of the simplified Newton method. What makes this method efficient is the need to only compute one fixed Jacobian matrix which is also of a smaller size and order than the HB Jacobian matrix. In addition, this approach does not require the computation of higher order derivatives of device model nonlinearities.

2.4.3 Fast IP3 Using Periodic Steady State Analysis

One of the approaches to improve the memory usage and time of computing the value of IP3 is to reduce the number of variables by using only single-tone inputs instead of the typical two tones. This is the motivation for the method illustrated in [30], [35] which first computes the periodic steady-state solution of the circuit using only a single frequency tone with a large signal (or a single-tone in addition to the LO for mixers). A second small signal tone with a frequency close to that of the first tone (one sideband spacing) is then applied using Periodic AC Analysis to compute the value of the intercept point with minimal additional CPU cost. This means that the first tone is used to drive the circuit hard enough to cause distortion, while the second small signal tone is used to cause intermodulation distortion. The value of IIP3 is then computed from the results of both sets of analysis using the relation given by

$$IP_3 = V_{L1} - \frac{V_{S3} - V_{S1}}{2} \tag{2.5}$$

where V_{L1} is the fundamental response due to the large signal tone, V_{S1} is the response due to the small signal tone and V_{S3} represents the intermodulation distortion. These are illustrated in Fig 2.4.

This approach was shown to present a speedup of around 6 times when compared with traditional two-tone steady-state simulations, but with results that slightly differ from the value of

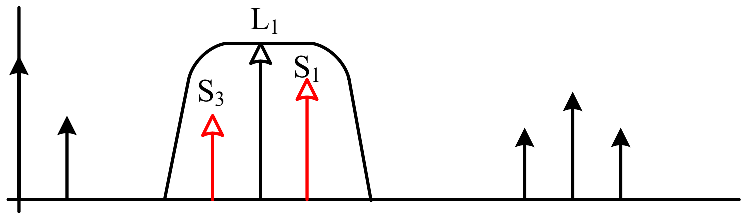

Fig. 2.4 Measurement of intermodulation distortion using periodic-steady-state / periodic AC analysis

the two-tone IP3 due to a difference in definition. While this method does significantly reduce the number of variables and thus the CPU cost, a steady-state analysis still needs to be performed which means systems of nonlinear equations still need to be solved using inefficient steady-state simulation methods.

2.4.4 Linear Centric Distortion Analysis

The linear centric distortion analysis approach is part of what is referred to as per-nonlinearity distortion analysis [4], [36], [37] methods of which Volterra series analysis is also a part. This methodology provides insight on the circuit linearity by splitting the output distortion obtained via a regular simulation to per-component distortion contributions in an efficient post-simulation step. The linear-centric circuit model can be used to perform distortion analysis with any steady-state simulation method as a post-simulation processing step. A good example of this is in conjunction with the Harmonic Balance method [38].

This distortion analysis approach relies on an iterative Successive Chord method in which the Jacobian matrix for the solution of the nonlinear system is constructed through the use of constant linearizations of nonlinear elements. The nonlinear effects only appear in the right-hand-side vector of the general circuit equations (see Chapter 3) through the use of nonlinear device model evaluations. Each nonlinear element is replaced by its linear centric model, which consists of a linear element in addition to a varying current source at each iteration. The final circuit can therefore be viewed as a constant linear circuit driven by external inputs, in addition to contributions to the right-hand-side vector representing the circuit nonlinearities. This concept is illustrated in Fig. 2.5 [4].

The linear centric models for most circuit elements are simple to determine, unlike traditional Volterra series. No higher order derivatives need to be evaluated explicitly during the process,

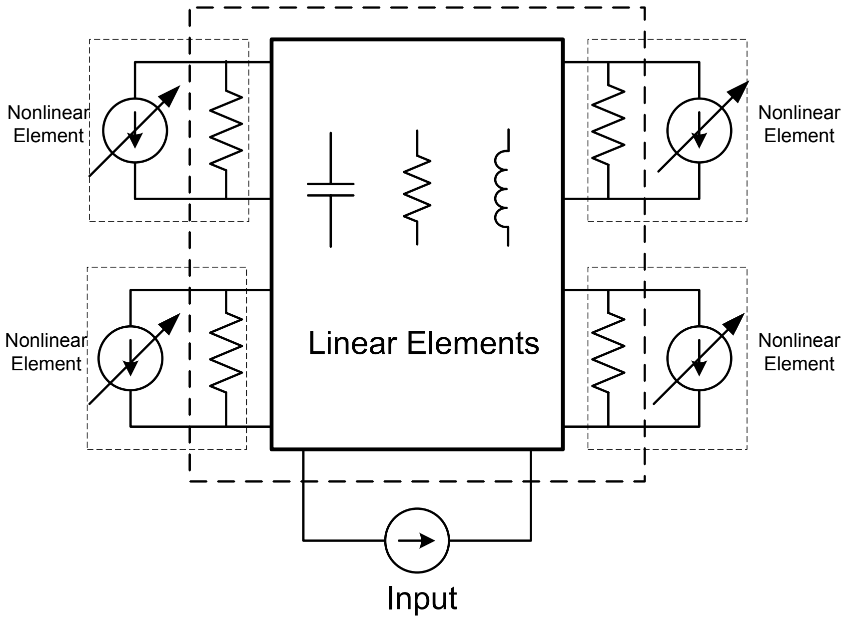

Fig. 2.5 Overall linear-centric circuit model showing how a nonlinear circuit can be viewed as a linearized one driven by external inputs in addition to chord current sources due to the nonlinearities [4]

which means the method is easily automated and directly applied to widely adopted device models. The method is applicable to both amplifiers and mixers. The CPU cost of this approach is the solution of one linear system of equations followed by simple device-model evaluations. The accuracy of the obtained results is quite high and is similar to the accuracy of general circuit-level simulation.

2.4.5 Weakly Nonlinear RF Circuit Reduction and Other Simulation Enhancement Methods

In the literature, there are many simulation based techniques for efficient intermodulation distortion analysis that enhance and optimize some of the existing approaches. One of the main trends in RF circuit simulation is to develop methods with the aim of reducing the size of the systems of equations by implementing model order reduction and macromodeling of weakly nonlinear RF circuits [39]–[42]. For these methods to work, the nonlinearity information information has to be preserved in the reduced order systems. Krylov subspace projection based reduction algorithms preserve the critical nonlinearity data necessary for accurate and efficient intermodulation distortion analysis.

Another current trend in circuit simulation is the development of algorithms that take advantage of emerging parallel hardware platforms which have become very popular recently. Distortion analysis algorithms and steady-state simulation methods are serial in nature, but there is a lot of work aimed at performing efficient parallel algorithms such as parallel Harmonic Balance implementations based on hierarchical HB preconditioners [43], [44] and domain decomposition methods [45]. This allows distortion analysis simulations to run faster on multi-core computing platforms.

2.5 Analytical Techniques for Distortion Analysis

The other general class of methods for analyzing nonlinear distortion is that of analytical techniques. Such methods are for the most part based on the Volterra Series [46], [47]. These methods rely on deriving complex analytical expressions for the different order nonlinearities in the circuit. The main advantage of such methods is that the equations provide insight into the sources of distortion in the circuit, which simplifies tasks such as performing a sensitivity analysis. The main limitation is that such methods are difficult to automate and apply in a general circuit simulator on arbitrary circuits and models. In this section, an overview of how to obtain the value of IP3 using Volterra series is presented.

2.5.1 Volterra Series Formulation

Consider the case of a general *linear* system with memory elements, that is excited by an input signal $v(t)$ and produces an output signal $x(t)$. The input-output relation of the system can be represented with the use of a transfer function $h(t)$. In the frequency domain, this would correspond to the relation

$$H(j\omega) = \frac{X(j\omega)}{V(j\omega)} \tag{2.6}$$

Now, consider the case of a *nonlinear* memoryless system (i.e. without the presence of inductors or capacitors). In this case the input-output relation of the system can be represented with the use of a power series expansion as follows

$$x = k_0 + k_1 v_{in} + k_2 v_{in}^2 + k_3 v_{in}^3 + \cdots = \sum_n k_n v^n \tag{2.7}$$

In this relation, k_n represents n^{th} order response of the circuit.

For the more general case of *nonlinear* systems *with memory*, a Volterra series can be used to represent the input output relation of the system. A time-domain Volterra series can be expressed using the expansion given by

$$x(t) = H_1\left[v(t)\right] + H_2\left[v(t)\right] + \cdots + H_n\left[v(t)\right] \tag{2.8}$$

In this relation, H_n is the n^{th} order Volterra operator and can be viewed as the n^{th} order transfer function when expressed in the frequency domain [3], [48]. The block diagram representation of a Volterra series is illustrated in Fig. 2.6. Each Volterra operator in (2.8) is a function of its

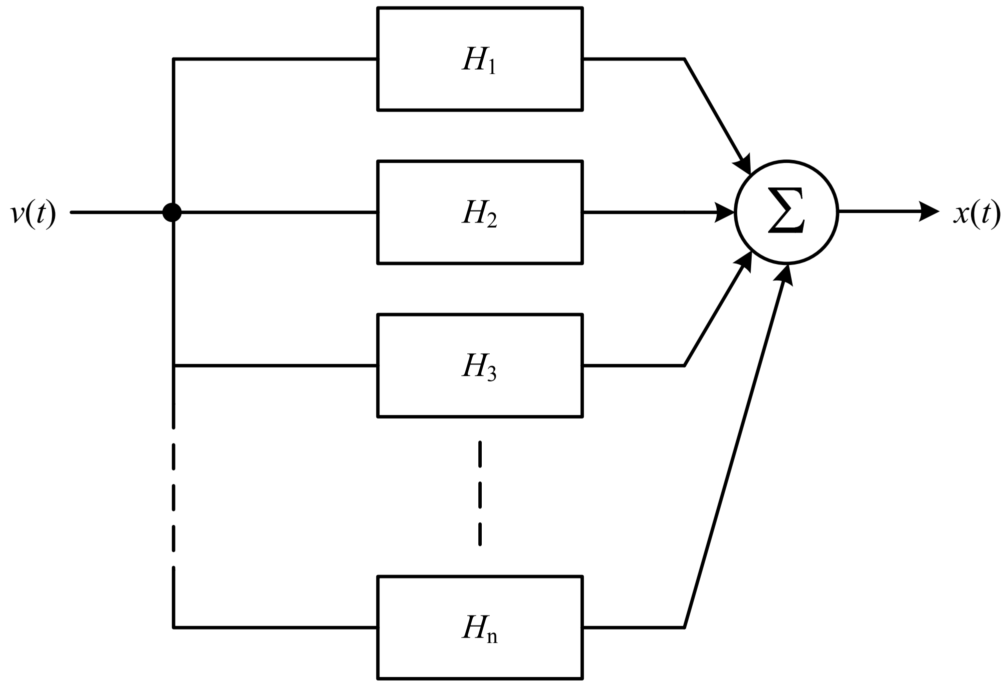

Fig. 2.6 Block diagram representation of a Volterra series

corresponding Volterra kernel and therefore can be expressed as

$$H_n\left[v(t)\right] = \int_{-\infty}^{\infty} \cdots \int_{-\infty}^{\infty} h_n(\tau_1, \cdots, \tau_n) \prod_{r=1}^{n} v(t-\tau_r)d\tau_r \tag{2.9}$$

for an input function $v(t)$, where $h_n\left(\tau_1, \tau_2, \ldots, \tau_n\right)$ is the n^{th} order Volterra kernel. It is also possible to represent a Volterra series in the frequency domain through the use of a Laplace or Fourier transform [3]. The multi-dimensional Laplace transform for functions of p variables, in this case $h_p(\tau_1, \ldots, \tau_n)$ is defined as

$$H_n(s_1, \cdots, s_p) = \int_{-\infty}^{\infty} \cdots\cdots \int_{-\infty}^{\infty} h_p(\tau_1, \cdots, \tau_p) e^{-(s_1\tau_1+\cdots+s_p\tau_p)} d\tau_1 \cdots d\tau_p \tag{2.10}$$

2.5.2 IP3 Computation Using Volterra Kernels

Consider the power series expansion of the input-output relationship of a memoryless nonlinear system given in (2.7). For simplicity, only the first four terms of the series in (2.7) will be accounted for. Now consider an input voltage signal consisting of two sinusoidal input tones given by $v_{in} = V_1 \cos \omega_1 t + V_2 \cos \omega_2 t$. By substituting this term into (2.7) and expanding using trigonometric identities, the frequency components shown in Table 2.1 are obtained.

Table 2.1 Summary of distortion components [6]

Frequency	**Component Amplitude**
DC	$k_0 + \frac{k_2}{2}(V_1^2 + V_2^2)$
ω_1	$k_1 V_1 + k_3 V_1(\frac{3}{4}V_1^2 + \frac{3}{2}V_2^2)$
ω_2	$k_1 V_2 + k_3 V_2(\frac{3}{4}V_2^2 + \frac{3}{2}V_1^2)$
$2\omega_1$	$\frac{k_2 V_1^2}{2}$
$2\omega_2$	$\frac{k_2 V_2^2}{2}$
$\omega_1 \pm \omega_2$	$k_2 V_1 V_2$
$\omega_2 \pm \omega_1$	$k_2 V_1 V_2$
$3\omega_1$	$\frac{k_3 V_1^3}{4}$
$3\omega_2$	$\frac{k_3 V_2^3}{4}$
$2\omega_1 \pm \omega_2$	$\frac{3}{4}k_3 V_1^2 V_2$
$2\omega_2 \pm \omega_1$	$\frac{3}{4}k_3 V_1 V_2^2$

The 3rd order intercept point is theoretically where the amplitude of the fundamental tone is the same as that of the intermodulation tones at either $2\omega_1 - \omega_2$ or $2\omega_2 - \omega_1$. To determine the value of the input third order intercept point voltage, we equate the linear part of the fundamental component to that at one of the third order intermodulation tones. Assuming the amplitudes of the two input signals are the same such that $V_1 = V_2 = V_{IP3}$, we obtain

$$k_1 V_{IP3} = \frac{3}{4} k_3 V_{IP3}^3 \tag{2.11}$$

which then simplifies to

$$V_{IP3} = \sqrt{\frac{4}{3}\frac{k_1}{k_3}} \tag{2.12}$$

The relation given by (2.12) is used to determine the value of the input third order intercept point voltage. To determine the output third order intercept point voltage, simply multiply this quantity by the voltage gain of the system.

For systems that contain memory elements such as inductors and capacitors, the input-output relationship given by (2.7) becomes a function of the Volterra kernels, where the n^{th} order kernel is given by $H_n(j\omega_1, \ldots, j\omega_n)$. In this case, the distortion components at each output frequency are summarized in Table 2.2. It can be shown that the value of the input third order intercept point voltage now becomes

$$V_{IP3} = \sqrt{\frac{4}{3}\frac{|H_1(j\omega_1)|}{|H_3(j\omega_1, j\omega_1, -j\omega_2)|}} \tag{2.13}$$

For the case of mixer circuits, the input signal is defined as $v = V_1 \cos(\omega_1 t) + V_2 \cos(\omega_2 t) + V_{LO} \cos(\omega_0 t)$, with ω_1 and ω_2 being two input radio frequency signals and ω_0 being the local oscillator frequency. In this case, the distortion components will be different to that of amplifier circuits and the expression for IP3 will be a function of the LO power. The intermodulation distortion analysis of mixers can be accomplished through the use of periodically time varying Volterra series and is outlined in section 2.5.3. The main difficulty of this approach is that, in order to obtain the Volterra kernels, complex analytical solutions of equations for each nonlinear element has to be performed [3]. Recently, several methods have been proposed in the literature with some modifications and variations on traditional Volterra series to make their application more intuitive and flexible [49]–[51]. However, the fundamental advantages and limitations of traditional Volterra series remain.

Table 2.2 Distortion components described by Volterra kernels at the corresponding output frequencies [3]

Frequency	Component Amplitude	Type of Response
DC	$\frac{1}{2}V_1^2\,\lvert H_2(j\omega_1,-j\omega_1)\rvert$	DC Shift
DC	$\frac{1}{2}V_2^2\,\lvert H_2(j\omega_2,-j\omega_2)\rvert$	DC Shift
ω_1	$V_1\,\lvert H_1(j\omega_1)\rvert$	Linear
ω_2	$V_2\,\lvert H_1(j\omega_2)\rvert$	Linear
$2\omega_1$	$\frac{1}{2}V_1^2\,\lvert H_2(j\omega_1,j\omega_1)\rvert$	2nd harmonic
$2\omega_2$	$\frac{1}{2}V_2^2\,\lvert H_2(j\omega_2,j\omega_2)\rvert$	2nd harmonic
$\omega_1+\omega_2$	$V_1V_2\,\lvert H_2(j\omega_1,j\omega_2)\rvert$	2nd order intermodulation
$\lvert\omega_1-\omega_2\rvert$	$V_1V_2\,\lvert H_2(j\omega_1,-j\omega_2)\rvert$	2nd order intermodulation
$3\omega_1$	$\frac{1}{4}V_1^3\,\lvert H_3(j\omega_1,j\omega_1,j\omega_1)\rvert$	3rd harmonic
$3\omega_2$	$\frac{1}{4}V_2^3\,\lvert H_3(j\omega_2,j\omega_2,j\omega_2)\rvert$	3rd harmonic
$2\omega_1+\omega_2$	$\frac{3}{4}V_1^2V_2\,\lvert H_3(j\omega_1,j\omega_1,j\omega_2)\rvert$	3rd order intermodulation
$\lvert 2\omega_2-\omega_1\rvert$	$\frac{3}{4}V_1^2V_2\,\lvert H_3(j\omega_1,j\omega_1,-j\omega_2)\rvert$	3rd order intermodulation
$\lvert\omega_1-2\omega_2\rvert$	$\frac{3}{4}V_1V_2^2\,\lvert H_3(j\omega_1,-j\omega_2,-j\omega_2)\rvert$	3rd order intermodulation
$\omega_1+2\omega_2$	$\frac{3}{4}V_1V_2^2\,\lvert H_3(j\omega_1,j\omega_2,j\omega_2)\rvert$	3rd order intermodulation
$2\omega_1-\omega_1=\omega_1$	$\frac{3}{4}V_1^3\,\lvert H_3(j\omega_1,-j\omega_1,-j\omega_1)\rvert$	3rd order compression
$2\omega_2-\omega_2=\omega_2$	$\frac{3}{4}V_2^3\,\lvert H_3(j\omega_2,j\omega_2,-j\omega_2)\rvert$	3rd order compression
$\omega_1+\omega_2-\omega_2=\omega_1$	$\frac{3}{2}V_1V_2^2\,\lvert H_3(j\omega_1,j\omega_2,-j\omega_2)\rvert$	3rd order desensitization
$\omega_1-\omega_1+\omega_2=\omega_2$	$\frac{3}{2}V_1^2V_2\,\lvert H_3(j\omega_1,-j\omega_1,j\omega_2)\rvert$	3rd order desensitization

2.5.3 Distortion Analysis Using Time-Varying Volterra Series

Traditional Volterra series are referred to as time invariant and are only applicable to weakly nonlinear amplifier circuits. However, extensions to an important class of strongly nonlinear circuits such as active switching mixers have been made using time-varying Volterra series [2], [52]. These types of circuits are typically driven by one large periodic input signal such as a local oscillator (LO) signal or a clock [4]. In this case, the input RF signal in the signal path is at a small level and therefore the circuit is considered to behave in a weakly nonlinear fashion about the periodically varying operating point that is generated by the LO or the clock. This then allows the strongly nonlinear circuits to be analyzed as periodically time varying weakly nonlinear systems with respect to a small-signal input of interest.

For nonlinear time-varying systems, a multi-frequency network function is given by

$$H_n(t, \omega_1, \cdots, \omega_n) = \int_{-\infty}^{\infty} \cdots\cdots \int_{-\infty}^{\infty} h_n(t, \tau_1, \cdots, \tau_n) e^{-j\omega_1(t-\tau_1)} \ldots e^{-j\omega_1(t-\tau_n)} d\tau_1 \cdots d\tau_n \tag{2.14}$$

where $h_n(t, \tau_1, \cdots, \tau_n)$ is the n^{th} order Volterra kernel. With these relations, the response of a nonlinear periodically time varying system to a two-tone sinusoidal input of $v(t) = A(cos\omega_1 t + cos\omega_2 t)$ is of the form [2]

$$\begin{aligned} x(t) \approx & \sum_{k=-\infty}^{\infty} \left[\frac{A^2}{2} H_{2,k} + \left(\frac{A}{2} H_{1,k} + \frac{9A^3}{8} H_{3,k} \right) e^{j\omega_1 t} + \left(\frac{A}{2} H_{1,k} + \frac{9A^3}{8} H_{3,k} \right) e^{j\omega_2 t} + \right. \\ & \frac{A^2}{4} H_{2,k} e^{j2\omega_1 t} + \frac{A^2}{4} H_{2,k} e^{j2\omega_2 t} + \frac{A^3}{8} H_{3,k} e^{j3\omega_1 t} + \frac{A^3}{8} H_{3,k} e^{j3\omega_2 t} + \\ & \left. \text{intermod.terms} \right] e^{jk\omega_0 t} \end{aligned} \tag{2.15}$$

where ω_0 is the frequency of the LO or clock. As can be seen from this relation, due to the periodically time varying nature of these systems, an output spectrum pattern that is similar to that in the base band will appear at multiples of ω_0.

2.5.4 Sensitivity Analysis Using Volterra Series

Sensitivity analysis of mildly nonlinear circuits can be performed from a Volterra series analysis since the closed form expressions for the Volterra kernels provide the necessary insight into the circuit. Having access to the closed form expressions allows for very efficient evaluation of sensitivity using software. Recently, a simulation based algorithm was implemented for computing the sensitivity using Volterra Series directly in the frequency domain [53], [54]. The method is based on Schetzen's multilinear theory for separating the nonlinear circuit into circuits of different order [55], in conjunction with Volterra series equivalent circuits. Sensitivity analysis performed with this approach was shown to be computationally efficient as it implemented the adjoint sensitivity approach to Volterra series and only required one LU decomposition of a sparse matrix for all the different order circuits. Since this method requires access to the equivalent higher order Volterra series circuits, its application to arbitrary circuit models and nonlinearities in a general purpose simulator is limited.

2.5.5 Rapid Estimation of IP3 Using the Three-Point Method

A very simple procedure for a rapid estimation of the value of IP3 that can easily be implemented in simulators like SPICE is presented in [29]. It relies on the fact that knowing the incremental gain of the circuit at three different input amplitudes is enough to be able to determine the power series coefficients needed for finding IP3 according to (2.12). The incremental gain (transconductance) is the derivative of the power series equation given by (2.7) [29] and is therefore approximately equal to

$$g(v) \approx k_1 + 2k_2 v + 3k_3 v^2 \tag{2.16}$$

Any three different input voltages would do the trick, but convenient ones are those at deviations of 0, V, -V from the DC bias value. With these choices of voltages, the incremental gains would be

$$\begin{aligned} g(0) &\approx k_1, && (2.17)\\ g(V) &\approx k_1 + 2k_2 V + 3k_3 V^2 && (2.18)\\ g(-V) &\approx k_1 - 2k_2 V + 3k_3 V^2 && (2.19) \end{aligned}$$

The coefficients of the power series then become

$$k_1 = g(0), \tag{2.20}$$

$$k_2 = \frac{g(V) - g(-V)}{4V} \tag{2.21}$$

$$k_3 = \frac{g(V) + g(-V) - 2g(0)}{6V^2} \tag{2.22}$$

Substituting into (2.12) then gives the final relation for the value of IIP3. The three-point method is used for a rapid estimation of the value of IP3 in the early stages of a design and is also valuable in guiding the selection of design parameters to maximize the value of IP3.

2.6 Moments Based Technique for the Distortion Analysis of Amplifier Circuits

Recently, a method based on the computation of the circuit moments was presented for obtaining the value of IP3 in weakly nonlinear amplifier circuits [56], [57]. The new approach was shown to be equivalent to the numerical computation of the values of the appropriate Volterra kernels at the frequencies of interest. This approach does not require any analytical manipulation but is rather applied directly to the MNA [21] formulation of the circuit. It can therefore be applied to circuits of arbitrary complexity. Furthermore, the computation of all the moments only requires one LU decomposition of the Jacobian evaluated at the DC operating point which is very sparse unlike the typical Harmonic Balance (HB) Jacobian which is usually both large and dense, especially for large RF circuits that exhibit strong nonlinearities. The computation is done numerically with the input frequencies known, and thus produces very accurate results. The methods presented in this thesis are based on the same methodology as that introduced in this technique, but have been developed extensively to cover more types of RF circuits, improve CPU efficiency and present new sensitivity information. In this section, the moments computation algorithm used in [56], [57] is introduced, followed by the presentation of the relation between the moments and the value of IP3 in amplifier circuits.

2.6.1 Moments Computation Algorithm

The moments are defined as the Taylor series coefficients of the expansion of the Harmonic Balance vector of unknowns $\boldsymbol{X}$, with respect to the signal amplitude voltage α, given by

$$\begin{aligned} \boldsymbol{X} &= \boldsymbol{M}_0 + \boldsymbol{M}_1\alpha + \boldsymbol{M}_2\alpha^2 + \boldsymbol{M}_3\alpha^3 + \dots && (2.23) \\ &= \sum_{i=0}^{\infty} \boldsymbol{M}_i\alpha^i && (2.24) \end{aligned}$$

These moments can be evaluated using a very efficient algorithm [17], [18]. The zeroth moment vector $\boldsymbol{M}_0$, is obtained by finding the DC solution of the general HB system of equations (Refer to Chapter 3 for more details on the HB formulation). If the nonlinear HB Jacobian, $\boldsymbol{J}$, is also expressed as a Taylor series expansion with respect to the signal amplitude voltage α as given by

$$\boldsymbol{J} = \sum_{i=0}^{\infty} \boldsymbol{T}_i\alpha^i, \tag{2.25}$$

then the remaining moment vectors $\boldsymbol{M}_n$ can be found by solving the system of equations given by [17]

$$\begin{aligned} \boldsymbol{\Phi M}_1 &= \boldsymbol{B}_{RF} && (2.26) \\ \boldsymbol{\Phi M}_n &= -\frac{1}{n}\sum_{j=1}^{n-1}(n-j)\boldsymbol{T}_j\boldsymbol{M}_{n-j}, \quad n \geq 2 && (2.27) \end{aligned}$$

where $\boldsymbol{\Phi}$ is the moments computation matrix, and $\boldsymbol{B}_{RF}$ is a vector containing the contributions of the RF input signal (Refer to Chapter 3 for more details). In these relations, the moment vectors can be obtained using one LU Decomposition to solve (2.26) and (2.27) recursively. It is important to note that the matrix $\boldsymbol{\Phi}$ has the same structure as that of the HB Jacobian matrix but with only the DC components present, which makes it very sparse. As can be seen from (2.26) and (2.27), the computation of the moment vectors is a solution of a set of linear algebraic equations where the left-hand-side matrix is the same throughout and is therefore very efficient.

2.6.2 Computation of IP3 From the Moments

In this section the relation between the circuit moments and the desired Volterra kernels is shown for general amplifier circuits. In order to simplify the presentation, a memoryless system is considered first where the output variable x is expressed as a power series of the input v as given by (2.7). Substituting $v = \alpha(\cos(\omega_1 t) + \cos(\omega_2 t))$ into (2.7), truncating after k_3, and expanding using trigonometric identities then gives

$$\begin{aligned} x \;=\; & k_0 + [k_1\cos(\omega_1 t) + k_1\cos(\omega_2 t)]\alpha + [k_2 + \frac{k_2}{2}\cos(2\omega_1 t) + k_2\cos((\omega_1+\omega_2)t) \\ & + k_2\cos((\omega_1-\omega_2)t) + \frac{k_2}{2}\cos(2\omega_2 t)]\alpha^2 + [\frac{9k_3}{4}\cos(\omega_1 t) + \frac{k_3}{4}\cos(3\omega_2 t) \\ & + \frac{9k_3}{4}\cos(\omega_2 t) + \frac{k_3}{4}\cos(3\omega_1 t) + \frac{3k_3}{4}\cos((2\omega_2-\omega_1)t) + \frac{3k_3}{4}\cos((2\omega_1+\omega_2)t) \\ & + \frac{3k_3}{4}\cos((2\omega_2+\omega_1)t) + \frac{3k_3}{4}\cos((2\omega_1-\omega_2)t)]\alpha^3 \end{aligned} \tag{2.28}$$

From (2.28) and (2.23) the relationship between k_n and the system moments can be deduced since the solution vector $\boldsymbol{X}$ in (2.23) is essentially the output variable x in (2.28). By equating the same powers of α in these two equations and noting the frequencies, the location of the k_n terms in the moment vectors $\boldsymbol{M}_k$ can be determined. In fact, their locations are given by

$$\underbrace{\left|\begin{array}{c} \text{DC} \\ 2\omega_1 \pm \omega_2 \\ \omega_1 \\ \omega_2 \\ 2\omega_2 \pm \omega_1 \\ 2\omega_1 \\ 2\omega_2 \\ \vdots \end{array}\right|}_{\text{Frequency}} \begin{array}{c} \rightarrow \\ \rightarrow \\ \rightarrow \\ \rightarrow \\ \rightarrow \\ \rightarrow \\ \rightarrow \\ \vdots \end{array} \underbrace{\begin{bmatrix} k_0 \\ 0 \\ 0 \\ 0 \\ 0 \\ 0 \\ 0 \\ \vdots \end{bmatrix}}_{\boldsymbol{M}_0} \underbrace{\begin{bmatrix} 0 \\ 0 \\ \mathbf{k_1} \\ \mathbf{k_1} \\ 0 \\ 0 \\ 0 \\ \vdots \end{bmatrix}}_{\boldsymbol{M}_1} \underbrace{\begin{bmatrix} k_2 \\ 0 \\ 0 \\ 0 \\ 0 \\ \frac{1}{2}k_2 \\ \frac{1}{2}k_2 \\ \vdots \end{bmatrix}}_{\boldsymbol{M}_2} \underbrace{\begin{bmatrix} 0 \\ \mathbf{\frac{3}{4}k_3} \\ \frac{9}{4}k_3 \\ \frac{9}{4}k_3 \\ \mathbf{\frac{3}{4}k_3} \\ 0 \\ 0 \\ \vdots \end{bmatrix}}_{\boldsymbol{M}_3} \tag{2.29}$$

For example, consider the first power of α and it be can seen that the vector $\boldsymbol{M}_1$ consists of k_1 at the frequency of ω_1 and also another k_1 at the frequency of ω_2. The relation in (2.29) shows the first 3 moment vectors in addition to the zeroth moment vector, with the entries at the sample frequencies of interest for the computation of the third order intercept point shown in bold [6].

In the case of systems with memory (i.e. containing energy storage elements such as capacitors and inductors), a fundamentally similar analysis can be performed. The additional complexity here comes from the fact that the output is now represented as a Volterra series rather than a power series. In this case a relation between the system moments and the Volterra kernels that is similar to equation (2.29) is developed. In order to derive these relationships, first consider the system representation in terms of the Volterra series as defined in (2.8). To determine the location of the kernels in the moment vectors, an input function with two tones of the same amplitude α defined as

$$\begin{aligned} v(t) &= \alpha(\cos(\omega_1 t) + \cos(\omega_2 t)) && (2.30)\\ &= \frac{\alpha}{2}e^{j\omega_1 t} + \frac{\alpha}{2}e^{-j\omega_1 t} + \frac{\alpha}{2}e^{j\omega_2 t} + \frac{\alpha}{2}e^{-j\omega_2 t} && (2.31) \end{aligned}$$

is substituted into (2.8). The resulting equations for each Volterra operator are then used to evaluate and express the Volterra kernels in the frequency domain [57]. The final expression, when arranged by grouping like powers of α and only considering the terms up to the third order (i.e. $n = 3$), is given by the following input output relation

$$\begin{aligned} y = {} & H_0 + \left[Re(H_1(j\omega_1)e^{j\omega_1 t}) + Re(H_1(j\omega_2)e^{j\omega_2 t})\right]\alpha + \\ & \Bigg[\frac{1}{2}Re(H_2(j\omega_1, -j\omega_1)) + \frac{1}{2}Re(H_2(j\omega_2, -j\omega_2)) + \frac{1}{2}Re(H_2(j\omega_1, j\omega_1)e^{j2\omega_1 t}) + \\ & Re(H_2(j\omega_1, j\omega_2)e^{j(\omega_1+\omega_2)t}) + Re(H_2(j\omega_1, -j\omega_2)e^{j(\omega_1-\omega_2)t}) + \\ & \frac{1}{2}Re(H_2(j\omega_2, j\omega_2)e^{j2\omega_2 t})\Bigg]\alpha^2 + \\ & \Bigg[\frac{3}{4}Re(H_3(j\omega_1, j\omega_1, -j\omega_2)e^{j(2\omega_1-\omega_2)t}) + \frac{3}{4}Re(H_3(-j\omega_1, j\omega_2, j\omega_2)e^{j(2\omega_2-\omega_1)t}) + \\ & \frac{3}{2}Re(H_3(j\omega_1, j\omega_2, -j\omega_2)e^{j\omega_1 t}) + \frac{3}{4}Re(H_3(j\omega_1, j\omega_1, -j\omega_1)e^{j\omega_1 t}) + \\ & \frac{3}{2}Re(H_3(j\omega_1, -j\omega_1, j\omega_2)e^{j\omega_2 t}) + \frac{3}{4}Re(H_3(j\omega_2, j\omega_2, -j\omega_2)e^{j\omega_2 t}) + \ldots\Bigg]\alpha^3 \quad (2.32) \end{aligned}$$

The Volterra Series expression in (2.32) is similar to the expression shown in (2.28) which proves that this method is essentially that of numerically computing the required Volterra kernels evaluated at the frequencies of interest. In a similar fashion to memoryless systems, the location of the parameters to compute the value of the third order intercept point are the entries in bold found in the moment vectors at the locations shown in

$$
\underbrace{\left|\begin{array}{c} \text{DC} \\ 2\omega_1 \pm \omega_2 \\ \omega_1 \\ \omega_2 \\ 2\omega_2 \pm \omega_1 \\ 2\omega_1 \\ 2\omega_2 \\ \vdots \end{array}\right|}_{\text{Frequency}}
\begin{array}{c} \rightarrow \\ \rightarrow \\ \rightarrow \\ \rightarrow \\ \rightarrow \\ \rightarrow \\ \rightarrow \\ \vdots \end{array}
\underbrace{\begin{bmatrix} 0 \\ 0 \\ |\mathbf{H_1(j\omega_1)}| \\ |\mathbf{H_1(j\omega_2)}| \\ 0 \\ 0 \\ 0 \\ \vdots \end{bmatrix}}_{\boldsymbol{M}_1}
\underbrace{\begin{bmatrix} 0 \\ \frac{\mathbf{3}}{\mathbf{4}}|\mathbf{H_3(j\omega_1, j\omega_1, -j\omega_2)}| \\ \frac{3}{2}|H_3(j\omega_1, j\omega_2, -j\omega_2)| + \frac{3}{4}|H_3(j\omega_1, j\omega_1, -j\omega_1)| \\ \frac{3}{2}|H_3(j\omega_2, j\omega_1, -j\omega_1)| + \frac{3}{4}|H_3(j\omega_2, j\omega_2, -j\omega_2)| \\ \frac{\mathbf{3}}{\mathbf{4}}|\mathbf{H_3(j\omega_1, -j\omega_2, -j\omega_2)}| \\ 0 \\ 0 \\ \vdots \end{bmatrix}}_{\boldsymbol{M}_3}
\tag{2.33}
$$

For the case of memoryless systems, the expressions for these kernels simplify to the terms k_1 and k_3 in (2.29). This method presents significant CPU speedup over traditional Harmonic Balance approaches and is fully automated. The main disadvantage of this approach is that it is limited to weakly nonlinear amplifier circuits. In addition, the number of equations in the general Harmonic Balance equations remains quite large due to the multi-tone inputs. The fact that the kernels are evaluated numerically also means that the numerical results give no insight to the circuit performance.

2.7 Conclusion

In this chapter, an overview of the significance of distortion analysis as a means for RF design engineers to analyze linearity has been discussed. In addition, a literature survey of some of the traditional and more recent approaches for computing IP3 and other distortion parameters for different types of circuits has been presented. A special emphasis was placed on Volterra Series since it is directly related to the contributions that are presented in the remainder of this thesis.

Chapter 3

Circuit Simulation Using Harmonic Balance

3.1 Introduction

There are several important design specifications for RF circuits, most of which are typically centered around the computation of key performance parameters that include gain, power, intermodulation distortion, noise and frequency bandwidth [1], [5], [6]. Such figures of merit require the computation of the steady-state response of the circuit after all the transients have died out, which is essentially computing the frequency domain response of the circuit. One way to obtain the frequency response is by using small signal analysis. This is achieved by first linearizing the circuit around the DC operating point followed by using small signal analysis to obtain the frequency response. This approximation, however, does not provide sufficient accuracy for the analysis of RF circuits, especially when computing the intermodulation distortion. In such a case, the nonlinear steady-state response is required. For circuits with constant inputs, the steady-state response is simply the DC response, while for circuits with periodic inputs, the output in the steady-state will also be periodic with the same period as the input. The brute force way to obtain the steady-state response is to perform a long transient analysis until all the transients die out. Such an approach is, however, very inefficient due to the very large number of time steps required, and suffers from several limitations such as the inability to determine exactly when the transients completely die out in addition to the resulting Fourier transform noise. Alternatively, the steady-state response of a nonlinear circuit can be obtained directly in an accurate and efficient manner using one of several algorithms that have been proposed in the literature [30]. These include time domain methods such as the Shooting method [5], [11], [58], and frequency domain methods such as the Harmonic Balance approach [5], [12], [13].

The Shooting method determines the steady-state response of a nonlinear circuit excited with a periodic input by solving a Boundary Value Problem (BVP). Standard circuit simulators such as SPICE [59] solve an initial value problem by integrating the differential algebraic equations (DAEs) representing the circuit in the time domain from a known initial condition. In order to directly find the steady-state response (also called the periodic solution), the Shooting method relies on the fact that for a periodic input, the output in the steady-state is also periodic and thus recasts the problem as a BVP which is then solved using Newton Iteration [11], [14], or using other iterative methods such as conjugate gradient [60] or Krylov techniques [61].

There are two problems that arise when trying to apply the Shooting method to analog and microwave circuits. The first problem is that shooting methods find the periodic steady-state response of a circuit by assuming that the periodicity constraint of $x(t) = x(t+T)$ for all t holds as a two-point boundary-value constraint [62]. However, the steady-state response of a mixer circuit, for example, is in general not periodic but rather quasi-periodic which makes the method inappropriate for such circuits. This has led to the development of mixed time frequency envelope techniques [30] that extend the applicability of this method. The second problem is that being a time domain method, it has difficulties with distributed elements such as transmission lines which are best described in the frequency domain. For each iteration, a new initial condition is computed. However, if the circuit contains distributed elements, then their initial conditions cannot be expressed using a finite set of numbers, but rather with functions which then result in significant complexity when applying the method [63].

The contributions presented in this thesis are based on the formulation of the nonlinear system in the frequency domain using the general Harmonic Balance equations. Therefore, this chapter will focus strictly on the HB approach as time-domain methods are not required. This Chapter begins with introducing the method for formulating a general nonlinear system in a circuit simulator based on the Modified Nodal Analysis (MNA) approach [21] and the general Harmonic Balance equations. This will provide the necessary background to the contributions presented in later chapters of this thesis which are all based on this general formulation. This is then followed by an analysis of steady-state nonlinear circuit simulation using the Harmonic Balance method. In particular, the various limitations of this approach are highlighted and some of the recent methods that have been proposed in the literature to address these issues are presented. In this chapter, the formulation for performing sensitivity analysis is also presented. The brute-force way to perform a sensitivity analysis is through perturbation which was first used by Rizzoli *et al.* to approximate gradients for design optimization [64], [65]. However this method is very inefficient and suffers from accuracy limitations. Other more efficient sensitivity analysis algorithms have been developed such as differentiation and the adjoint approach [27], [28] which are presented in this chapter.

3.2 Modified Nodal Analysis Formulation

The formulation of the MNA circuit equations corresponds to the summation of currents according to Kirchoff's Current Law (KCL) at the circuit nodes as well as additional equations for dealing with voltage sources, inductors and other special elements [66]. The MNA formulation provides a simple and general approach that allows for the automated representation of circuits containing both linear and nonlinear elements as a set of equations in matrix form.

Consider a non-linear circuit excited by one or more input tones. The MNA circuit equations can be expressed in the time domain as [21]

$$\boldsymbol{G}\boldsymbol{x}(\boldsymbol{t}) + \boldsymbol{C}\dot{\boldsymbol{x}}(\boldsymbol{t}) + \boldsymbol{f}(\boldsymbol{x}) = \boldsymbol{b}(t), \tag{3.1}$$

where

- $\boldsymbol{x}(t) \in \mathbb{R}^n$ is the vector of n unknown voltages and currents,
- $\boldsymbol{G} \in \mathbb{R}^{n\times n}$ is the matrix that contains the contributions of the linear memoryless circuit elements,
- $\boldsymbol{C} \in \mathbb{R}^{n\times n}$ is the matrix that contains the contributions of the linear memory circuit elements,
- $\boldsymbol{f}(\boldsymbol{x}) \in \mathbb{R}^n$ is a vector of nonlinear algebraic scalar functions of the form

$$\boldsymbol{f}(\boldsymbol{x}(t)) = [f_1(\boldsymbol{x}), f_2(\boldsymbol{x}), \cdots, f_N(\boldsymbol{x})]^T \tag{3.2}$$

- $\boldsymbol{b}(t)$ is a vector that contains the independent input sources.
- n is the total number of variables in the circuit equations.

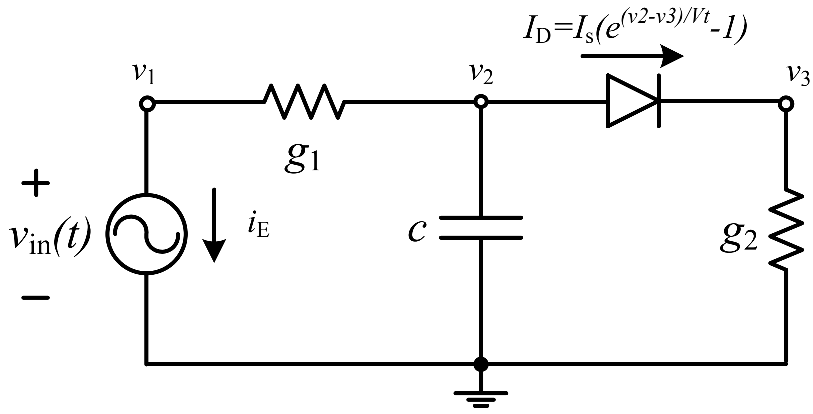

Fig. 3.1 Simple nonlinear circuit

As an example, consider the simple non-linear circuit shown in Fig. 3.1. Applying KCL to all three nodes would give us the following set of equations:

$$g_1\left(v_1 - v_2\right) - i_E = 0 \tag{3.3}$$

$$g_1\left(v_2 - v_1\right) + c\left(\dot{v}_2\right) + I_s\left(e^{\frac{v_2-v_3}{V_t}} - 1\right) = 0 \tag{3.4}$$

$$-I_s\left(e^{\frac{v_2-v_3}{V_t}} - 1\right) + g_2 v_3 = 0 \tag{3.5}$$

$$v_1 = v_{in}(t) \tag{3.6}$$

The MNA equations for this circuit can be obtained by expressing (3.3)-(3.6) in matrix form using the matrices defined in (3.1). Doing so results in the following MNA formulation for this particular circuit:

$$\underbrace{\begin{bmatrix} g_1 & -g_1 & 0 & 1 \\ -g_1 & g_1 & 0 & 0 \\ 0 & 0 & g_2 & 0 \\ 1 & 0 & 0 & 0 \end{bmatrix}}_{\boldsymbol{G}} \underbrace{\begin{bmatrix} v_1 \\ v_2 \\ v_3 \\ i_E \end{bmatrix}}_{\boldsymbol{x}(t)} + \underbrace{\begin{bmatrix} 0 & 0 & 0 & 0 \\ 0 & c & 0 & 0 \\ 0 & 0 & 0 & 0 \\ 0 & 0 & 0 & 0 \end{bmatrix}}_{\boldsymbol{C}} \underbrace{\begin{bmatrix} \dot{v}_1 \\ \dot{v}_2 \\ \dot{v}_3 \\ \dot{i}_E \end{bmatrix}}_{\dot{\boldsymbol{x}}(t)} + \underbrace{\begin{bmatrix} 0 \\ I_s(e^{v_2-v_3/V_t} - 1) \\ -I_s(e^{v_2-v_3/V_t} - 1) \\ 0 \end{bmatrix}}_{\boldsymbol{f}(x)} = \underbrace{\begin{bmatrix} 0 \\ 0 \\ 0 \\ v_{in} \end{bmatrix}}_{\boldsymbol{b}(t)} \tag{3.7}$$

Note that one of the key advantages of the MNA formulation is that these MNA systems of equations can be automatically generated by a computer with the use of component signatures, or ‘stamps’ [9], [67], for each circuit element. Several stamps for common circuit elements can be found in [9]. Another advantage is that the resulting system of equations is typically very sparse.

3.3 Harmonic Balance Formulation

The Harmonic Balance (HB) method is a technique for obtaining the steady-state response due to a periodic input directly in the frequency domain. A number of variations of this approach designed to improve the CPU efficiency have been proposed such as piecewise Harmonic Balance [12], [13], domain decomposition [68], Harmonic Balance using inexact Newton [69], and model order reduction based methods [17]. All these models are based on the one fundamental concept behind Harmonic Balance that is, given a periodic input, the steady-state output will also be periodic and can thus be expressed as a Fourier series. The HB algorithm reformulates the system of nonlinear differential algebraic equations into a system of nonlinear algebraic equations where the unknowns are the Fourier coefficients. In this section, the HB approach is explained in detail since the formulation of the HB equations is used as a basis for the contributions in this thesis.

Consider a circuit containing linear and nonlinear elements described by its MNA equations as shown in (3.1). Given a periodic input $\boldsymbol{b}(t)$, the response is also known to be periodic in the steady-state. The Harmonic Balance approach expresses the periodic solution as a truncated series of sine and cosine functions at the frequencies of the harmonics of the inputs as well as the intermodulation products. For a single tone simulation, the Harmonic Balance solution vector simplifies to a truncated Fourier Series including the first H harmonics since there would be no intermodulation frequencies present. In general, the solution vector can then be represented as

$$\boldsymbol{x}(t) = \boldsymbol{A}_0 + \sum_{k=1}^{H} (\boldsymbol{A}_k \cos(\omega_k t) + \boldsymbol{B}_k \sin(\omega_k t)) \tag{3.8}$$

where

- ω_k are the harmonic and intermodulation frequencies present in the circuit.
- $\boldsymbol{A}_0 \in \mathbb{R}^n$ is a vector containing the DC amplitudes of all n variables.
- $\boldsymbol{A}_k \in \mathbb{R}^n$ is a vector containing the amplitudes of all the cosine terms at frequency ω_k
- $\boldsymbol{B}_k \in \mathbb{R}^n$ is a vector containing the amplitudes of all the sine terms at frequency ω_k.

Substituting (3.8) into the MNA equations in (3.1) and equating the coefficients of the sine and cosine terms results in a set of nonlinear algebraic equations in the form of

$$\bar{\boldsymbol{G}}\boldsymbol{X} + \bar{\boldsymbol{C}}\boldsymbol{X} + \boldsymbol{F}(\boldsymbol{X}) = \boldsymbol{B_{dc}} + \boldsymbol{B_{ac}}, \tag{3.9}$$

where

- $\boldsymbol{X} \in \mathbb{R}^{N_h}$ is a vector of unknown cosine and sine coefficients for each of the variables in $\boldsymbol{x}(t)$.
- $\boldsymbol{B_{dc}} \in \mathbb{R}^{N_h}$ and $\boldsymbol{B_{ac}} \in \mathbb{R}^{N_h}$ represent the contributions of the DC and AC independent sources respectively.
- $\bar{\boldsymbol{G}} \in \mathbb{R}^{N_h \times N_h}$ is a block matrix $\bar{\boldsymbol{G}} = [\boldsymbol{G}_{ij}]$ representing the contribution of the linear memoryless elements of the network to the frequency components. The blocks $\boldsymbol{G}_{ij} \in \mathbb{R}^{N_b \times N_b}$ are diagonal matrices given by

$$\boldsymbol{G}_{ij} = \mathrm{diag}(g_{ij}, \cdots, g_{ij}) \tag{3.10}$$

  with g_{ij} being the corresponding entry in the $\boldsymbol{G}$ matrix in (3.1).

- $\bar{\boldsymbol{C}} \in \mathbb{R}^{N_h \times N_h}$ is a block matrix $\bar{\boldsymbol{C}} = [\boldsymbol{C}_{ij}]$ representing the contribution of the linear memory elements of the network to the frequency components. The blocks $\boldsymbol{C}_{ij} \in \mathbb{R}^{N_b \times N_b}$ are diagonal matrices given by

$$\boldsymbol{C}_{ij} = \begin{bmatrix} 0 & 0 & 0 & \cdots & 0 & 0 \\ 0 & 0 & \omega_1 & \cdots & 0 & 0 \\ 0 & -\omega_1 & 0 & \cdots & 0 & 0 \\ \vdots & \vdots & \vdots & \ddots & \vdots & \vdots \\ 0 & 0 & 0 & \cdots & 0 & \omega_k \\ 0 & 0 & 0 & \cdots & -\omega_k & 0 \end{bmatrix} \tag{3.11}$$

  where $\omega_1 \rightarrow \omega_k$ are the harmonics of the operating frequency and with c_{ij} being the corresponding entry in the $\boldsymbol{C}$ matrix in (3.1).

- $\boldsymbol{F}(\boldsymbol{X})$ contains the sine and cosine coefficients of the nonlinear vector $\boldsymbol{f}(\boldsymbol{x})$ defined in

(3.1) and is expressed as

$$\boldsymbol{F}(\boldsymbol{X}) = \begin{bmatrix} F_1(\boldsymbol{X}) \\ F_2(\boldsymbol{X}) \\ \vdots \\ F_N(\boldsymbol{X}) \end{bmatrix} \tag{3.12}$$

- N_b is the expanded number of variables for each original unknown variable in $\boldsymbol{x}(t)$. For a system excited with a single frequency input tone, this is equal to $2H + 1$ if H harmonics are considered. For multi-tone systems, this number becomes significantly higher.

- N_h is total number of variables for the HB system of equations and is given by $N_h = n \times N_b$. For a single-tone excited system this would be equal to $N_h = n(2H + 1)$. This quantity is usually very large even for modest size systems.

The relation between the vectors $\boldsymbol{X}$, $\boldsymbol{f}(\boldsymbol{x}(t))$ and $\boldsymbol{F}(\boldsymbol{X})$ is established through the use of the Fast Fourier Transform (FFT) and the Inverse Fast Fourier Transform (IFFT) [70]. These transforms are utilized while performing Newton Iterations to obtain the solution of the HB equations and are explained in the following section.

To illustrate how much bigger the HB matrices become relative to the original system, the simple 3-node circuit shown in Fig. 3.1 is taken as an example. If only 2 Harmonics are considered (i.e. H=2), then $\bar{\boldsymbol{G}}$ becomes a 20×20 matrix, as seen in equation (3.13).

$$
\bar{G} = \underbrace{\left[\begin{array}{ccccc|ccccc|ccccc|ccccc}
g_1 & & & & & -g_1 & & & & & 0 & & & & & 1 & & & & \\
& g_1 & & & & & -g_1 & & & & & 0 & & & & & 1 & & & \\
& & g_1 & & & & & -g_1 & & & & & 0 & & & & & 1 & & \\
& & & g_1 & & & & & -g_1 & & & & & 0 & & & & & 1 & \\
& & & & g_1 & & & & & -g_1 & & & & & 0 & & & & & 1 \\
\hline
-g_1 & & & & & g_1 & & & & & 0 & & & & & 0 & & & & \\
& -g_1 & & & & & g_1 & & & & & 0 & & & & & 0 & & & \\
& & -g_1 & & & & & g_1 & & & & & 0 & & & & & 0 & & \\
& & & -g_1 & & & & & g_1 & & & & & 0 & & & & & 0 & \\
& & & & -g_1 & & & & & g_1 & & & & & 0 & & & & & 0 \\
\hline
0 & & & & & 0 & & & & & g_2 & & & & & 0 & & & & \\
& 0 & & & & & 0 & & & & & g_2 & & & & & 0 & & & \\
& & 0 & & & & & 0 & & & & & g_2 & & & & & 0 & & \\
& & & 0 & & & & & 0 & & & & & g_2 & & & & & 0 & \\
& & & & 0 & & & & & 0 & & & & & g_2 & & & & & 0 \\
\hline
1 & & & & & 0 & & & & & 0 & & & & & 0 & & & & \\
& 1 & & & & & 0 & & & & & 0 & & & & & 0 & & & \\
& & 1 & & & & & 0 & & & & & 0 & & & & & 0 & & \\
& & & 1 & & & & & 0 & & & & & 0 & & & & & 0 & \\
& & & & 1 & & & & & 0 & & & & & 0 & & & & & 0
\end{array}\right]}_{\text{dimensions}=20\times 20} \tag{3.13}
$$

Alternatively, if 20 harmonics are needed in the simulation, then the size of the matrix would become 164×164, and for multi-tone inputs, this number would be much larger. This dramatic increase in size presents a significant CPU cost problem. Despite the fact that the matrices $\bar{\boldsymbol{G}}$ and $\bar{\boldsymbol{C}}$ are sparse, this is not the case with the HB Jacobian matrix which is usually very dense, and has to be manipulated at each Newton Iteration, as will be explained more clearly in the following sections.

3.4 Solution of the Harmonic Balance Equations

The solution to the set of nonlinear algebraic HB equations, where the unknowns are the Fourier coefficients of the steady state solution, is obtained by applying iterative numerical techniques such as Newton Iteration [71], [72] or the Conjugate Gradient method [32]. However, each iteration of the solution is very CPU expensive without a guarantee of convergence [67]. A number of relaxation based techniques have been introduced to improve the CPU cost of iterative solutions [12], [73], [74]. In this chapter the Newton Raphson Iteration, which benefits from quadratic convergence near the solution, is presented.

To apply the Newton Raphson iteration, the HB equations in (3.9) are reformulated as

$$\boldsymbol{\Psi}(\boldsymbol{X}) = \bar{\boldsymbol{G}}\boldsymbol{X} + \bar{\boldsymbol{C}}\boldsymbol{X} + \boldsymbol{F}(\boldsymbol{X}) - \boldsymbol{B} = 0 \tag{3.14}$$

where $\boldsymbol{\Psi}(\boldsymbol{X})$ is referred to as the objective function. In this expression, the terms $\boldsymbol{B}_{ac}$ and $\boldsymbol{B}_{dc}$ have been combined into one vector such that $\boldsymbol{B} = \boldsymbol{B}_{ac} + \boldsymbol{B}_{dc}$. The target solution vector $\boldsymbol{X}$ is found iteratively using Newton Raphson Iteration [31] by starting with an initial guess and then updating the solution at each iteration until convergence occurs. At each iteration, the solution vector is updated using

$$\boldsymbol{X}^{(i+1)} = \boldsymbol{X}^{(i)} - \boldsymbol{J}_{HB}(\boldsymbol{X}^{(i)})^{-1}\boldsymbol{\Psi}(\boldsymbol{X}^{(i)}) \tag{3.15}$$

where i is the iteration number, $\boldsymbol{X}^{(i)}$ is the old guess and $\boldsymbol{J}_{HB}(\boldsymbol{X}^{(i)})$ is the Jacobian Matrix defined as

$$\boldsymbol{J}_{HB}(\boldsymbol{X}^{(i)}) = \frac{\partial \boldsymbol{\Psi}(\boldsymbol{X})}{\partial \boldsymbol{X}}\bigg|_{\boldsymbol{X}^{(i)}} = \bar{\boldsymbol{G}} + \bar{\boldsymbol{C}} + \frac{\partial \boldsymbol{F}(\boldsymbol{X})}{\partial \boldsymbol{X}}\bigg|_{\boldsymbol{X}^{(i)}} \tag{3.16}$$

To solve for the harmonic balance solution vector $\boldsymbol{X}$, the following steps are applied

1. Select a good initial guess for the solution vector to be used in (3.15) for the first iteration. A good initial guess is one that is close to the solution vector which will in turn lead to faster convergence and thus result in a lower CPU cost.

2. Compute the objective function using the current value of the vector $\boldsymbol{X}$ which includes the evaluation of the nonlinear vector $\boldsymbol{F}(\boldsymbol{X})$.

3. Evaluate the Jacobian matrix according to (3.16) using the current value of the vector $\boldsymbol{X}$.

4. Determine the new updated solution $\boldsymbol{X}_{new}$ according to (3.15).

5. Check if the error between $\boldsymbol{X}_{new}$ and $\boldsymbol{X}_{old}$ is less than a predetermined error tolerance value ϵ, if not then repeat from step 2 using the latest value of $\boldsymbol{X}$ as $\boldsymbol{X}_{old}$ until the error between $\boldsymbol{X}_{new}$ and $\boldsymbol{X}_{old}$ is smaller than the acceptable tolerance value, in which case the solution would have converged and the iteration loop is stopped.

To evaluate the value of the objective function, $\boldsymbol{\Psi}(\boldsymbol{X})$, all the terms in (3.14) with the exception of the nonlinear vector $\boldsymbol{F}(\boldsymbol{X})$ are found by expanding the original MNA matrices into block matrix forms as highlighted earlier. The evaluation of the nonlinear vector $\boldsymbol{F}(\boldsymbol{X})$ given by (3.12) is a bit more complex as use of the Direct Fourier Transform (DFT) is required. Thus, an overview of the DFT algorithm is provided before proceeding with the method for evaluating $\boldsymbol{F}(\boldsymbol{X})$.

3.4.1 Direct Fourier Transform

The Fourier Transform is used in the calculation of the objective function and the Jacobian matrix at each Newton iteration of the HB algorithm. Consider a periodic signal $x(t)$ with a period $T = \frac{2\pi}{\omega}$ expressed as a Fourier Series given by

$$\boldsymbol{x}(t_n) = a_0 + \sum_{k=1}^{H} (a_k \cos(k\omega t_n) + b_k \sin(k\omega t_n)) \tag{3.17}$$

This signal is then sampled at N_b time points $[t_0, t_1, \cdots, t_{N_b-1}]$ that are equally spaced across the interval $[0, T]$ with

$$t_n = n\frac{T}{N_b}; n = 0, 1, \cdots, N_b - 1 \tag{3.18}$$

The Fourier Series expressions at each sampled time point results in

$$\boldsymbol{x}(t_0) = a_0 + \sum_{k=1}^{H} (a_k \cos(k\omega t_0) + b_k \sin(k\omega t_0)) \tag{3.19}$$

$$\boldsymbol{x}(t_1) = a_0 + \sum_{k=1}^{H} (a_k \cos(k\omega t_1) + b_k \sin(k\omega t_1)) \tag{3.20}$$

$$\vdots \tag{3.21}$$

$$\boldsymbol{x}(t_{N_b-1}) = a_0 + \sum_{k=1}^{H} (a_k \cos(k\omega t_{N_b-1}) + b_k \sin(k\omega t_{N_b-1})) \tag{3.22}$$

which can be re-written in matrix form as

$$\begin{bmatrix} x(t_0) \\ x(t_1) \\ \vdots \\ x(t_{N_b-1}) \end{bmatrix} = \begin{bmatrix} 1 & cos(\omega t_0) & sin(\omega t_0) & \cdots & cos(H\omega t_0) & sin(H\omega t_0) \\ 1 & cos(\omega t_1) & sin(\omega t_1) & \cdots & cos(H\omega t_1) & sin(H\omega t_1) \\ \vdots & \vdots & \vdots & \ddots & \vdots & \vdots \\ 1 & cos(\omega t_{N_b-1}) & sin(\omega t_{N_b-1}) & \cdots & cos(H\omega t_{N_b-1}) & sin(H\omega t_{N_b-1}) \end{bmatrix} \begin{bmatrix} a_0 \\ a_1 \\ b_1 \\ \vdots \\ a_H \\ b_H \end{bmatrix} \quad (3.23)$$

This relation is that of the Inverse Direct Fourier Transform (IDFT), with the times samples obtained by multiplying the vector of Fourier coefficients with the IDFT matrix, which will be referred to as $\mathbf{\Gamma}$. Similarly the DFT can be performed with the use of $\mathbf{\Gamma}^{-1}$. The arguments in matrix $\mathbf{\Gamma}$ of the form $k\omega t_n$ can be re-written as

$$k\omega t_n = k\left(\frac{2\pi}{T}\right) n \left(\frac{T}{N_b}\right) = kn\left(\frac{2\pi}{N_b}\right) \quad (3.24)$$

which shows that the arguments are independent of frequency. In fact, matrix $\mathbf{\Gamma}$ can be expressed independently of frequency as

$$\mathbf{\Gamma} = \begin{bmatrix} 1 & cos(\Theta_{0,1}) & sin(\Theta_{0,1}) & \cdots & cos(\Theta_{0,H}) & sin(\Theta_{0,H}) \\ \vdots & \vdots & \vdots & \ddots & \vdots & \vdots \\ 1 & cos(\Theta_{n,1}) & sin(\Theta_{n,1}) & \cdots & cos(\Theta_{n,H}) & sin(\Theta_{n,H}) \\ \vdots & \vdots & \vdots & \ddots & \vdots & \vdots \\ 1 & cos(\Theta_{N_b-1,1}) & sin(\Theta_{N_b-1,1}) & \cdots & cos(\Theta_{N_b-1,H}) & sin(\Theta_{N_b-1,H}) \end{bmatrix} \quad (3.25)$$

with

$$\Theta_{n,k} = kn\left(\frac{2\pi}{N_b}\right) \quad (3.26)$$

3.4.2 Evaluation of the Nonlinear Vector $\boldsymbol{F}(\boldsymbol{X})$

To simplify matters, only one nonlinear scalar function from the vector $\boldsymbol{f}(\boldsymbol{x})$ shown in (3.2) is considered. The evaluation of the other functions is done in a similar fashion. $\boldsymbol{f}(\boldsymbol{x})$ is also assumed to be a function of one variable x_1.

To evaluate the nonlinear vector $\boldsymbol{F}(\boldsymbol{X}_1)$, as a function of $\boldsymbol{X}_1$, which is the vector containing the sine and cosine coefficients of $x_1(t)$, the following relation is used

$$\boldsymbol{F}(\boldsymbol{X}_1) = \boldsymbol{\Gamma}^{-1}\boldsymbol{F}_s \tag{3.27}$$

where $\boldsymbol{F}_s$ is the vector that contains the time samples of $f(x(t))$ and is given by

$$\boldsymbol{F}_s = [f(x_0), f(x_1), \ldots, f(x_{N_h})]^T \tag{3.28}$$

and $\boldsymbol{\Gamma}$ is the inverse DFT matrix. The vector of time samples $\boldsymbol{X}_s = [x_0, x_1, \ldots, x_{N_h}]^T$ needed to determine $\boldsymbol{F}_s$ is also evaluated by using the DFT, namely

$$\boldsymbol{X}_s = \boldsymbol{\Gamma}\boldsymbol{X}_1 \tag{3.29}$$

3.5 Harmonic Balance Jacobian

The computation, storage and inversion of the HB Jacobian matrix at each iteration of the Newton Raphson algorithm constitutes the bulk of the CPU cost for obtaining the HB solution as this matrix is usually very large and dense, especially when simulating circuits with multi-tone inputs. The number of iterations needed to obtain the final solution vector also varies and can be quite large, therefore requiring that the expensive process of manipulating the Jacobian matrix be repeated several times.

The HB Jacobian matrix is evaluated using the expression shown in (3.16). The matrices $\bar{\boldsymbol{G}}$ and $\bar{\boldsymbol{C}}$ are the same as those defined in (3.9). The remaining term is found using

$$\frac{\partial \boldsymbol{F}(\boldsymbol{X})}{\partial \boldsymbol{X}} = \begin{bmatrix} \frac{\partial F_1}{\partial X_1} & \cdots & \frac{\partial F_1}{\partial X_n} \\ \vdots & \ddots & \vdots \\ \frac{\partial F_n}{\partial X_1} & \cdots & \frac{\partial F_n}{\partial X_n} \end{bmatrix} \tag{3.30}$$

where $\boldsymbol{F}_n$ and $\boldsymbol{X}_n$ contain the Fourier coefficients of $\boldsymbol{f}_n$ and $\boldsymbol{x}_n$ respectively. Each of the terms in (3.30) is a matrix in itself, forming a block matrix structure. Each term is evaluated using

$$\frac{\partial \boldsymbol{F}_n}{\partial \boldsymbol{X}_n} = \boldsymbol{\Gamma}^{-1}\frac{\partial \boldsymbol{F}_s}{\partial \boldsymbol{X}_n} = \boldsymbol{\Gamma}^{-1}\frac{\partial \boldsymbol{F}_s}{\partial \boldsymbol{X}_s}\frac{\partial \boldsymbol{X}_s}{\partial \boldsymbol{X}_n} = \boldsymbol{\Gamma}^{-1}\frac{\partial \boldsymbol{F}_s}{\partial \boldsymbol{X}_s}\boldsymbol{\Gamma} \tag{3.31}$$

where $\boldsymbol{\Gamma}$ is the DFT matrix and

$$\frac{\partial \boldsymbol{F}_s}{\partial \boldsymbol{X}_s} = \operatorname{diag}\left[\frac{df(x(t_0))}{dx(t_0)}, \cdots, \frac{df(x(t_{N_b-1}))}{dx(t_{N_b-1})}\right] \tag{3.32}$$

In practice, the multiplication by $\boldsymbol{\Gamma}$ and $\boldsymbol{\Gamma}^{-1}$ is not done, and is replaced by the FFT and IFFT algorithms. It is also important to note that although $\frac{\partial F_s}{\partial X_s}$ is a diagonal matrix, the multiplication by $\boldsymbol{\Gamma}$ and $\boldsymbol{\Gamma}^{-1}$ makes $\frac{\partial F_n}{\partial X_n}$ a full matrix, which then makes the Jacobian matrix dense. As an example of the density of the HB Jacobian matrix, Fig. 3.2 shows the sparsity pattern for the HB Jacobian matrix of the simple nonlinear circuit of Fig. 3.1. As can be seen, the matrix contains dense blocks at the location of the nonlinear function in the MNA equations.

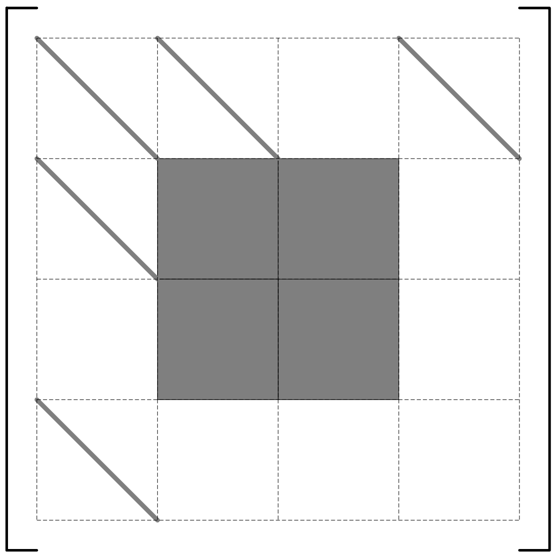

Fig. 3.2 Sparsity pattern of the Harmonic Balance Jacobian matrix. White space shows location of zero entries, dark space shows location of non-zero entries.

3.6 Harmonic Balance Difficulties and Improvements to the Harmonic Balance Method

The Harmonic Balance method for steady state analysis comes with significant problems. One of the method's major problems is that of convergence since there is a dependence on numerical iterations to achieve the solution. Convergence can be improved through the use of a good initial guess which can lead to two major improvements. The first is to reduce the number of iterations by choosing an initial guess that is closer to the solution, and the second is to improve the chances of converging to the correct solution. Although Newton Iteration benefits from quadratic convergence near the solution, convergence is not guaranteed. In recent years, there have been several improvements and refinements to the classical Harmonic Balance algorithm in order to improve CPU efficiency and memory requirements.

3.6.1 Continuation Methods

A number of techniques such as Gauss-Jacobi Newton harmonic relaxation [12] and inexact Newton Iteration [69] have been presented to improve convergence. The main challenge is that there are no rules for selecting a good initial guess. Continuation or homotopy methods [75]–[77] have been introduced to circuit simulation to address the issue of convergence in locally convergent iterative methods such as Newton Iteration. The main idea behind continuation methods is to augment the system of equations $\boldsymbol{\Psi}(\boldsymbol{X})$ shown in (3.14) with a new variable μ as a continuation parameter to form a new set of equations $\boldsymbol{\Omega}(\boldsymbol{X}, \mu)$ with a trivial solution when $\mu = 0$, and the solution of the original system when $\mu = 1$, such that $\boldsymbol{\Omega}(\boldsymbol{X}, 1) = \boldsymbol{\Psi}(\boldsymbol{X})$. The continuation parameter is swept from 0 to 1 using a discrete number of values, and the solution at each value is obtained and tracked, such that the solution at each value is used as the initial guess for the obtaining the next solution.

3.6.2 Use of Preconditioning

Convergence of a system can be made much more robust through the use of preconditioners [78]. A preconditioner matrix is selected and applied to the original system that is a good approximation of the solution of the system of equations and relatively easy to invert. For example, consider the linear system of equations given by

$$\boldsymbol{A}\boldsymbol{X} = \boldsymbol{B} \tag{3.33}$$

Then applying a preconditioner matrix $\boldsymbol{A}_p$ to this system would give

$$\boldsymbol{A}_p^{-1}\boldsymbol{A}\boldsymbol{X} = \boldsymbol{A}_p^{-1}\boldsymbol{B} \tag{3.34}$$

Recent linear iterative techniques such as the quasi-minimal residual (QMR) [79] and the generalized minimal residual (GMRES) [80] approaches were used for solving the HB equations. However, the efficiency of these techniques depends heavily on the ability to select a good preconditioner. If a poor preconditioner matrix is selected, this could end up making the solution more CPU expensive. The challenge therefore shifts to selecting a good preconditioner. There are a number of techniques in the literature for selecting a preconditioner [43], [81]. The first and most simplest is the averaging diagonal preconditioner [79]. In this case, the preconditioner is a block diagonal matrix with each block having the sparsity structure of the circuit transient matrix, meaning the matrix can be easily inverted. This technique works extremely well for circuits with only mild nonlinearities and is probably the best preconditioner for such circuits [43].

As the circuit becomes more strongly nonlinear, the off-diagonal entries in the Jacobian matrix become larger and therefore the diagonal preconditioner becomes less effective. In this case, a one step correction can be applied [43] or super diagonals can be included [81]. In the latter case, when harmonics are large, only the super diagonal entries of one ore more harmonics can be included, while the sub-diagonal entries can be discarded. The resulting matrix becomes an upper triangular one, which can be more easily inverted than a full one. However, discarding entries for a system with a large harmonic index makes the preconditioner less effective, especially in the case of systems with multi-tone inputs, where the artificial frequency mapping may place significant harmonics far away from the diagonal [81].

Alternatively the preconditioner of the finite difference Jacobian can be used for circuits that are highly nonlinear. However, this technique is limited to circuits with only single-tone inputs. The Schur-complement preconditioner can be also used assuming the number of columns containing nonlinear elements is small relative to the size of the overall system, and that permuting these columns to the side of the matrix does not cause significant fill-ins [80], [81].

3.7 Fourier Transform for Almost Periodic Input Signals

When a circuit is excited with an input signal that contains multiple tones, the signal is usually quasi-periodic, i.e. the two input frequencies are non-commensurate, and are therefore not multiples of each other [67]. These frequency values thus create problems when performing Fourier Transforms and also when calculating the Jacobian matrix [67]. A number of algorithms in the literature have been proposed to address this problem [82]–[85]. A simple and efficient way to address this problem is through the use of frequency mapping techniques presented in [5] which are known as the Diamond and Block truncation methods for two input tones. This analysis can also be extended for the case of greater input tones. These truncation methods are used to map actual harmonic frequencies (including intermodulation terms) to arbitrary artificial frequencies. In particular, the fundamentals of the input signal are chosen to be multiples of some arbitrary frequency so that the resulting signals will be periodic and can also be expressed as shown in (3.8). This trick is best illustrated with an example. Consider a nonlinear circuit with an input-output relation as follows

$$f(v(t)) = v(t)^2 \tag{3.35}$$

Assuming that the input signal consists of a voltage signal with two input tones as follows

$$v(t) = A\cos(\alpha t) + B\cos(\beta t) \tag{3.36}$$

Substituting (3.36) into (3.35) and expanding using trigonometric identities the output function becomes

$$f(v(t)) = \frac{A}{2} + \frac{B}{2} + \frac{A}{2}\cos(2\alpha t) + \frac{B}{2}\cos(2\beta t) + \frac{AB}{2}\cos(\alpha t + \beta t) + \frac{AB}{2}\cos(\alpha t - \beta t) \tag{3.37}$$

It is important to note how the coefficients of the cosine terms are independent of the actual values of the frequencies α and β, therefore allowing the possibility of mapping these frequencies to convenient values. The type of truncation algorithm selected depends on the type of circuit and the frequencies used in the analysis.

3.7.1 Block Truncation

The Block Truncation algorithm is applied when a two-tone input is used with frequencies ω_1 and ω_2 that are well spaced out from each other on the frequency spectrum i.e. $\omega_1 >> \omega_2$. Consider the following set of frequencies given by

$$\omega_k = k_1\omega_1 + k_2\omega_2; 0 \leq k_1 \leq H_1, |k_2| \leq H_2, k_1 \neq 0 \text{ if } k_2 < 0 \tag{3.38}$$

where H_1 and H_2 are the number of harmonics of ω_1 and ω_2 respectively. The new artificial set of frequencies that are equally spaced and do not overlap is given by $k\omega = \alpha_1 k_1 \omega_1 + \alpha_2 k_2 \omega_2$, with the scaling factors for the two fundamental frequencies (α_1 and α_2) being

$$\alpha_1 = 1; \alpha_2 = \frac{\omega_1}{\omega_2(2H_2 + 1)} \tag{3.39}$$

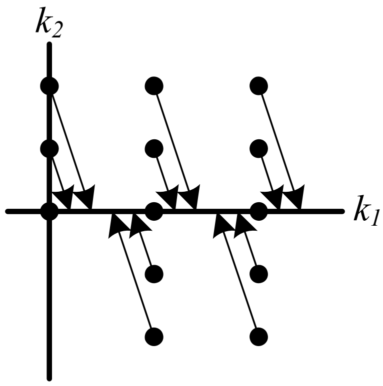

Fig. 3.3 Frequency mapping using block truncations [5]

The mapping of the quasiperiodic frequencies to periodic frequencies using Block truncations is graphically illustrated in Fig. 3.3.

3.7.2 Diamond Truncation

For the more frequent case in RF circuits where the two fundamental frequencies of the input signal are very close to each other on the output spectrum such that $\omega_1 \approx \omega_2$, the Diamond Truncation algorithm is used. Considering the set of frequencies given by

$$\omega_k = k_1\omega_1 + k_2\omega_2; |k_1| + |k_2| \leq H, k_1 + k_2 \geq 0, k_1 \neq k_2 \text{ if } k_2 > 0 \tag{3.40}$$

where H is the highest order of harmonics of ω_1 and ω_2 that is accounted for. The new artificial set of frequencies that are equally spaced and do not overlap is given by $k\omega = \alpha_1 k_1\omega_1 + \alpha_2 k_2\omega_2$, with the scaling factors for the two fundamental frequencies (α_1 and α_2) being

$$\alpha_1 = 1; \alpha_2 = \frac{H\omega_1}{\omega_2(H+1)} \tag{3.41}$$

The mapping of the quasiperiodic frequencies to periodic frequencies using Diamond truncation is shown in Fig. 3.4.

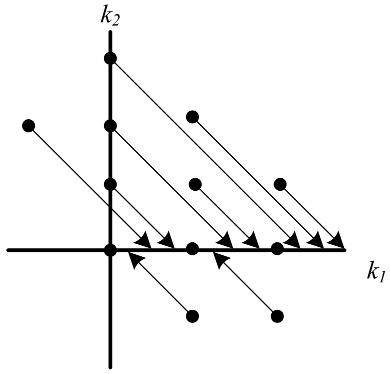

Fig. 3.4 Frequency mapping using diamond truncations [5]

3.7.3 Three Tone Truncation

In some cases, there is a need to simulate the circuit with three input frequency tones. In the case of mixer circuits, for example, there could be two RF input tones present (ω_1 and ω_2) in addition to one local oscillator tone (ω_3). For this reason, a three-tone truncation algorithm is required, which is a natural extension of the two-tone diamond and block truncation algorithms. Consider the set of frequencies given by

$$\omega_k = k_1\omega_1 + k_2\omega_2 + k_3\omega_3; |k_1| + |k_2| \leq H, k_3 \leq H, k_1 + k_2 \geq 0, k_1 \neq k_2 \text{ if } k_2 > 0 \quad (3.42)$$

The new artificial set of frequencies that are equally spaced, do not overlap and account for the mixing property would be given by $k\omega = \alpha_1 k_1\omega_1 + \alpha_2 k_2\omega_2 + \alpha_3 k_3\omega_3$. For the case of $k_3 = 0$, this algorithm would be the same as that of diamond truncation. For the case of $k_3 > 0$ the mapping of these frequencies would correspond to those illustrated in Fig. 3.5 and the corresponding scaling factors are

$$\alpha_1 = \frac{(H+1)\omega_3}{\omega_1(2H(H+1)+1)}; \alpha_2 = \frac{H\omega_3}{\omega_2(2H(H+1)+1)}; \alpha_3 = 1 \quad (3.43)$$

The resulting scaled set of frequencies is equally spaced with no two frequencies overlapping. Other implementations of three-tone truncation algorithms is possible, however this implementation works well with the frequency characteristics of mixer circuits and thus is the one selected.

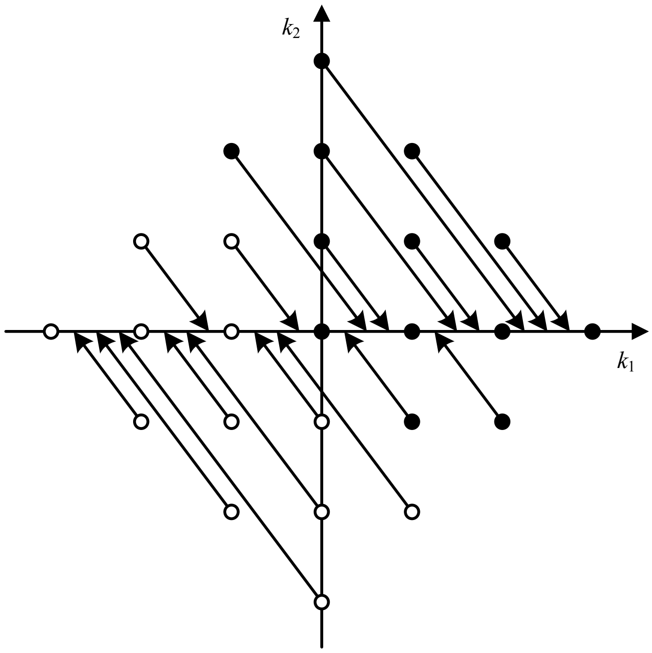

Fig. 3.5 Frequency mapping using three-tone truncation with $k_3 > 0$

3.8 Sensitivity Analysis Techniques

Sensitivity analysis is of particular importance for circuit designers as it is critical for performing several applications, including design centering, yield analysis, optimization and computing group delay. In this section an overview of some of the main methods used for performing sensitivity analysis in the frequency domain is presented. First, the general formulation and definitions of sensitivity are presented, followed by the sensitivity analysis methods.

3.8.1 Sensitivity Analysis Formulation

The absolute sensitivity of a variable V with respect to a general circuit parameter λ is defined as

$$D_{\lambda}^{V} = \frac{\partial V}{\partial \lambda} \tag{3.44}$$

The above definition is not scale free and therefore makes it difficult to compare the sensitivities of various elements. In practical applications, it is more useful to quantify sensitivities as relative or normalized quantities. In such a case, the relative sensitivity of a variable V with respect to a general circuit parameter λ is defined as

$$\boldsymbol{S}_\lambda^V = \frac{\lambda}{V}\frac{\partial V}{\partial \lambda} = \frac{\lambda}{V} D_\lambda^Y \tag{3.45}$$

while the normalized sensitivity is given by

$$S_\lambda^V = \lambda \frac{\partial V}{\partial \lambda} = \lambda D_\lambda^V \tag{3.46}$$

3.8.2 Perturbation

The brute-force approach to performing a sensitivity analysis is through the perturbation of the system. To apply this approach on a linear system described by the set of equations

$$\boldsymbol{AX} = \boldsymbol{B}, \tag{3.47}$$

first, the nominal solution of the system $\boldsymbol{X}$ is determined. Next, the parameter λ of interest is modified by a small delta amount $\Delta\lambda$ such that the new system of equations becomes

$$(\boldsymbol{A} + \boldsymbol{\Delta A})(\boldsymbol{X} + \boldsymbol{\Delta X}) = \boldsymbol{B} \tag{3.48}$$

The solution of the perturbed system $(\boldsymbol{X} + \boldsymbol{\Delta X})$ is then determined. The sensitivity of the system to the parameter λ can now be computed by evaluating

$$D_\lambda^F = \frac{\partial \boldsymbol{X}}{\partial \lambda} = \frac{\Delta \boldsymbol{X}}{\Delta \lambda} \tag{3.49}$$

The Perturbation sensitivity approach has several major problems. The first problem is that it is very computationally inefficient. This approach computes the sensitivity of one variable with respect to one parameter. Therefore an entire simulation must be performed for each different parameter and each variable. In addition, this approach suffers from issues with round-off errors depending on the size of the $\Delta\lambda$ used, which varies on a case by case basis [9].

3.8.3 Differentiation

A more efficient sensitivity analysis technique is that of differentiation. Consider the same set of linear equations given by

$$\boldsymbol{A}\boldsymbol{X} = \boldsymbol{B} \tag{3.50}$$

The partial derivative of (3.50) with respect to λ (assuming $\boldsymbol{B}$ is not a function of a λ) is given by

$$\frac{\partial \boldsymbol{A}}{\partial \lambda}\boldsymbol{X} + \boldsymbol{A}\frac{\partial \boldsymbol{X}}{\partial \lambda} = 0 \tag{3.51}$$

Rearranging this relation results in an expression that can be solved for determining $\frac{\partial X}{\partial \lambda}$

$$\boldsymbol{A}\frac{\partial \boldsymbol{X}}{\partial \lambda} = -\frac{\partial \boldsymbol{A}}{\partial \lambda}\boldsymbol{X} \tag{3.52}$$

It is important to observe that for different cases of λ, the equation above will have a different right-hand-side, but will retain the same left-hand-side. This method therefore finds the sensitivity of all variables with respect to one parameter and is more computationally efficient than brute-force perturbation. This approach is often referred to in the literature as the sensitivity network approach [9]. However, the sensitivity of all components of $\boldsymbol{X}$ is rarely required. A more probable scenario is the need to determine the sensitivity of one scalar variable with respect to many parameters. Therefore, significant CPU saving can be achieved if the sensitivity with respect to all the circuit parameters can be found at once.

3.8.4 Adjoint Sensitivity

The Adjoint sensitivity approach is a very popular and common traditional sensitivity analysis technique [27], [28]. It is attractive because it exhibits very low incremental CPU cost and also computes the sensitivity of one scalar variable with respect to all the parameters in the system. Suppose the output scalar variable of interest is V_{out} and we would like to determine its sensitivity with respect to a parameter λ. In this case, V_{out} can be extracted from the solution vector $\boldsymbol{X}$ with the aid of a selection vector d by using the relation

$$V_{out} = \boldsymbol{d}^T\boldsymbol{X} \tag{3.53}$$

To compute the sensitivity, the first step is to take the derivative of this relation with respect to λ which yields

$$\frac{\partial V_{out}}{\partial \lambda} = \boldsymbol{d}^T \frac{\partial \boldsymbol{X}}{\partial \lambda} \tag{3.54}$$

For a general linear system of equations $\boldsymbol{AX} = \boldsymbol{B}$, an expression for $\frac{\partial X}{\partial \lambda}$ can be obtained by re-arranging the expression in (3.52) as

$$\frac{\partial \boldsymbol{X}}{\partial \lambda} = -\boldsymbol{A}^{-1} \frac{\partial \boldsymbol{A}}{\partial \lambda} \boldsymbol{X} \tag{3.55}$$

Substituting (3.55) into (3.54) results in the general Adjoint sensitivity equation given by

$$\frac{\partial V_{out}}{\partial \lambda} = (\boldsymbol{X_a})^T \frac{\partial \boldsymbol{X}}{\partial \lambda} \tag{3.56}$$

where $\boldsymbol{X_a}$ is the Adjoint solution vector and is defined as

$$(\boldsymbol{X_a})^T = -\boldsymbol{d}^T \boldsymbol{A}^{-1} \tag{3.57}$$

The adjoint sensitivity algorithm thus simplifies to following steps:

1. Solve the original network $\boldsymbol{AX} = \boldsymbol{B}$.
2. Solve the adjoint network $\boldsymbol{A}^T \boldsymbol{X_a} = -\boldsymbol{d}$.
3. For each parameter λ, determine $\frac{\partial A}{\partial \lambda}$ and compute the sensitivity according to (3.56).

It is important to note that the matrix $\frac{\partial A}{\partial \lambda}$ is an extremely sparse matrix which makes the CPU cost of the final step negligible to that of the first two. As can be seen, the same left-hand-side matrix $\boldsymbol{A}$ is used to determine solutions of both the original network and the adjoint network, meaning only one decomposition of the matrix $\boldsymbol{A}$ is needed for determining the sensitivity of all the parameters in the circuit.

Adjoint sensitivity analysis can also be performed on the solution of nonlinear circuits using methods such as Harmonic Balance [7]. In this case, the adjoint solution vector $\boldsymbol{X}_a$ for nonlinear circuits is defined using the general relation given by

$$\boldsymbol{J}^T \boldsymbol{X}_a = \boldsymbol{d} \tag{3.58}$$

where

$$\boldsymbol{J} = \boldsymbol{A} + \frac{\partial \boldsymbol{F}(\boldsymbol{X})}{\partial \boldsymbol{X}} \tag{3.59}$$

is the Harmonic Balance Jacobian matrix. The sensitivity of the output variable V_{out} with respect to any parameter connected to branch b can then be obtained by solving the simplified expression given by

$$\frac{\partial V_{out}}{\partial \lambda} = \begin{cases} -\sum_k \text{Real}\left[X_b(k)X_b^*(k)G_b^*(k)\right] & \text{if } x \in \text{linear subnetwork}, \\ -\sum_k \text{Real}\left[X_b(k)G_b^*(k)\right] & \text{if } x \in \text{nonlinear VCCS or nonlinear resistor}, \\ -\sum_k \text{Imag}\left[X_b(k)G_b^*(k)\right] & \text{if } x \in \text{nonlinear capacitor}. \end{cases} \tag{3.60}$$

In these equations, k is the k^{th} harmonic and $G_b^*(k)$ is the appropriate parameter from Table 3.1.

Table 3.1 Harmonic Balance adjoint sensitivity expressions for different elements [7]

Type of Element	$G_b(k)$
Linear G	1
Linear R	$-\frac{1}{R^2}$
Linear C	$j\omega_k$
Linear L	$-\frac{1}{j\omega_k L^2}$
Nonlinear VCCS or R with $i = i(x(t), \lambda)$	[kth Fourier coefficient of $\frac{\partial i}{\partial x}$]
Nonlinear C with $q = q(x(t), \lambda)$	ω_k[kth Fourier coefficient of $\frac{\partial q}{\partial x}$]

3.9 Conclusion

In this chapter, the formulation of nonlinear circuits using the Modified Nodal Analysis equations and the general Harmonic Balance equations was presented. In addition, the steady-state simulation of nonlinear RF circuits using classic Harmonic Balance and an overview of the fundamentals for performing exact and efficient sensitivity analysis were presented. For intermodulation distortion analysis applications, the Harmonic Balance approach presents several limitations and computational bottlenecks, thereby making it a very CPU expensive approach. In this thesis, a new approach for the intermodulation distortion analysis of RF circuits based on the Harmonic Balance moments is presented to address some of the critical CPU bottlenecks.

Chapter 4

Moments Based Computation of Intermodulation Distortion of Mixer Circuits

4.1 Introduction

Mixer circuits such as the doubly-balanced Gilbert cell [86] are widely encountered in modern telecommunication circuits and their main purpose is to convert a signal from one frequency to another. In a receiver circuit, this conversion is from the Radio Frequency (RF) to the Intermediate Frequency (IF). Mixer circuits are therefore inherently nonlinear devices since nonlinearity is necessary to generate the new frequencies [6]. In addition to the desired nonlinearity, mixer circuits also contain undesired nonlinearities in the RF signal path. The increased complexity of modern circuits in addition to the reduction of supply voltages and the scaling of MOS devices into deep sub-micron regions have aggravated the effect of the nonlinear device characteristics in these circuits [2]. Therefore, it is of particular importance to be able to perform efficient and accurate nonlinear distortion analysis for mixer circuits, especially for wireless applications. Simulation of intermodulation distortion can be performed in either the time domain or the frequency domain. Frequency domain approaches such as Harmonic Balance are more effective for weakly nonlinear circuits. However, there are several challenges to simulating intermodulation distortion in mixer circuits. As mentioned in Chapter 1, the number of frequency tones in the Harmonic Balance equations becomes extremely large due to the mixing of the two RF tones in addition to the LO tone. In addition, for complete switching in mixer circuits, the LO power is typically quite large, thereby causing strong nonlinearities outside the signal path which means a high order of harmonics have to be accounted for in the steady-state simulations.

In section 2.6, a simulation approach based on computing the moments of the harmonic balance equations was described for obtaining the third order intercept point of mildly nonlinear circuits. This method eliminated the complex analytical computations required for Volterra analysis by numerically computing the Volterra kernels of a circuit with an arbitrary topology. The approach is, however, limited to weakly nonlinear circuits such as low noise amplifiers. In this chapter, the method in section 2.6 is extended to address circuits such as mixers which are designed to be highly linear in the signal path, but contain highly nonlinear internal switching due to the large signal local oscillator input (i.e. weakly nonlinear periodically time varying circuits) [19], [20]. Using such an approach, the circuit moments expansion around the local oscillator power is used to compute the value of IP3. This approach does not require any analytical manipulation but is rather applied directly to the general MNA Harmonic Balance formulation of the circuit. It can therefore be fully automated in a general simulator environment and applied to circuits of arbitrary topology and complexity. It is important to note that the value of IP3 is in fact obtained from the general Harmonic Balance equations without the need to compute the steady-state harmonic balance solution, which requires a large computational cost due to the dense nature of the Jacobian and the number of Newton iterations required. Furthermore, the computation of all the moments only requires one LU decomposition of a moments computation matrix that has the same structure as a Jacobian matrix, except it is very sparse unlike the typical Harmonic Balance Jacobian which is usually both large and dense. In addition, the computation is done numerically around a given LO input power (operating point) and with the input frequencies and the local oscillator power known, and thus produces very accurate results.

The general steps of the moments based approach for computing the IP3 of mixer circuits are as follows. First the moments of the harmonic balance equations with respect to the input radio frequency power are computed. Second, the values of the relevant distortion analysis terms are extracted from the appropriate locations in the moment vectors. Finally, the third order intercept point is obtained from the computed terms. This chapter is organized into seven sections. After the introduction, section 4.2 formulates the computation of IP3 in mixer circuits using series expansion. This is followed by section 4.3 which presents the moments computation algorithm for mixer circuits including the sparsity pattern analysis of the moments computation matrix. The main method is then presented in sections 4.4 and 4.5. A numerical example is shown in section

4.6 in order to illustrate the speedup and accuracy of the new method, followed by the conclusion in section 4.7.

4.2 Obtaining the IP3 From Series Expansion

Consider the following power series expansion of the input-output relationship of a memoryless nonlinear system

$$x = k_0 + k_1 v_{in} + k_2 v_{in}^2 + k_3 v_{in}^3 + \cdots = \sum_n k_n v^n \tag{4.1}$$

Now consider an input voltage signal consisting of two sinusoidal RF input tones given by $v = V_{RF}(\cos(\omega_1 t) + \cos(\omega_2 t)) + V_{LO}\cos(\omega_0 t)$, with ω_1 and ω_2 being two input radio frequency signals and ω_0 being the local oscillator frequency. Substituting this term into (4.1) and expanding using trigonometric identities results in the frequency components shown in Table 4.1.

Table 4.1 Summary of distortion components in mixer circuits

Frequency	Component Amplitude
DC	$k_0 + k_2 V_{RF}^2$
$\omega_0 \pm \omega_1$	$k_2 V_{RF} V_{LO} + k_4 V_{RF} V_{LO}(\frac{3}{2}V_{LO}^2 + \frac{9}{2}V_{RF}^2)$
$\omega_0 \pm \omega_2$	$k_2 V_{RF} V_{LO} + k_4 V_{RF} V_{LO}(\frac{3}{2}V_{LO}^2 + \frac{9}{2}V_{RF}^2)$
$\omega_0 \pm 2\omega_1$	$\frac{3}{4}k_3 V_{RF}^2 V_{LO}$
$\omega_0 \pm 2\omega_2$	$\frac{3}{4}k_3 V_{RF}^2 V_{LO}$
$\omega_0 \pm (\omega_1 \pm \omega_2)$	$\frac{3}{2}k_3 V_{RF}^2 V_{LO}$
$\omega_0 \pm (\omega_2 \pm \omega_1)$	$\frac{3}{2}k_3 V_{RF}^2 V_{LO}$
$\omega_0 \pm 3\omega_1$	$\frac{1}{2}k_4 V_{RF}^3 V_{LO}$
$\omega_0 \pm 3\omega_2$	$\frac{1}{2}k_4 V_{RF}^3 V_{LO}$
$\omega_0 \pm (2\omega_1 \pm \omega_2)$	$\frac{3}{2}k_4 V_{RF}^3 V_{LO}$
$\omega_0 \pm (2\omega_2 \pm \omega_1)$	$\frac{3}{2}k_4 V_{RF}^3 V_{LO}$

The 3rd order intercept point is theoretically where the amplitude of the fundamental tone is the same as that of the intermodulation tones at either $\omega_0 \pm (2\omega_1 - \omega_2)$ or $\omega_0 \pm (2\omega_2 - \omega_1)$ [87]. To determine the value of the input third order intercept point voltage, the linear part of the fundamental component is equated to that at one of the third order intermodulation tones. Solving for $V_{RF} = V_{IP3}$ is done by evaluating

$$\left(k_2 V_{LO} + \frac{3}{2} k_4 V_{LO}^3 + \ldots\right) V_{IP3} = \left(\frac{3}{2} k_4 V_{LO} + \ldots\right) V_{IP3}^3 \tag{4.2}$$

which then simplifies to

$$V_{IP3} = \sqrt{\frac{\left(k_2 V_{LO} + \frac{3}{2} k_4 V_{LO}^3 + \ldots\right)}{\left(\frac{3}{2} k_4 V_{LO} + \ldots\right)}} \tag{4.3}$$

The relation given by (4.3) is used to determine the value of the input third order intercept point voltage. For systems that contain memory elements such as inductors and capacitors, the input output relationship given by (4.1) becomes a function of the Volterra kernels, where the n^{th} order kernel is given by $H_n(j\omega_1, \ldots, j\omega_n)$. In this case the value of the input third order intercept point voltage becomes

$$V_{IP3} = \sqrt{\frac{|V_{LO} H_2(j\omega_0, j\omega_1) + \frac{3V_{LO}^3}{2} H_4(j\omega_0, j\omega_0, -j\omega_0, j\omega_1) + \ldots|}{|\frac{3V_{LO}}{2} H_4(j\omega_0, j\omega_1, j\omega_1, -j\omega_2) + \ldots|}} \tag{4.4}$$

To determine the output third order intercept point voltage, this quantity is multiplied by the voltage gain of the system. The fundamental difference between computing IP3 in mixers and in amplifier circuits using circuit expansion is that the mixer relations are a function of the LO power. It is important to observe that in order to determine the value of IP3 accurately using the above formulations, several terms of the summations need to be accounted for since the value of the LO power is typically quite large. In the new moments based approach, the moments expansion is performed around the LO power which makes the computation of IP3 very accurate.

4.3 Definition and Calculation of the Moments For Mixers

The computation cost of the overall algorithm is essentially the CPU cost of computing the Harmonic Balance moments from the general Harmonic Balance equations. Once the moments are determined, the distortion analysis parameters can be obtained. In this section, the definition of the system moments and the method used to compute them efficiently for mixer circuits is presented [67].

4.3.1 System Formulation

The system moments are essentially the derivatives of the unknown Harmonic Balance solution vector $\boldsymbol{X}$ defined in (3.9) with respect to the input radio frequency voltage amplitude [18] evaluated with the amplitude set to zero. To develop the algorithm for calculating the moments efficiently, it is useful to express the Harmonic Balance equations defined in (3.9) in the following format

$$\bar{\boldsymbol{G}}\boldsymbol{X} + \bar{\boldsymbol{C}}\boldsymbol{X} + \boldsymbol{F}(\boldsymbol{X}) - \boldsymbol{B}_{DC} - \beta\boldsymbol{B}_{LO} - \alpha\boldsymbol{B}_{RF} = 0 \tag{4.5}$$

where

- α is the amplitude of the input RF signals.
- β is the power of the local oscillator tone.
- $\boldsymbol{B}_{RF}$ is a vector with the only non-zero entries being entries of value '1' at the input radio frequencies of interest.
- $\boldsymbol{B}_{LO}$ is a vector containing the contributions of the Local Oscillator input.
- $\boldsymbol{B}_{DC}$ contains the values of the DC independent sources.
- $\bar{\boldsymbol{G}}$, $\bar{\boldsymbol{C}}$, $\boldsymbol{F}(\boldsymbol{X})$ and $\boldsymbol{X}$ remain as defined in section 3.3.

The system moments $\boldsymbol{M}_0 \dots \boldsymbol{M}_q$ are defined as the coefficients of the Taylor series expansion of the Harmonic Balance solution vector $\boldsymbol{X}$ as a function of α in

$$\boldsymbol{X} \;=\; \boldsymbol{M}_0 + \boldsymbol{M}_1\alpha + \boldsymbol{M}_2\alpha^2 + \boldsymbol{M}_3\alpha^3 + \cdots = \sum_{k=0}^{q}\boldsymbol{M}_k\alpha^k \tag{4.6}$$

where $\boldsymbol{M}_k$ is the k^{th} moment vector of the system.

4.3.2 Moments Computation Algorithm

The derivation of the moments computation algorithm begins by substituting (4.6) into (4.5), which results in the following expression:

$$\bar{\boldsymbol{G}}\sum_{k=0}^{q}\boldsymbol{M}_k\alpha^k + \bar{\boldsymbol{C}}\sum_{k=0}^{q}\boldsymbol{M}_k\alpha^k + \sum_{k=0}^{q}\boldsymbol{D}_k\alpha^k - \boldsymbol{B}_{DC} - \beta\boldsymbol{B}_{LO} - \alpha\boldsymbol{B}_{\boldsymbol{RF}} = 0 \tag{4.7}$$

The terms $\boldsymbol{D}_k$ are the Taylor expansion coefficients of $\boldsymbol{F}(\boldsymbol{X})$ with respect to α given by

$$\boldsymbol{F}(\boldsymbol{X}) = \sum_{k=0}^{q} \boldsymbol{D}_k \alpha^k \tag{4.8}$$

To solve for the zeroth moment $\boldsymbol{M}_0$, the value of α in (4.7) is set to zero. Setting $\alpha = 0$ gives:

$$\bar{\boldsymbol{G}}\boldsymbol{M}_0 + \bar{\boldsymbol{C}}\boldsymbol{M}_0 + \boldsymbol{F}(\boldsymbol{M}_0) = \boldsymbol{B}_{DC} + \beta \boldsymbol{B}_{LO} \tag{4.9}$$

Note that equation (4.9) is a Harmonic Balance equation with only one input tone at the local oscillator frequency and can thus be solved very efficiently. To solve for the remaining moments ($\boldsymbol{M}_n$; n $\geq$ 1), like powers of α are equated on both sides of (4.7). Equating the first power of α results in

$$\bar{\boldsymbol{G}}\boldsymbol{M}_1 + \bar{\boldsymbol{C}}\boldsymbol{M}_1 + \boldsymbol{D}_1 = \boldsymbol{B}_{\boldsymbol{RF}} \tag{4.10}$$

It is useful to apply the chain rule to rewrite $\boldsymbol{D}_1 = \frac{\partial F}{\partial \alpha}|_{\alpha=0}$ as $\boldsymbol{D}_1 = \frac{\partial F}{\partial X} \cdot \frac{\partial X}{\partial \alpha}|_{\alpha=0} = \boldsymbol{T}_0 \boldsymbol{M}_1$. Substituting this expression into (4.10) then yields

$$\underbrace{(\bar{\boldsymbol{G}} + \bar{\boldsymbol{C}} + \boldsymbol{T}_0)}_{\boldsymbol{\Phi}} \boldsymbol{M}_1 = \boldsymbol{B}_{RF} \tag{4.11}$$

The first moment can now be obtained using one LU Decomposition to solve (4.11). It is important to note that the matrix $\boldsymbol{\Phi} = (\bar{\boldsymbol{G}} + \bar{\boldsymbol{C}} + \boldsymbol{T}_0)$ is simply the sparse Jacobian matrix which is already computed when obtaining the initial solution. To obtain the remaining moments, the n^{th} power of α on both sides of (4.7) is equated to obtain:

$$\bar{\boldsymbol{G}}\boldsymbol{M}_n + \bar{\boldsymbol{C}}\boldsymbol{M}_n + \boldsymbol{D}_n = 0 \qquad n > 1 \tag{4.12}$$

To solve the system given in (4.12) efficiently for each value of n, D_n needs to be expressed using a different notation. Applying the chain rule means that D_n can be expressed as

$$\frac{\partial \boldsymbol{F}}{\partial \alpha} = \frac{\partial \boldsymbol{F}}{\partial \boldsymbol{X}} \cdot \frac{\partial \boldsymbol{X}}{\partial \alpha} = \boldsymbol{T} \frac{\partial \boldsymbol{X}}{\partial \alpha} \tag{4.13}$$

where $\boldsymbol{T}_n$ are the moments of the nonlinear Jacobian matrix and represent the coefficients of the Taylor series expansion of $\frac{\partial F(X)}{\partial X}$ as given by

$$\boldsymbol{T}(\alpha) = \frac{\partial \boldsymbol{F}(\boldsymbol{X})}{\partial \boldsymbol{X}} = \sum_{k=0} \boldsymbol{T}_k \alpha^k \tag{4.14}$$

Substituting (4.6), (4.8) and (4.14) into (4.13) then gives

$$\sum_{i=1}^{q} i\boldsymbol{D}_i \alpha^{i-1} = \sum_{i=0}^{q} \boldsymbol{T}_i \alpha^i \sum_{i=1}^{q} i\boldsymbol{M}_i \alpha^{i-1} \tag{4.15}$$

Taking the n^{th} derivative of (4.15) and setting α to zero means that $\boldsymbol{D}_n$ can be expressed as

$$\boldsymbol{D}_n = \boldsymbol{T}_0 \boldsymbol{M}_n + \frac{1}{n} \sum_{j=1}^{n-1} (n-j) \boldsymbol{T}_j \boldsymbol{M}_{n-j} \tag{4.16}$$

Finally by substituting (4.16) into (4.12) and rearranging yields

$$\underbrace{(\bar{\boldsymbol{G}} + \bar{\boldsymbol{C}} + \boldsymbol{T}_0)}_{\boldsymbol{\Phi}} \boldsymbol{M}_n = -\frac{1}{n} \sum_{j=1}^{n-1} (n-j) \boldsymbol{T}_j \boldsymbol{M}_{n-j} \tag{4.17}$$

This recursive relationship is used to calculate the remaining moment vectors. The right-hand side of equation (4.17) is calculated using the values of the previous moments ($\boldsymbol{M}_{n-j}$) that have already been obtained, in addition to the values of $\boldsymbol{T}_j$ which are the moments of the nonlinear Jacobian evaluated with only the DC and LO tones. All that remains is to show how to compute $\boldsymbol{T}_j$. Since $\boldsymbol{F}(\boldsymbol{X})$ and $\boldsymbol{X}$ are vectors, the term $\boldsymbol{T}(\alpha)$ in (4.14) will be a matrix of the form

$$\boldsymbol{T}(\alpha) = \frac{\partial \boldsymbol{F}(\boldsymbol{X})}{\partial \boldsymbol{X}} = \begin{bmatrix} \frac{\partial F_1}{\partial X_1} & \cdots & \frac{\partial F_1}{\partial X_n} \\ \vdots & \ddots & \vdots \\ \frac{\partial F_n}{\partial X_1} & \cdots & \frac{\partial F_n}{\partial X_n} \end{bmatrix} \tag{4.18}$$

where each $\frac{\partial F_j}{\partial X_i}$ term is a block matrix in itself. To simplify the presentation of calculating these terms, only one of the terms in the $\boldsymbol{T}(\alpha)$ matrix shown in (4.18), $\frac{\partial F_1}{\partial X_1}$, will be considered. Let

$\frac{\partial F_1}{\partial X_1}$ be the matrix $\boldsymbol{T}^{11}$, then its Taylor series expansion with respect to α is given by

$$\frac{\partial F_1}{\partial X_1} = \boldsymbol{T}^{11} = \boldsymbol{P} = \sum_{j=0} \boldsymbol{P}_j \alpha^j \tag{4.19}$$

where the Taylor coefficient $\boldsymbol{P}_j$ is entered in $\boldsymbol{T}_j$ at the location corresponding to $\frac{\partial F_1}{\partial X_1}$. The $\boldsymbol{P}_j$ matrices are computed using

$$\boldsymbol{P}_j = \boldsymbol{\Gamma}^{-1} \begin{bmatrix} \frac{\partial f_1(x_1(t_1))}{\partial x_1}_j & & 0 \\ & \ddots & \\ 0 & & \frac{\partial f_1(x_1(t_s))}{\partial x_1}_j \end{bmatrix} \boldsymbol{\Gamma} \tag{4.20}$$

where t_1 to t_s are time sample points that are equally spaced over the fundamental period (note that frequency mapping and truncation methods [5] are used in order to handle quasi-periodic inputs efficiently using the Fast Fourier Transform as described in section 3.7), and $\boldsymbol{\Gamma}$ is the Inverse Direct Fourier Transform matrix shown in (3.25). Note that the matrix vector multiplication with $\boldsymbol{\Gamma}$ can be done efficiently by taking advantage of the Fast Fourier Transform algorithm. The moments of the derivatives of the nonlinear functions with respect to each variable in the solution vector are also determined using an efficient algorithm that is very similar to that of the regular harmonic balance moments. The analytical expressions are derived once for each device model and then evaluated in the simulator for each moment. A list of common nonlinearities and their derivatives can be found in [18], [67].

It is to be noted that the moments computation matrix is the same for all moments as can be seen from (4.11) and (4.17). Furthermore, this matrix is very sparse since it is evaluated with only the LO tones present. A detailed analysis of the sparsity of this matrix is presented in the next section.

4.3.3 Sparsity of the Moments Computation Matrix

One of the key advantages of the new method is that the moments computation matrix $\boldsymbol{\Phi}$ in equations (4.11) and (4.17) is very sparse compared to the typical Harmonic Balance Jacobian, as will be illustrated in the examples. In this section, the sparsity pattern for the moment computation matrix $\boldsymbol{\Phi}$ of mixer circuits is presented. The definition of the matrix $\boldsymbol{\Phi}$ in equation (4.11) which has the same structure as a Harmonic Balance Jacobian is given by

$$\boldsymbol{\Phi} = \bar{\boldsymbol{G}} + \bar{\boldsymbol{C}} + \left.\frac{\partial \boldsymbol{F}(\boldsymbol{X})}{\partial \boldsymbol{X}}\right|_{\alpha=0} \tag{4.21}$$

Note that the matrices $\bar{\boldsymbol{G}}$ and $\bar{\boldsymbol{C}}$ are sparse, and the Jacobian of the nonlinear vector $\boldsymbol{F}(\boldsymbol{X})$ is given by

$$\frac{\partial \boldsymbol{F}(\boldsymbol{X})}{\partial \boldsymbol{X}} = \begin{bmatrix} \frac{\partial F_1}{\partial X_1} & \cdots & \frac{\partial F_1}{\partial X_n} \\ \vdots & \ddots & \vdots \\ \frac{\partial F_n}{\partial X_1} & \cdots & \frac{\partial F_n}{\partial X_n} \end{bmatrix} \tag{4.22}$$

In a standard Harmonic Balance Jacobian, each $\boldsymbol{\phi}_{ji} = \frac{\partial F_j}{\partial X_i}$ term is, when present, a full block matrix [17] which is computed from the relation

$$\boldsymbol{\phi}_{ji} = \boldsymbol{\Gamma}^{-1} \boldsymbol{\psi}_{ji} \boldsymbol{\Gamma} \tag{4.23}$$

where $\boldsymbol{\Gamma}$ is the Direct Fourier Transform matrix [70] and

$$\boldsymbol{\psi}_{ji} = \begin{bmatrix} \left.\frac{\partial f_j(x_i(t))}{\partial x_i}\right|_{(t=t_0)} & & 0 \\ & \ddots & \\ 0 & & \left.\frac{\partial f_j(x_i(t))}{\partial x_i}\right|_{(t=t_{Nh-1})} \end{bmatrix} \tag{4.24}$$

The dense blocks $\boldsymbol{\psi}_{ji}$ are the main reasons why a Harmonic Balance Jacobian matrix is dense. Note however, that for the case of the moment computation matrix $\boldsymbol{\Phi}$, the term $\frac{\partial F}{\partial X}$ is evaluated with the RF input set to zero. This makes the matrix $\boldsymbol{\phi}_{ji}$ very sparse as will be shown next.

In order to analyze the sparsity of the matrix $\boldsymbol{\phi}_{ji}$, we must first look at the structure of the Direct Fourier Transform (DFT) matrix $\boldsymbol{\Gamma}$ used in (4.23) and given by

$$\begin{aligned} \boldsymbol{\Gamma} &= \begin{bmatrix} 1 & \cos(\omega t_0) & \sin(\omega t_0) & \cdots & \cos(H\omega t_0) & \sin(H\omega t_0) \\ 1 & \cos(\omega t_1) & \sin(\omega t_1) & \cdots & \cos(H\omega t_1) & \sin(H\omega t_1) \\ \vdots & \vdots & \vdots & \ddots & \vdots & \vdots \\ 1 & \cos(\omega t_{N_{h-1}}) & \sin(\omega t_{N_{h-1}}) & \cdots & \cos(H\omega t_{N_{h-1}}) & \sin(H\omega t_{N_{h-1}}) \end{bmatrix} && (4.25) \\ &= [\boldsymbol{\lambda}_0, \boldsymbol{\lambda}_1, \ldots, \boldsymbol{\lambda}_i] && (4.26) \end{aligned}$$

From equation (4.25) we note that each column $\boldsymbol{\lambda}_i$ of $\boldsymbol{\Gamma}$ is a sampled time function of a time domain waveform which contains only one spectral component. Next, consider the diagonal entries of the matrix $\boldsymbol{\psi}_{ji}$. These are essentially a sampled time version of the function $\frac{\partial f_j}{\partial x_i}$. For the case of the moment computation matrix, the spectral components present in this function are only DC and the harmonics of the local oscillator frequency.

If the matrix resulting from the product of $\boldsymbol{\psi}_{ji}\boldsymbol{\Gamma}$ in (4.23) is now considered, and the subscript is dropped for simplicity of notation, the product can be expressed as:

$$\begin{aligned} \boldsymbol{\psi\Gamma} &= [\boldsymbol{\psi\lambda}_0, \boldsymbol{\psi\lambda}_1, \ldots, \boldsymbol{\psi\lambda}_i] && (4.27)\\ &= [\boldsymbol{C}_0, \boldsymbol{C}_1, \ldots, \boldsymbol{C}_i] && (4.28) \end{aligned}$$

Note that in this case, the columns $\boldsymbol{C}_i = \boldsymbol{\psi\lambda}_i$ are sampled time functions whose spectral components are those of the local oscillator frequency mixed with the one frequency corresponding to the column $\boldsymbol{\lambda}_i$. Finally if the matrix $\boldsymbol{\phi}_{ji}$ is re-written as

$$\boldsymbol{\phi} = \boldsymbol{\Gamma}^{-1}[\boldsymbol{\psi\Gamma}] = \boldsymbol{\Gamma}^{-1}[\boldsymbol{C}_0, \boldsymbol{C}_1, \ldots, \boldsymbol{C}_i] \quad (4.29)$$

it can be seen that the columns of $\boldsymbol{\phi}$ contain the spectral components of $\boldsymbol{C}_0$ to $\boldsymbol{C}_i$ respectively, and given the sparsity of those spectral components discussed earlier, the matrix $\boldsymbol{\phi}$ will be very sparse. Finally, it is important to note that since the frequencies being used are non-commensurate, in order to benefit from the use of the DFT operation the frequency mapping technique, and more specifically the three tone truncation algorithm in section 3.7.3, is used. As an example, the sparsity pattern for one frequency tone f_1 and one LO tone f_0 with the harmonic limit set at 2 in the three tone truncation algorithm is that shown in Fig. 4.1 where an X shows the location of a non-zero entry.

4.4 Derivation of the Link Between the Moments and the IP3 Terms

Linear circuits produce output frequencies that are the same as the input frequencies, which implies that no mixing can occur in purely linear circuits. Mixers are therefore inherently nonlinear devices with both desired and undesired nonlinearities. Intermodulation distortion analysis measures the amount of undesired nonlinear distortion at the translated IM3 frequency relative to the desired nonlinearity at the translated fundamental frequency. Therefore, measuring the third order intercept point in mixer circuits is performed in a similar manner to amplifier circuits ex-

	DC	f_1	$2f_1$	f_0-$2f_1$	f_0-f_1	f_0	f_0+f_1	f_0+$2f_1$	$2f_0$-$2f_1$	$2f_0$-f_1	$2f_0$
DC	X					X					X
f_1		X			X		X			X	
$2f_1$			X	X				X	X		
f_0-f_1			X	X				X	X		
f_0-$2f_1$		X			X		X			X	
f_0	X					X					X
f_0+f_1		X			X		X				
f_0+$2f_1$			X	X				X			
$2f_0$-$2f_1$			X	X					X		
$2f_0$-f_1		X			X					X	
$2f_0$	X					X					X

Fig. 4.1 Sparsity pattern of a single block in the moments computation matrix of mixer circuits

cept that now there is a frequency translation [6]. This means that the desired 'linear' signal is essentially the result of a second order response (linear response mixed with the LO), and the 'third order' intermodulation signal is essentially the result of a fourth order response (third order nonlinearity mixed with the LO). In this section, the derivation of the link between the moment vectors and the higher order terms required for computing IP3 is presented. In order to simplify the presentation, the case of memoryless systems is considered first, followed by the derivation for general circuits that contain memory elements.

4.4.1 Memoryless Systems

In the case of memoryless systems, the output x can be written as a power series expansion of the input v as given by

$$x = k_0 + k_1 v + k_2 v^2 + k_3 v^3 + k_4 v^4 + \dots \tag{4.30}$$

In mixers, the input signal is defined as

$$v = \alpha(\cos(\omega_1 t) + \cos(\omega_2 t)) + \beta \cos(\omega_0 t), \tag{4.31}$$

where

- ω_1 and ω_2 are the two input radio frequencies.
- ω_0 is the local oscillator frequency.
- α is the amplitude of the RF signal.
- β is the amplitude of the LO voltage.

Substituting this expression into (4.30), expanding using trigonometric identities and grouping terms with equal powers of α together results in

$$\begin{aligned}
x = \; & \left[k_0 + \left(k_2 + 3k_4\beta^2 + \ldots\right)\alpha^2\right] + \\
& \left[(k_1\beta + \ldots) + (3k_3\beta + \ldots)\,\alpha^2\right]\cos(\omega_0 t) + \\
& \left[\left(\frac{3k_4\beta}{2} + \ldots\right)\alpha^3\right]\cos((\omega_0 + 2\omega_1 - \omega_2)t) + \\
& \left[\left(k_2\beta + \frac{3k_4\beta^3}{2} + \ldots\right)\alpha + \left(\frac{9k_4\beta}{2} + \ldots\right)\alpha^3\right]\cos((\omega_0 + \omega_1)t) + \\
& \left[\left(k_2\beta + \frac{3k_4\beta^3}{2} + \ldots\right)\alpha + \left(\frac{9k_4\beta}{2} + \ldots\right)\alpha^3\right]\cos((\omega_0 + \omega_2)t) + \\
& \left[\left(\frac{3k_4\beta}{2} + \ldots\right)\alpha^3\right]\cos((\omega_0 + 2\omega_2 - \omega_1)t) + \\
& \left[\left(\frac{3k_3\beta}{4} + \ldots\right)\alpha^2\right]\cos((\omega_0 + 2\omega_2)t) + \ldots
\end{aligned} \tag{4.32}$$

Due to the large number of harmonics present at the output, only the components at the frequencies of interest for the calculation of the third order intercept point are shown in (4.32). By comparing (4.32) with the general equation for the moments defined in (4.6), the location of the k_n terms in the system moment vectors $\boldsymbol{M}_k$ is determined. This is more clearly seen when the moments are represented in vector form by

$$\underbrace{\begin{vmatrix} \vdots \\ \omega_0-(2\omega_1\pm\omega_2) \\ \omega_0-\omega_1 \\ \omega_0-\omega_2 \\ \omega_0-(2\omega_2\pm\omega_1) \\ \omega_0-\omega_1+\omega_2 \\ \omega_0 \\ \omega_0+\omega_1+\omega_2 \\ \omega_0+(2\omega_1\pm\omega_2) \\ \omega_0+\omega_1 \\ \omega_0+\omega_2 \\ \omega_0+(2\omega_2\pm\omega_1) \\ \vdots \end{vmatrix}}_{\text{Frequency}} \begin{matrix} \vdots \\ \rightarrow \\ \rightarrow \\ \rightarrow \\ \rightarrow \\ \rightarrow \\ \rightarrow \\ \rightarrow \\ \rightarrow \\ \rightarrow \\ \rightarrow \\ \rightarrow \\ \vdots \end{matrix} \underbrace{\begin{bmatrix} \vdots \\ 0 \\ 0 \\ 0 \\ 0 \\ 0 \\ k_1\beta+k_3\frac{3}{4}\beta^3+\dots \\ 0 \\ 0 \\ 0 \\ 0 \\ 0 \\ \vdots \end{bmatrix}}_{\boldsymbol{M}_0} \underbrace{\begin{bmatrix} \vdots \\ 0 \\ \mathbf{k_2}\beta+\frac{\mathbf{3}}{\mathbf{2}}\mathbf{k_4}\beta^{\mathbf{3}}+\dots \\ \mathbf{k_2}\beta+\frac{\mathbf{3}}{\mathbf{2}}\mathbf{k_4}\beta^{\mathbf{3}}+\dots \\ 0 \\ 0 \\ 0 \\ 0 \\ 0 \\ \mathbf{k_2}\beta+\frac{\mathbf{3}}{\mathbf{2}}\mathbf{k_4}\beta^{\mathbf{3}}+\dots \\ \mathbf{k_2}\beta+\frac{\mathbf{3}}{\mathbf{2}}\mathbf{k_4}\beta^{\mathbf{3}}+\dots \\ 0 \\ \vdots \end{bmatrix}}_{\boldsymbol{M}_1} \underbrace{\begin{bmatrix} \vdots \\ 0 \\ 0 \\ 0 \\ 0 \\ \frac{3}{2}k_3\beta+\dots \\ 3k_3\beta+\dots \\ \frac{3}{2}k_3\beta+\dots \\ 0 \\ 0 \\ 0 \\ 0 \\ \vdots \end{bmatrix}}_{\boldsymbol{M}_2} \underbrace{\begin{bmatrix} \vdots \\ \frac{\mathbf{3}}{\mathbf{2}}\mathbf{k_4}\beta+\dots \\ \frac{9}{2}k_4\beta+\dots \\ \frac{9}{2}k_4\beta+\dots \\ \frac{\mathbf{3}}{\mathbf{2}}\mathbf{k_4}\beta+\dots \\ 0 \\ 0 \\ 0 \\ \frac{\mathbf{3}}{\mathbf{2}}\mathbf{k_4}\beta+\dots \\ \frac{9}{2}k_4\beta+\dots \\ \frac{9}{2}k_4\beta+\dots \\ \frac{\mathbf{3}}{\mathbf{2}}\mathbf{k_4}\beta+\dots \\ \vdots \end{bmatrix}}_{\boldsymbol{M}_3} \tag{4.33}$$

The relation in (4.33) shows the contents of the first four moments vectors with the entries of interest for the computation of IP3 shown in bold at the fundamental frequencies of $(\omega_0 \pm \omega_{1,2})$ and third order intermodulation frequencies of $(\omega_0 \pm (2\omega_{1,2} - \omega_{2,1}))$.

4.4.2 Systems With Memory Elements

For the more general case of mixer circuits that contain memory elements, the circuit expansion is represented by a Volterra series with terms up to the 4th order Volterra operator included in the derivation. The Volterra series representation of a nonlinear system with memory is given by

$$x(t) = H_1[v(t)] + H_2[v(t)] + H_3[v(t)] + H_4[v(t)] + \dots \tag{4.34}$$

To determine the location of the Volterra terms in the moment vectors, the three frequency input function defined in (4.31) is re-written as

$$\begin{aligned} v(t) &= \beta\cos(\omega_0 t) + \alpha(\cos(\omega_1 t) + \cos(\omega_2 t)) && (4.35)\\ &= \frac{\beta}{2}e^{j\omega_0 t} + \frac{\beta}{2}e^{-j\omega_0 t} + \frac{\alpha}{2}e^{j\omega_1 t} + \frac{\alpha}{2}e^{-j\omega_1 t} + \frac{\alpha}{2}e^{j\omega_2 t} + \frac{\alpha}{2}e^{-j\omega_2 t} && (4.36)\\ &= v_a(t) + v_b(t) + v_c(t) + v_d(t) + v_e(t) + v_f(t) && (4.37) \end{aligned}$$

This function is then substituted into (4.34). The resulting expressions for each Volterra operator are too large to be stated in their entirety. Instead, only the expressions at the frequencies of interest are shown. At the fundamental intermediate frequency of an up-conversion mixer at $\omega_0 + \omega_1$, a combination of second order, fourth order and higher even order terms appear. The second order response at this specific frequency can be represented as

$$H_2\left[v(t)\right]_{\omega_0+\omega_1} = H_2\{v_a, v_c\} + H_2\{v_c, v_a\} + H_2\{v_b, v_d\} + H_2\{v_d, v_b\} \qquad (4.38)$$

The first term of (4.38) is now written in terms of the second-order Volterra kernel using the two-dimensional convolution [3]

$$\begin{aligned} H_2\{v_a, v_c\} &= \int_{-\infty}^{\infty}\int_{-\infty}^{\infty} h_2(\tau_1,\tau_2)v_a(t-\tau_1)v_b(t-\tau_2)d\tau_1 d\tau_2 && (4.39)\\ &= \frac{\alpha\beta}{4}\int_{-\infty}^{\infty}\int_{-\infty}^{\infty} h_2(\tau_1,\tau_2)e^{j\omega_0(t-\tau_1)}e^{j\omega_1(t-\tau_2)}d\tau_1 d\tau_2 && (4.40)\\ &= \frac{\alpha\beta}{4}e^{j\omega_0 t}e^{j\omega_1 t}\int_{-\infty}^{\infty}\int_{-\infty}^{\infty} h_2(\tau_1,\tau_2)e^{-j\omega_0\tau_1}e^{-j\omega_1\tau_2}d\tau_1 d\tau_2 && (4.41)\\ &= \frac{\alpha\beta}{4}H_2(j\omega_0, j\omega_1)e^{j(\omega_0+\omega_1)t} && (4.42) \end{aligned}$$

In a similar fashion, the remaining terms in (4.38) can also be expressed in terms of the second order kernel and are given by

$$\begin{aligned} H_2\{v_c, v_a\} &= \frac{\alpha\beta}{4}H_2(j\omega_1, j\omega_0)e^{j(\omega_1+\omega_0)t} && (4.43)\\ H_2\{v_b, v_d\} &= \frac{\alpha\beta}{4}H_2(-j\omega_0, -j\omega_1)e^{-j(\omega_0+\omega_1)t} && (4.44)\\ H_2\{v_d, v_b\} &= \frac{\alpha\beta}{4}H_2(-j\omega_1, -j\omega_0)e^{-j(\omega_1+\omega_0)t} && (4.45) \end{aligned}$$

If the second order kernel h_2 is assumed to be symmetric, then its Fourier transform can also be considered symmetric such that

$$H_2(j\omega_0, j\omega_1) = H_2(j\omega_1, j\omega_0) \tag{4.46}$$

Then (4.38) can be re-written as

$$H_2\left[v(t)\right]_{\omega_0+\omega_1} = 2\left(\frac{\alpha\beta}{4}\right) H_2(j\omega_0, j\omega_1)e^{j(\omega_0+\omega_1)t} + 2\left(\frac{\alpha\beta}{4}\right) H_2(-j\omega_0, -j\omega_1)e^{-j(\omega_0+\omega_1)t} \tag{4.47}$$

The two terms in (4.47) are complex conjugates of each other since it easy to prove that

$$H_2(-j\omega_0, -j\omega_1) = H_2^*(j\omega_0, j\omega_1) \tag{4.48}$$

This reduces the final result to the expression

$$H_2\left[v(t)\right]_{\omega_0+\omega_1} = \alpha\beta\mathrm{Re}\left(H_2(j\omega_0, j\omega_1)e^{j(\omega_0+\omega_1)t}\right) \tag{4.49}$$

The fourth order responses at $\omega_0 + \omega_1$ are due to the combination of frequencies at $\omega_0 + \omega_0 - \omega_0 + \omega_1$, at $\omega_0 + \omega_1 + \omega_1 - \omega_1$ and at $\omega_0 + \omega_1 + \omega_2 - \omega_2$. Assuming the fourth order kernels to be symmetric, a similar analysis to that of the second order response is considered which gives

$$\begin{aligned} H_4\left[v(t)\right]_{\omega_0+\omega_1} &= 12H_4\{v_a, v_a, v_b, v_c\} + 12H_4\{v_b, v_b, v_a, v_d\} \\ &\quad +12H_4\{v_a, v_c, v_c, v_d\} + 12H_4\{v_b, v_d, v_d, v_c\} \\ &\quad +24H_4\{v_a, v_c, v_e, v_f\} + 24H_4\{v_b, v_d, v_f, v_e\} \end{aligned} \tag{4.50}$$

When the above expressions are expressed using Volterra kernels they would simply to

$$\begin{aligned} H_4\left[v(t)\right]_{\omega_0+\omega_1} &= \frac{3}{2}\alpha\beta^3\mathrm{Re}\left(H_4(j\omega_0, j\omega_0, -j\omega_0, j\omega_1)e^{j(\omega_0+\omega_1)t}\right) \\ &\quad +\frac{3}{2}\alpha^3\beta\mathrm{Re}\left(H_4(j\omega_0, j\omega_1, j\omega_1, -j\omega_1)e^{j(\omega_0+\omega_1)t}\right) \\ &\quad +\frac{6}{2}\alpha^3\beta\mathrm{Re}\left(H_4(j\omega_0, j\omega_1, j\omega_2, -j\omega_2)e^{j(\omega_0+\omega_1)t}\right) \end{aligned} \tag{4.51}$$

At the translated 3rd order intermodulation frequency of $\omega_0 + 2\omega_1 - \omega_2$, only fourth order terms appear in addition to higher even-order terms. At this frequency, the fourth order Volterra operator can be written as

$$H_4\left[v(t)\right]_{\omega_0+2\omega_1-\omega_2} = 12H_4\{v_a, v_c, v_c, v_f\} + 12H_4\{v_b, v_d, v_d, v_e\} \tag{4.52}$$

By following a similar analysis to that performed at the fundamental frequency, the above expression would simplify to

$$H_4\left[v(t)\right]_{\omega_0+2\omega_1-\omega_2} = \frac{3}{2}\alpha\beta^3 \mathrm{Re}\left(H_4(j\omega_0, j\omega_1, j\omega_1, -j\omega_2)e^{j(\omega_0+2\omega_1-2\omega_2)t}\right) \tag{4.53}$$

By substituting (4.49), (4.51), (4.53) and expressions at other frequencies into (4.34) then rearranging by grouping like powers of α, the following input output relation is obtained

$$\begin{aligned} X \;=\; & \mathrm{Re}\left[\left(\beta H_2(j\omega_0, j\omega_1) + \frac{3\beta^3}{2}H_4(j\omega_0, j\omega_0, -j\omega_0, j\omega_1) + \ldots\right)\alpha e^{j(\omega_0+\omega_1)t}\right] + \\ & \mathrm{Re}\left[\left(\beta H_2(j\omega_0, j\omega_2) + \frac{3\beta^3}{2}H_4(j\omega_0, j\omega_0, -j\omega_0, j\omega_2) + \ldots\right)\alpha e^{j(\omega_0+\omega_2)t}\right] + \\ & \mathrm{Re}\left[\left(\frac{3\beta}{2}H_4(j\omega_0, j\omega_1, j\omega_1, j\omega_2) + \ldots\right)\alpha^3 e^{j(\omega_0+2\omega_1+\omega_2)t}\right] + \\ & \mathrm{Re}\left[\left(\frac{3\beta}{2}H_4(j\omega_0, j\omega_1, j\omega_1, -j\omega_2) + \ldots\right)\alpha^3 e^{j(\omega_0+2\omega_1-\omega_2)t}\right] + \\ & \mathrm{Re}\left[\left(\frac{3\beta}{2}H_4(j\omega_0, j\omega_1, j\omega_2, j\omega_2) + \ldots\right)\alpha^3 e^{j(\omega_0+2\omega_2+\omega_1)t}\right] + \\ & \mathrm{Re}\left[\left(\frac{3\beta}{2}H_4(j\omega_0, -j\omega_1, j\omega_2, j\omega_2) + \ldots\right)\alpha^3 e^{j(\omega_0+2\omega_2-\omega_1)t}\right] + \ldots \end{aligned} \tag{4.54}$$

This expression can be re-written in terms of magnitudes and angles which results in the following notation that is easier to follow

$$
\begin{aligned}
X \;=\; & \left[\left|\beta H_2(j\omega_0, j\omega_1) + \frac{3\beta^3}{2} H_4(j\omega_0, j\omega_0, -j\omega_0, j\omega_1) + \ldots\right| \alpha\right] \cos((\omega_0+\omega_1)t + \Theta_1) + \\
& \left[\left|\beta H_2(j\omega_0, j\omega_2) + \frac{3\beta^3}{2} H_4(j\omega_0, j\omega_0, -j\omega_0, j\omega_2) + \ldots\right| \alpha\right] \cos((\omega_0+\omega_2)t + \Theta_2) + \\
& \left[\left|\frac{3\beta}{2} H_4(j\omega_0, j\omega_1, j\omega_1, j\omega_2) + \ldots\right| \alpha^3\right] \cos((\omega_0+2\omega_1+\omega_2)t + \Theta_3) + \\
& \left[\left|\frac{3\beta}{2} H_4(j\omega_0, j\omega_1, j\omega_1, -j\omega_2) + \ldots\right| \alpha^3\right] \cos((\omega_0+2\omega_1-\omega_2)t + \Theta_4) + \\
& \left[\left|\frac{3\beta}{2} H_4(j\omega_0, j\omega_1, j\omega_2, j\omega_2) + \ldots\right| \alpha^3\right] \cos((\omega_0+2\omega_2+\omega_1)t + \Theta_5) + \\
& \left[\left|\frac{3\beta}{2} H_4(j\omega_0, -j\omega_1, j\omega_2, j\omega_2) + \ldots\right| \alpha^3\right] \cos((\omega_0+2\omega_2-\omega_1)t + \Theta_6) + \ldots
\end{aligned} \tag{4.55}
$$

It can be seen that the Volterra series expression in (4.55) is similar to the expression shown in (4.32), which means that the contents of the first moment vector, $\boldsymbol{M}_1$, at the fundamental frequencies are

$$
\underbrace{\left|\begin{array}{c}
\vdots \\
\omega_0-(2\omega_1\pm\omega_2) \\
\omega_0-\omega_1 \\
\omega_0-\omega_2 \\
\omega_0-(2\omega_2\pm\omega_1) \\
\omega_0-\omega_1+\omega_2 \\
\omega_0 \\
\omega_0+\omega_1+\omega_2 \\
\omega_0+(2\omega_1\pm\omega_2) \\
\omega_0+\omega_1 \\
\omega_0+\omega_2 \\
\omega_0+(2\omega_2\pm\omega_1) \\
\vdots
\end{array}\right|}_{\text{Frequency}}
\begin{array}{c}
\vdots \\ \rightarrow \\ \rightarrow \\ \rightarrow \\ \rightarrow \\ \rightarrow \\ \rightarrow \\ \rightarrow \\ \rightarrow \\ \rightarrow \\ \rightarrow \\ \rightarrow \\ \vdots
\end{array}
\underbrace{\begin{bmatrix}
\vdots \\
0 \\
\left|H_2(j\omega_0,-j\omega_1)\beta + \frac{3}{2}H_4(j\omega_0,j\omega_0,-j\omega_0,-j\omega_1)\beta^3 + \ldots\right| \\
\left|H_2(j\omega_0,-j\omega_2)\beta + \frac{3}{2}H_4(j\omega_0,j\omega_0,-j\omega_0,-j\omega_2)\beta^3 + \ldots\right| \\
0 \\
0 \\
0 \\
0 \\
0 \\
\left|H_2(j\omega_0,j\omega_1)\beta + \frac{3}{2}H_4(j\omega_0,j\omega_0,-j\omega_0,j\omega_1)\beta^3 + \ldots\right| \\
\left|H_2(j\omega_0,j\omega_2)\beta + \frac{3}{2}H_4(j\omega_0,j\omega_0,-j\omega_0,j\omega_2)\beta^3 + \ldots\right| \\
0 \\
\vdots
\end{bmatrix}}_{\boldsymbol{M}_1}
\tag{4.56}
$$

Similarly, the third moment vector $\boldsymbol{M}_3$ contains the distortion terms given by

$$
\underbrace{\left|\begin{array}{c}
\vdots \\
\omega_0-(2\omega_1-\omega_2) \\
\omega_0-\omega_1 \\
\omega_0-\omega_2 \\
\omega_0-(2\omega_2-\omega_1) \\
\omega_0-\omega_1+\omega_2 \\
\omega_0 \\
\omega_0+\omega_1+\omega_2 \\
\omega_0+(2\omega_1-\omega_2) \\
\omega_0+\omega_1 \\
\omega_0+\omega_2 \\
\omega_0+(2\omega_2-\omega_1) \\
\vdots
\end{array}\right|}_{\text{Frequency}}
\begin{array}{c}
\vdots \\ \rightarrow \\ \rightarrow \\ \rightarrow \\ \rightarrow \\ \rightarrow \\ \rightarrow \\ \rightarrow \\ \rightarrow \\ \rightarrow \\ \rightarrow \\ \rightarrow \\ \vdots
\end{array}
\underbrace{\begin{bmatrix}
\vdots \\
|\frac{3}{2}H_4(j\omega_0,-j\omega_1,-j\omega_1,j\omega_2)\beta+\ldots| \\
|\frac{3}{2}H_4(j\omega_0,-j\omega_1,-j\omega_1,j\omega_1)\beta+\frac{6}{2}H_4(j\omega_0,j\omega_1,j\omega_2,-j\omega_2)\beta+\ldots| \\
|\frac{3}{2}H_4(j\omega_0,-j\omega_2,-j\omega_2,j\omega_2)\beta+\frac{6}{2}H_4(j\omega_0,j\omega_2,j\omega_1,-j\omega_1)\beta+\ldots| \\
|\frac{3}{2}H_4(j\omega_0,-j\omega_2,-j\omega_2,j\omega_1)\beta+\ldots| \\
0 \\
0 \\
0 \\
|\frac{3}{2}H_4(j\omega_0,j\omega_1,j\omega_1,-j\omega_2)\beta+\ldots| \\
|\frac{3}{2}H_4(j\omega_0,j\omega_1,j\omega_1,-j\omega_1)\beta+\frac{6}{2}H_4(j\omega_0,j\omega_1,j\omega_2,-j\omega_2)\beta+\ldots| \\
|\frac{3}{2}H_4(j\omega_0,j\omega_2,j\omega_2,-j\omega_2)\beta+\frac{6}{2}H_4(j\omega_0,j\omega_2,j\omega_1,-j\omega_1)\beta+\ldots| \\
|\frac{3}{2}H_4(j\omega_0,j\omega_2,j\omega_2,-j\omega_1)\beta+\ldots| \\
\vdots
\end{bmatrix}}_{\boldsymbol{M}_3}
\tag{4.57}
$$

It is important to observe that the terms required for computing IP3 are a function of the LO power β, which means that for large LO powers, several higher order terms need to be accounted for. The moment vectors contain the values equivalent to that of the whole summations, rather than individual distortion components, which means that this method does not suffer from ill-conditioning and problems with convergence.

4.5 Computation of the IP3 From the Moments

To determine the value of the input third order intercept point, we use the relation developed in section 4.4. The relations shown in (4.3) and (4.4) can be generalized to obtain the following expression for the input third order intercept point referred to below as $IIP3$

$$
IIP3 = \sqrt{\frac{m_{1,1}}{m_{3,3}}} \tag{4.58}
$$

The terms $m_{1,1}$ and $m_{3,3}$ represent the entries in the first moment vector at the fundamental frequency, and in the third moment vector at the third order intermodulation frequency, respectively.

For memoryless systems, these terms correspond to

$$m_{1,1} = k_2\beta + \frac{3\beta^3}{2}k_4 + \dots \tag{4.59}$$

$$m_{3,3} = \frac{3\beta}{2}k_4 + \dots \tag{4.60}$$

In the presence of memory elements such as capacitors and inductors, the entries in the moment vectors are equivalent to the Volterra kernels, which means that

$$m_{1,1} = |\beta H_2(j\omega_0, j\omega_1) + \frac{3\beta^3}{2}H_4(j\omega_0, j\omega_0, -j\omega_0, j\omega_1) + \dots| \tag{4.61}$$

$$m_{3,3} = |\frac{3\beta}{2}H_4(j\omega_0, j\omega_1, j\omega_1, -j\omega_2) + \dots| \tag{4.62}$$

A summary of the main steps of the algorithm can be found in Fig. 4.2. It is important to notice that the relation for the moments based computation of IP3 in amplifier circuits presented in section 2.6 is actually very similar to the one given by (4.58), with only the contents of the moments at the terms $m_{1,1}$ and $m_{3,3}$ differing between the two approaches. This means that the relation in (4.58) can now be used as part of a unified framework for the moments based computation of IP3 in general RF circuits. It is to be noted that the computation cost required for obtaining IP3 using this algorithm is only one LU decomposition of the moments computation matrix. Furthermore, this matrix is evaluated at either the DC operating point, or with only the local oscillator tones present for the case of mixers, and it is therefore very sparse unlike a typical HB Jacobian matrix. In contrast, the brute force steady-state simulation based approach requires the solution of a system of equations with a dense Jacobian at each Newton iteration, which requires a high computational cost.

It is important to note that, although the derivation of the algorithm for computing the moments is quite involved, its application is systematic and can be easily automated. Furthermore, all the moments are solutions of systems of linear equations where the left hand side matrix remains the same, and is very sparse as compared to the Harmonic Balance Jacobian which is both large and dense. In addition, although the proofs showing the link between the circuit moments and Volterra kernels require complex analytical manipulations, these proofs are only done once for the general harmonic balance equations, and the results presented here are thus general. From an implementation perspective, the portion of the new algorithm linking the moments to the distortion terms is trivial and requires a negligible computational expense as the value of the third order intercept point is computed from the system moments which only require one LU decomposition of a sparse matrix.

1. Set up the system equations in the frequency domain according to the formulation shown in (4.5)
2. Calculate the zeroth moment $\boldsymbol{M_0}$ as defined in (4.6) by finding the solution of the sparse system shown in (4.9)
3. Calculate the first moment $\boldsymbol{M_1}$ by solving the formulation in (4.11)
4. Calculate the remaining moments ($\boldsymbol{M_n}; n > 1$) by solving (4.17) recursively
5. Obtain the Volterra kernels from the entries in the moment vectors at the fundamental frequencies ($\omega_0 + \omega_{1,2}$) and at the third order intermodulation frequencies ($\omega_0 + 2\omega_{1,2} - \omega_{2,1}$) as outlined in (4.33)
6. Determine the distortion by calculating the third order intercept point according to (4.58)

Fig. 4.2 Summary of the moments based algorithm for computing IP3 in mixer circuits.

4.6 Numerical Example

In this section, the numerical results of IP3 simulations performed on an example circuit are shown in detail in order to illustrate the accuracy and speedup of the new method. The value of the third order intercept point obtained using the moments technique, which does not require a harmonic balance solution, is compared with that obtained using the brute force method which is based on multi-tone harmonic balance simulation. The new method was also tested on several other circuit topologies, the numerical results of which are shown at the end of Chapter 6.

4.6.1 Detailed Analysis of a Doubly Balanced Mixer Circuit

The example considered for a detailed analysis is an active doubly-balanced (Gilbert Cell) up-conversion Mixer with a local oscillator frequency of 1 GHz and input and output matching networks as shown in Fig. 4.3 [20]. The power of the local oscillator signal is -16 dBm. To measure the linearity of the circuit, the brute force method was first used by applying two -53.5

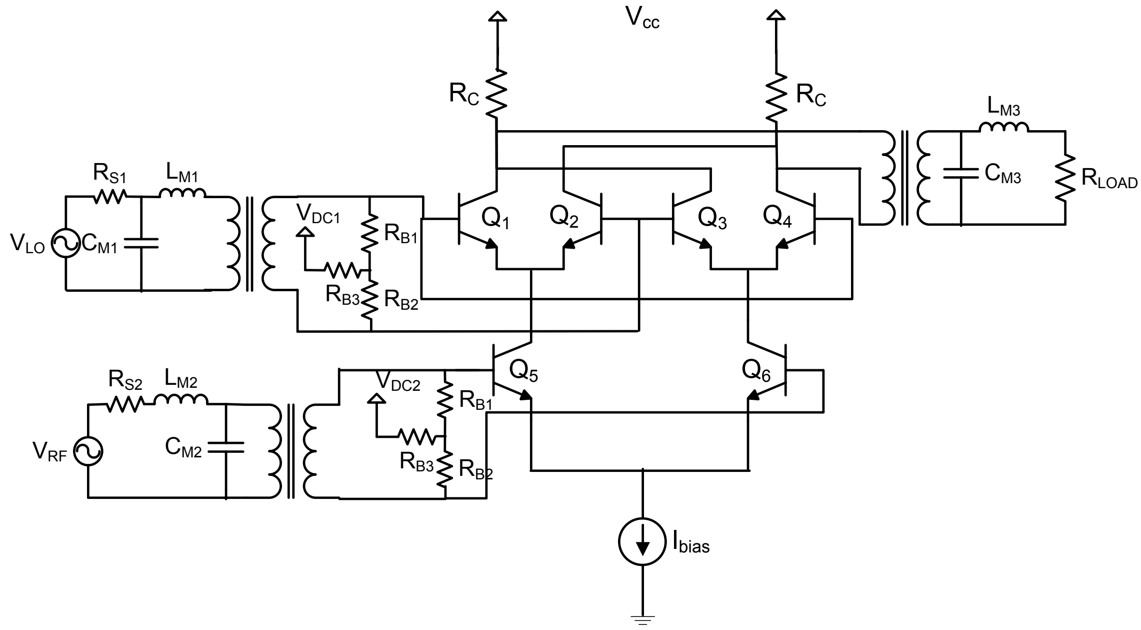

Fig. 4.3 Active doubly-balanced mixer (Gilbert Cell) circuit diagram.

dBm tones at the RF signal input, with f_1 = 99.5 MHz and f_2 = 100.5 MHz, and performing a standard harmonic balance analysis. The results are shown in Fig. 4.4 and Fig. 4.5. The calculated input third order intercept point in this case was 13.774 dBm and the output third order intercept point was found to be 33.36 dBm.

The distortion was then analyzed using the new approach by computing the moments of the system and extracting the Volterra summations at the appropriate frequencies. The resulting values of the input third order intercept point and the output third order intercept point were found to be 13.772 dBm and 33.36 dBm respectively. As can be seen, the results are consistent with the brute force approach based on Harmonic Balance simulations. The error between the two methods was less than 0.01%.

In order to illustrate the differences between the HB Jacobian matrix used in the brute-force approach and the moments computation matrix used in the new method, Figs. 4.6 and 4.7 show the sparsity pattern of the HB Jacobian while Figs. 4.8 and 4.9 show the sparsity pattern of the moments matrix. Since the two matrices are significant in size, to clearly illustrate the difference in block sparsity between the two, the diagram in Fig. 4.7 shows the sparsity pattern of a section of the Harmonic Balance Jacobian, while Fig. 4.9 shows the sparsity pattern of the same corresponding section of the moments matrix, which contains only the DC and the local oscillator

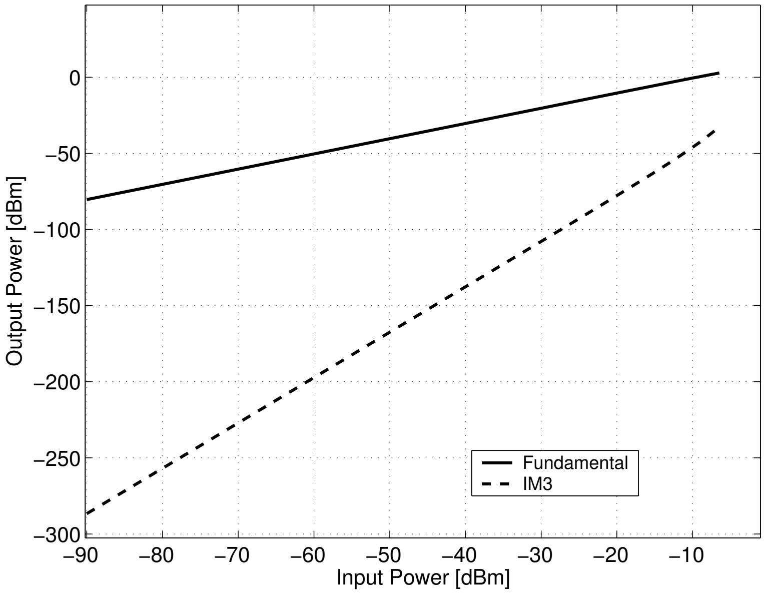

Fig. 4.4 Output power of the fundamental and the 3^{rd} order intermodulation (IM3) frequency tones using Harmonic Balance.

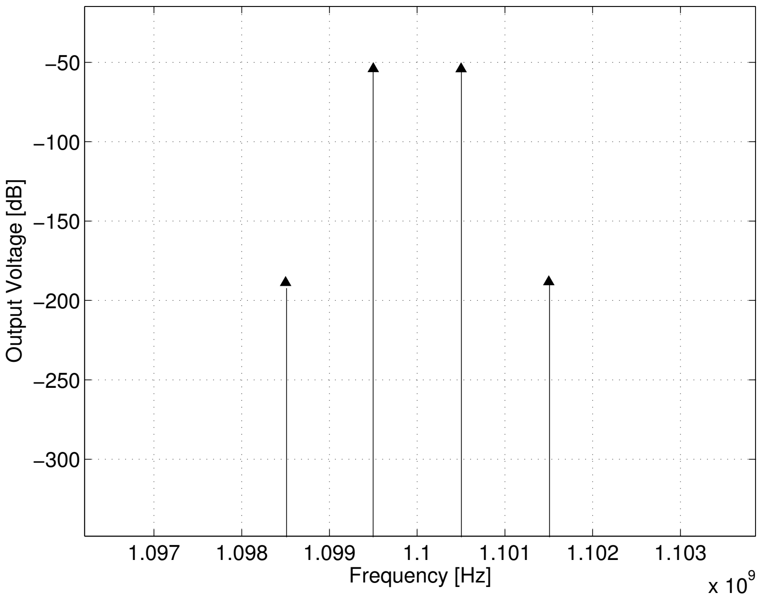

Fig. 4.5 Output voltage spectrum at the IF frequencies using Harmonic Balance.

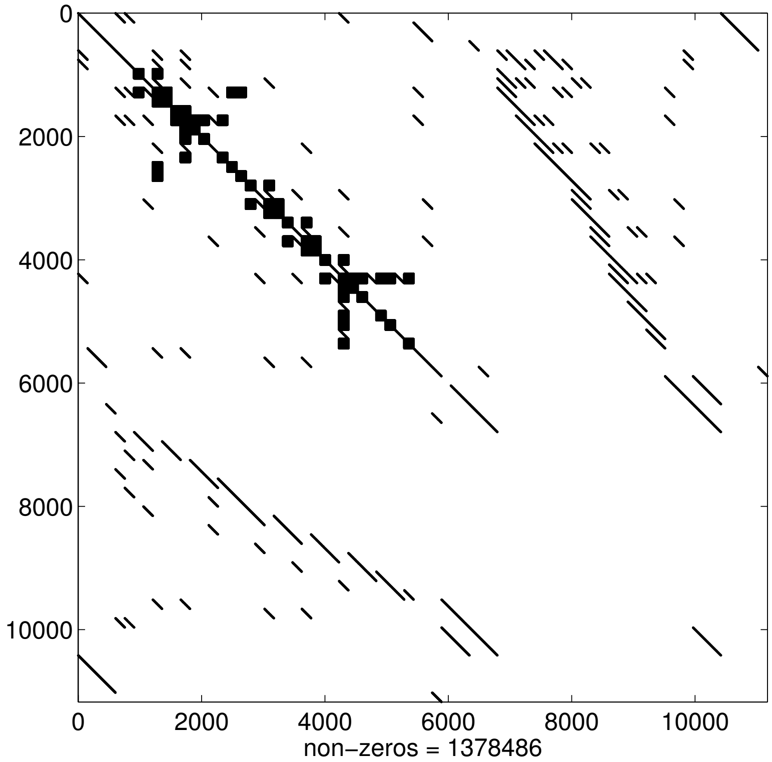

Fig. 4.6 Sparsity pattern of the Harmonic Balance Jacobian for the doubly balanced mixer circuit example.

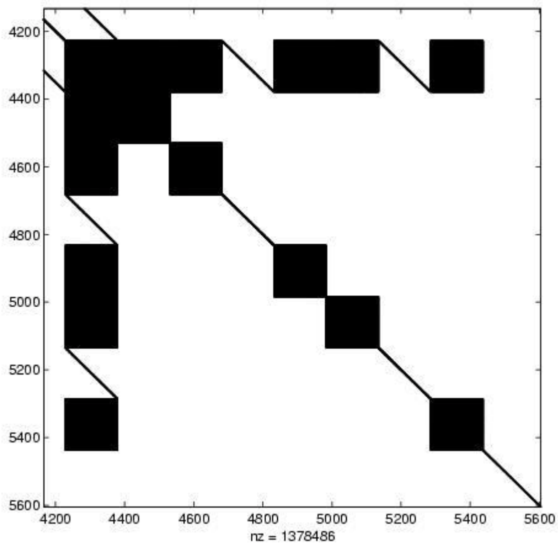

Fig. 4.7 Sparsity pattern of the dense blocks of the Harmonic Balance Jacobian matrix.

tones.

4.6.2 Computation Cost Comparison

The data in Table 4.2 shows a comparison of the computation times and the speed-up between the new moments method and the Harmonic Balance solution obtained using a prototype MATLAB simulator. The hardware platform on which the simulations were run was a single-core Intel Xeon machine with a clock speed of 3.6 GHz and 4GB of RAM. The speed-up over a Harmonic Balance simulation was 39.7 times for this particular circuit when run with 4 harmonics. This speed-up is due to three main reasons. First of all, the moments used in the new method are found by solving a linear equation without the need for any Newton Iteration. The second reason is that the left-hand-side matrix in (4.17) for finding the moments is the same for all moments, while the Harmonic Balance Jacobian is different at each Newton Iteration. Finally the Harmonic Balance Jacobian is significantly more dense than the Jacobian used for solving for the moments as was shown earlier. For this specific example, the $11,174 \times 11,174$ Harmonic Balance Jacobian contains $1,378,486$ non-zero elements as shown in Fig. 4.6, while the $11,174 \times 11,174$ matrix for finding the moments contains only $122,927$ non-zeros as shown in Fig. 4.8. It is also important to note that the greater the number of non-linear elements present in the system, the more significant the speed-up will become between the two approaches.

4.7 Conclusion

In this chapter, a new simulation method for measuring distortion at the output of a non-linear system based on the calculation of the system moments was presented. It was demonstrated that by using this new simulation based approach to compute the third order intercept point from the moments, it becomes significantly more efficient to analyze distortion in RF mixer circuits while remaining as accurate as Harmonic Balance methods. It was also shown that the method is general and applicable in a fully automated simulator on arbitrary circuit topologies and nonlinearities.

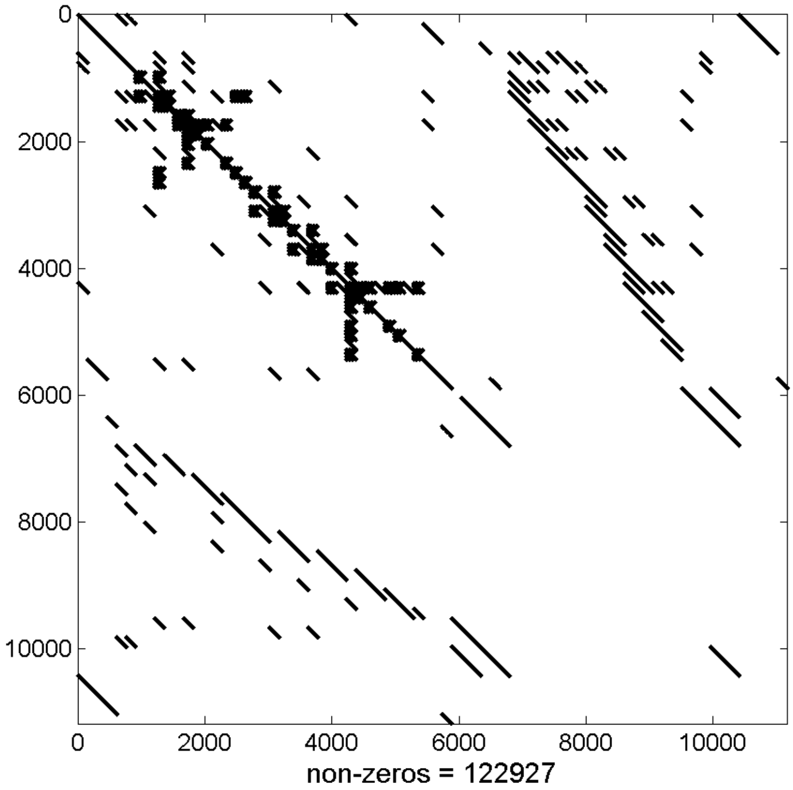

Fig. 4.8 Sparsity pattern of the moments computation matrix $\mathbf{\Phi}$ for the doubly balanced mixer circuit example.

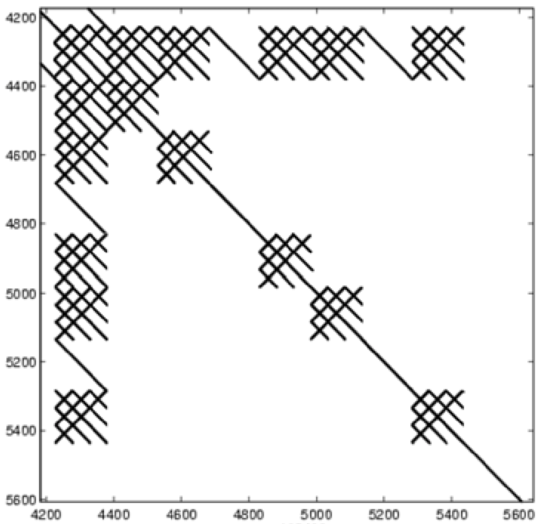

Fig. 4.9 Sparsity pattern of the sparse blocks of the moments computation matrix.

Table 4.2 Comparison of computation times between the moments method and the Harmonic Balance solution

	Harmonic Balance CPU time (s)	Moments Method CPU time (s)	**Speed-up**
IP3 Computation	154.02	3.88	**39.7 times**

Chapter 5

Computation of IP3 Using Single-Tone Moments Analysis

5.1 Introduction

Nonlinear distortion is due to the inherent nonlinearity of circuit components and results in the harmonics of input tones, as well as the intermodulation products, being present at the output. Radio Frequency circuits are typically designed to be as linear as possible in order to reduce such nonlinear distortion. Of particular interest are third order intermodulation products because they mix back into the frequency band of operation and result in many undesirable effects such as gain compression and adjacent channel interference [1]. The third order nonlinearity is a result of, and is proportional to, the third order term in the Taylor expansion of memoryless nonlinear systems, or to the third order Volterra kernel of a nonlinear circuit with memory [3], [16]. The most common metric for characterizing and quantifying the third order nonlinearity is the third order intercept point (IP3) [6]. In a typical measurement setup, IP3 is obtained by applying a 2-tone input and measuring the third order intermodulation product which mixes back into the passband of the circuit. Note that applying a single-tone input and attempting to characterize the third order nonlinearity by measuring the third harmonic is not a suitable approach because the third harmonic typically falls outside the passband of the circuit. This has lead to the popularity of IP3 which is based on the measurement of the third order intermodulation product of a two-tone input as a figure of merit for linearity. It is important to note, however, that the fundamental quantity behind IP3 is the third order Taylor coefficient or the third order Volterra kernel.

In a simulation environment, the most common approach for determining IP3 is to mimic a laboratory measurement by applying a two-tone input and performing a steady-state analysis using techniques such as the Harmonic Balance method. This approach is general and gives very accurate results; however, the Harmonic Balance simulation requires a large CPU cost because of the large number of variables present due to the two-tone input. This is particularly the case for mixer circuits which would, in this instance, have a three-tone input (the local oscillator tone in addition to the two RF tones). The moments based approach described in Chapter 4 does not attempt to mimic laboratory measurements by applying a two-tone input and performing a steady-state analysis. Instead, the linearity figures of merit are computed directly from the Harmonic Balance equations. In this case, the nonlinear Harmonic Balance equations do not need to be solved, and the computational complexity of obtaining IP3 is reduced to the solution of a set of sparse linear equations. Furthermore, given that this approach is based on the Harmonic Balance formulation, it is general and can be applied to any arbitrary circuit topology. Note that while the moments method reduces the computational complexity of computing IP3 to that of solving a set of very sparse linear equations, the size of this system of equations remains large. This is because the number of variables is the same as the Harmonic Balance equations which can be very large for amplifier circuits requiring two input tones, and even much higher for mixer circuits requiring three-tone inputs.

In this chapter, a new method for the fast estimation of the value of IP3 in nonlinear RF circuits using only a single-tone RF input is presented [22], [23]. The computation complexity of this method is that of solving a set of linear equations and does not require the solution of the nonlinear Harmonic Balance equations. Furthermore the number of variables is the same as a Harmonic Balance formulation with a *single-tone* input, thus making the size of the system of linear equations that need to be solved considerably smaller than the two-tone moments method while still being very sparse. This results in a considerable reduction in computation cost as will be seen in the examples. For mixer circuits, the necessary distortion terms are computed numerically from the moments of the Harmonic Balance equations with only two input tones (one RF in addition to one local oscillator) instead of the traditional three tones. The new method presents a fast alternative to the two-tone method presented in Chapter 4 for an estimation of the value of IP3.

The general idea behind the new method is to numerically compute the value of IP3 directly from the single-tone Harmonic Balance circuit equations by separating the linear response from the third order distortion terms at the fundamental frequency. To that end, a mathematical relation is derived linking the value of IP3 to the single tone moments of the circuit. The computation of IP3 is thus reduced to the computation of these single-tone moments. It is important to note that, while the solution of the Harmonic Balance equations is not needed, the starting point of the new method is the Harmonic Balance formulation. This makes it general to any circuit topology and easily automated unlike traditional Volterra series based methods.

This chapter is organized into six sections. Following the introduction, section 5.2 provides a brief background on the effects of third order nonlinear distortion on system performance and highlights some of the main differences between different approaches for obtaining the third order intercept point. The main algorithm is presented in section 5.3 including the single-tone definition of IP3 and the derivation of the link between the single-tone moments and the value of IP3. The computational cost analysis of the method is presented in section 5.4. Two numerical examples are shown in section 5.5 (one amplifier circuit and one mixer circuit) in order to illustrate the speedup and accuracy of the new method, followed by the conclusion in section 5.6.

5.2 Third Order Nonlinearity and IP3 Definitions

In this section the importance of third order nonlinear distortion and its effects on system performance is presented. In addition, the various approaches for computing the third order intercept point are outlined in order to provide the necessary background for the remainder of this chapter.

Consider a memoryless nonlinear system. Its input-output relationship can be expressed as follows

$$X = k_0 + k_1 v_{in} + k_2 v_{in}^2 + k_3 v_{in}^3 + \cdots = \sum_n k_n v^n, \tag{5.1}$$

where X is the output, v_{in} is the input and k_n are the Taylor Series coefficients. For Radio Frequency circuits, the third order nonlinearity caused by k_3 is of particular interest to designers. For the more general case of nonlinear circuits with memory, the Taylor series in (5.1) is replaced by a Volterra series. In this case, the third order nonlinearity is represented by the Laplace transform of the third order Volterra kernel $H_3(j\omega_1, j\omega_2, j\omega_3)$ [3]. This third order nonlinearity causes signal distortion which can be an important bottleneck in the system performance. This distortion manifests itself in two important ways.

The first is through gain compression where the third order nonlinearity k_3 is mixed back down to the fundamental frequency causing gain compression at high input powers as illustrated in Fig. 5.1. As can be seen from the summary of frequency components shown in Table 2.1, the

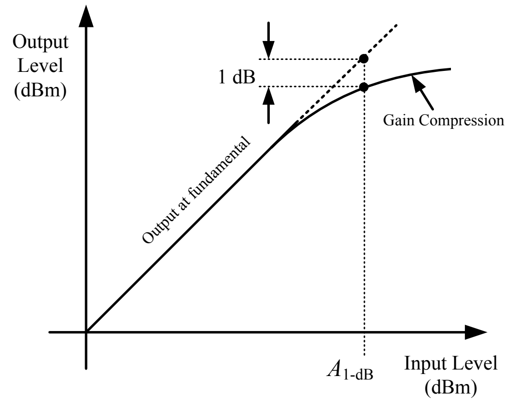

Fig. 5.1 Definition of the 1-dB compression point

amplitude of the fundamental frequency tone (ω_1) consists of the terms $(k_1V_1 + \frac{3}{4}k_3V_1^3)$, where k_1V_1 represents the linear response, and $\frac{3}{4}k_3V_1^3$ represents the nonlinear distortion. As can be seen from Fig. 5.1, the effects of gain compression are more significant at high input powers. The main figure of merit used to quantify this effect is the "1-dB compression point" (A_{1dB}), defined as the input signal power at which the gain drops by 1-dB as illustrated in Fig. 5.1.

The second significant effect of the third order nonlinearity is the intermodulation distortion observed in the presence of multi-tone inputs. When a nonlinear circuit is excited with two input tones (ω_1 and ω_2), the third order intermodulation product (IM3) results in tones at ($2\omega_1 - \omega_2$) and ($2\omega_2 - \omega_1$) which falls within the system bandwidth and interferes with adjacent channels. As shown in Fig. 5.2, if a weak signal accompanied by two strong interferers experiences third order nonlinear distortion, then one of the IM3 products will appear within the passband of the desired channel, thereby corrupting the desired component. The primary figure of merit used to quantify this type of distortion is the third order intercept point (IP3).

In order to compute the value of IP3, first there is a need to determine the numerical values of both the k_1 and k_3 terms from the series expansion in (5.1). Since the two components k_1V_1 and $\frac{3}{4}k_3V_1^3$ are impossible to separate from a single measurement of the output amplitude, the only way to determine the value of k_3 in a single-tone simulation is by measuring the amplitude of the output spectral component at $3\omega_1$ which corresponds to $\frac{1}{4}k_3V_1^3$. While this measurement might be accurate for memoryless circuits, unfortunately such a measurement often results in inaccurate results for quantifying the third order nonlinearity in circuits with memory elements since measuring $3\omega_1$ typically involves measuring an output outside the pass-band of the system

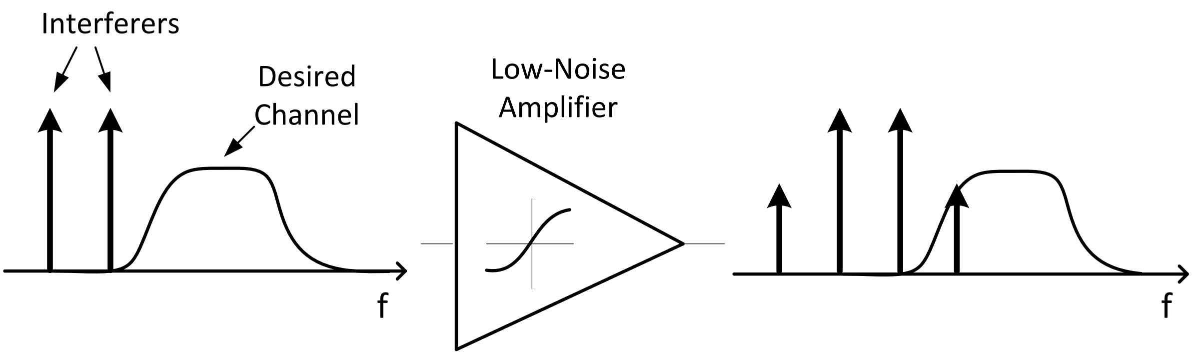

Fig. 5.2 Adjacent channel interference due to intermodulation distortion [1]

as illustrated in Fig. 5.3 (a). To tackle this problem, a two-tone input must be applied to the circuit in order to measure the third order nonlinearity at either $2\omega_1 - \omega_2$ or $2\omega_2 - \omega_1$ which would fall in the pass-band as illustrated in Fig. 5.3 (b). Unfortunately, such a solution would add significant and unnecessary computation cost overhead.

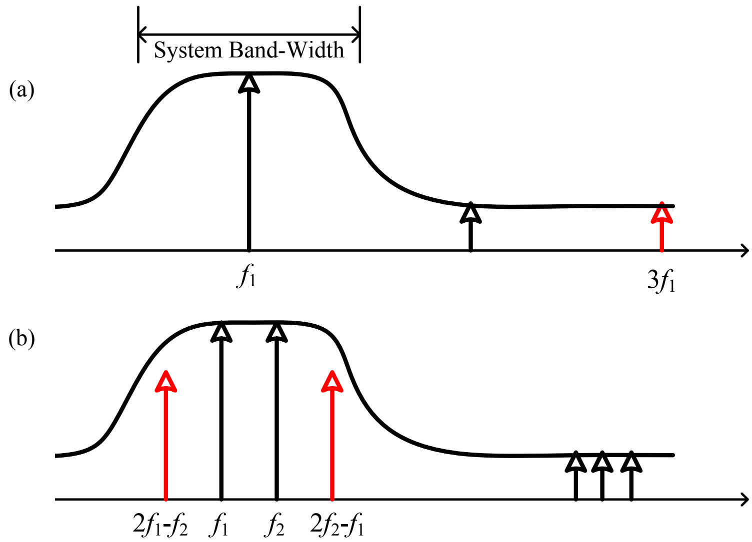

Fig. 5.3 Single-tone vs. two-tone third order nonlinearity and system bandwidth

5.2.1 Evaluation of IP3 From the 1-dB Compression Point

Both the 1-dB compression point and IP3 are due to the same third order nonlinearity and are thus related. It is possible to show that the value of IP3 is related to the 1-dB compression point using the following relation [1],

$$\frac{A_{1-dB}}{IIP3} = \frac{\sqrt{0.145}}{\sqrt{4/3}} \approx -9.6\text{dB} \tag{5.2}$$

It is important to point out however that the 1-dB compression point is determined by the circuit behavior (measured or simulated) at a relatively high input power and can thus be affected by nonlinearities that are only activated in the device models at those power levels. The expression in (5.2) is thus considered only a first order approximation for IP3.

It is possible to determine the value of IP3 using only simulations or measurements with a single-tone input. This is accomplished by evaluating the 1-dB compression point and then using the relation in (5.2). However such an approach has several limitations. First of all, it is not a computationally efficient method. In order to obtain the 1-dB compression point, the input power of the RF circuit must be swept, and the output power must be computed at each sweep point using steady-state analysis techniques. In order to obtain accurate results, the number of sweep points needs to be large. Another limitation of using such an approach is that the gain compression that occurs at high input powers does not always follow such a typical curve as that illustrated in Fig. 5.1. Finally, designers usually rely on the 1-dB compression point as a useful tool for measuring distortion at high input powers, whereas the third order intercept point is utilized to measure distortion at lower input powers.

5.2.2 Computing IP3 Using Volterra Series

In addition to the simulation based approaches discussed above, it is possible to obtain IP3 by performing an analysis of the circuit using Volterra series as described in section 2.5 [16]. Consider a nonlinear circuit containing energy storage elements such as capacitors and inductors. The input-output relation of this circuit can be expressed as [16]

$$x(t) = H_0 + H_1[v_{in}(t)] + H_2[v_{in}(t)] + H_3[v_{in}(t)] + \ldots, \tag{5.3}$$

where H_n is the n^{th} Volterra operator. For memoryless circuits the expression in (5.3) simplifies to a Taylor expansion as expressed in (5.1). It is possible to derive analytical expressions relating IP3 to the expressions in (5.1) and (5.3). These relations are outlined next for both amplifier and mixer circuits.

Amplifier Circuits

Consider an amplifier with an input given by $v_{in} = V_1 \cos(\omega_1 t) + V_2 \cos(\omega_2 t)$. By substituting this input signal into (5.1) and expanding the terms, the following analytical expression for the third order intercept point voltage can be derived [6].

$$V_{IP3} = \sqrt{\frac{4}{3}\frac{k_1}{k_3}} \tag{5.4}$$

For the general case of circuits with memory, the value of IP3 can also be expressed analytically in terms of the Volterra kernels. Note that in this case, it is possible to define IP3 in terms of both the upper side tones and the lower side tones as follows [3],

$$IIP3_L = \sqrt{\frac{4}{3}\frac{|H_1(j\omega_1)|}{|H_3(j\omega_1, j\omega_1, -j\omega_2)|}} \tag{5.5}$$

$$IIP3_U = \sqrt{\frac{4}{3}\frac{|H_1(j\omega_2)|}{|H_3(j\omega_2, j\omega_2, -j\omega_1)|}} \tag{5.6}$$

Both definitions of IP3 in (5.5) and (5.6) are equally valid, and since the two fundamental tones are typically chosen in the passband and close enough to each other on the frequency spectrum such that

$$H_1(j\omega_1) \approx H_1(j\omega_2), \tag{5.7}$$

$$H_3(j\omega_1, j\omega_1, -j\omega_2) \approx H_3(j\omega_2, j\omega_2, -j\omega_1), \tag{5.8}$$

the value of IP3 found using either (5.5) or (5.6) would be approximately the same. In other words, the standard definition of IP3 assumes that the approximations in (5.7) and (5.8) are valid [16].

Mixer Circuits

Consider a mixer with an input signal $v_{in} = V_0 \cos(\omega_0 t) + V_1 \cos(\omega_1 t) + V_2 \cos(\omega_2 t)$, with ω_1 and ω_2 being two input radio frequencies and ω_0 being the local oscillator frequency. By substituting this input signal into (5.3) and expanding the terms, the following expressions for the lower and upper side IP3 can be derived [19]

$$IIP3_L = \sqrt{\frac{|V_0 H_2(j\omega_0, j\omega_1) + \frac{3V_0^3}{2} H_4(j\omega_0, j\omega_0, -j\omega_0, j\omega_1) + \ldots|}{|\frac{3V_0}{2} H_4(j\omega_0, j\omega_1, j\omega_1, -j\omega_2) + \ldots|}} \tag{5.9}$$

$$IIP3_U = \sqrt{\frac{|V_0 H_2(j\omega_0, j\omega_2) + \frac{3V_0^3}{2} H_4(j\omega_0, j\omega_0, -j\omega_0, j\omega_2) + \ldots|}{|\frac{3V_0}{2} H_4(j\omega_0, j\omega_2, j\omega_2, -j\omega_1) + \ldots|}} \tag{5.10}$$

For the case of mixer circuits without memory, these expressions simplify to the following relation in terms of the power series expansion coefficients given in (5.1)

$$IIP3 = \sqrt{\frac{V_0 k_2 + \frac{3V_0^3}{2} k_4 + \ldots}{\frac{3V_0}{2} k_4 + \ldots}} \tag{5.11}$$

Note that both the numerators and the denominators in (5.9) and (5.10) are power series of the local oscillator power V_0. Notice that these power series terms are difficult to converge for large values of V_0, as is often the case in mixer circuits. Similarly to the case of amplifier circuits, the two fundamental RF tones are typically chosen in the passband and close enough to each other on the frequency spectrum such that the following approximations can be made [16]

$$H_2(j\omega_0, j\omega_1) \approx H_2(j\omega_0, j\omega_2) \tag{5.12}$$

$$H_4(j\omega_0, j\omega_1, j\omega_1, -j\omega_2) \approx H_4(j\omega_0, j\omega_2, j\omega_2, -j\omega_1) \tag{5.13}$$

5.3 Computation of IP3 Using Single-Tone Moments

In Section 5.2.2 the value of IP3 was expressed as a function of the Volterra kernels of the circuit. However, obtaining IP3 from these relations has not been practical due to two main reasons. First, it is very difficult to obtain analytical expressions for the Volterra kernels and to automate this process for arbitrary circuit topologies. Second, the formula for the IP3 of mixer circuits contains a power series of the local oscillator power which does not easily converge, therefore limiting such an approach to weakly nonlinear circuits such as low noise amplifiers. In this section, a new method is presented where the expressions needed for computing IP3 from the relations given in (5.4)–(5.5) and (5.9)–(5.11) are numerically evaluated, without the need to explicitly compute the analytical expressions for the Volterra kernels or the power series terms in (5.1), and with only a single RF input frequency (ω_1) rather than the traditional two input frequencies (ω_1 and ω_2). To that end a closed form relation between the moments of the Harmonic Balance equations and the terms in the single-tone Volterra series relations for obtaining IP3 is derived, which reduces the problem of finding IP3 to that of computing the circuit moments. Although the expressions are extracted from the Harmonic Balance moments, there is no need to perform a full Harmonic Balance simulation. In fact the CPU cost of the moments computation algorithm is reduced to finding the solution of a set of linear algebraic equations with only one LU-decomposition of a sparse moments computation matrix that is significantly smaller in size than a Harmonic Balance Jacobian matrix. This makes this method computationally much cheaper than than traditional multi-tone simulation methods. Also, since the expressions are obtained numerically, this method is automated and can easily be applied to arbitrary circuit topologies and nonlinearities.

In this section the details of the new algorithm are presented, beginning with the single-tone IP3 formulation using Volterra series in section 5.3.1. This is then followed by the derivation of the relation between these moments and IP3 for both amplifiers and mixers in section 5.3.3.

5.3.1 IP3 Formulation Using Single-Tone Volterra Kernels

It has been shown earlier that the IP3 of a nonlinear circuit can be obtained by first determining the Volterra kernels of the circuit, then using the relation in (5.5) or (5.6) for amplifiers, and the relation in (5.9) or (5.10) for mixers. Note however, that the presence of two input tones in these formulations is simply to be consistent with measurement and simulation based approaches where two input tones are necessary in order to obtain the intermodulation products. When the values of the Volterra kernels can be analytically obtained for a given frequency, the approximations in (5.7) and (5.8) are no longer necessary because for $\omega_1 \approx \omega_2$,

$$H_3(j\omega_1, j\omega_1, -j\omega_2) \approx H_3(j\omega_1, j\omega_1, -j\omega_1) \tag{5.14}$$

and the intercept point IP3 can be defined using only a single input frequency as

$$IIP3 = \sqrt{\frac{4}{3} \frac{|H_1(j\omega_1)|}{|H_3(j\omega_1, j\omega_1, -j\omega_1)|}} \tag{5.15}$$

It is important to note that with the condition given by (5.14), the formulation in (5.15) gives similar results as that of the two-tone IP3 in (5.5), and any variations are due to a difference of definition rather than numerical error.

A fundamentally similar analysis can be applied to mixer circuits. The standard definition of IP3 assumes that the approximations in (5.12) and (5.13) are valid. If the two RF input fundamental frequencies are chosen sufficiently far away from each other such that (5.12) and (5.13) are no longer valid, the standard definition of IP3 in mixer circuits is no longer valid. In other words, similar to the case of amplifier circuits, when using Volterra series analysis it is possible to determine the input IP3 of mixer circuits using only a single RF frequency in addition to the local oscillator because for $\omega_1 \approx \omega_2$,

$$H_4(j\omega_0, j\omega_1, j\omega_1, -j\omega_2) \approx H_4(j\omega_0, j\omega_1, j\omega_1, -j\omega_1) \tag{5.16}$$

In the case where the condition given by (5.16) is true, then the following single RF tone relation can be used:

$$IIP3 = \sqrt{\frac{|V_0 H_2(j\omega_0, j\omega_1) + \frac{3V_0^3}{2} H_4(j\omega_0, j\omega_0, -j\omega_0, j\omega_1) + \ldots|}{|\frac{3V_0}{2} H_4(j\omega_0, j\omega_1, j\omega_1, -j\omega_1) + \ldots|}} \tag{5.17}$$

A general relation for computing the third order intercept point using a single-tone input for both mixers and amplifiers is provided at the end of section 5.3.3.

5.3.2 Definition of Single-Tone Moments

The Harmonic Balance equations for a general nonlinear system, as described in detail in Chapter 3, are of the form [17]

$$\bar{\boldsymbol{G}}\boldsymbol{X} + \bar{\boldsymbol{C}}\boldsymbol{X} + \boldsymbol{F}(\boldsymbol{X}) = \boldsymbol{B}_{DC} + \alpha \boldsymbol{B}_{RF} + \beta \boldsymbol{B}_{LO}, \tag{5.18}$$

where

- $\bar{\boldsymbol{G}} \in \mathbb{R}^{N_h \times N_h}$ is a block matrix representing the contributions of the linear memoryless elements.
- $\bar{\boldsymbol{C}} \in \mathbb{R}^{N_h \times N_h}$ is a block matrix representing the contributions of the linear memory elements.
- $\boldsymbol{X} \in \mathbb{R}^{N_h}$ is a vector of unknown cosine and sine coefficients for each of the variables in $\boldsymbol{x}(t)$.
- The vectors $\boldsymbol{B}_{DC} \in \mathbb{R}^{N_h}$ and $\boldsymbol{B}_{LO} \in \mathbb{R}^{N_h}$ show the contributions of the DC independent sources and, if present, the LO frequency tone, respectively.
- $\boldsymbol{B}_{RF} \in \mathbb{R}^{N_h}$ shows the location of the single-tone RF input (a vector of all zero entries except for a '1' at the location of the RF frequency).
- α refers to the amplitude of the input RF voltage signal
- β refers to the amplitude of the LO voltage. Note that β is only present in mixer circuits, and is otherwise equal to zero.
- $\boldsymbol{F}(\boldsymbol{X}) \in \mathbb{R}^{N_h}$ is the vector of nonlinear equations.

The moments of the system are defined as the Taylor series expansion of the output solution vector $\boldsymbol{X}$ with respect to the input RF amplitude α. This can be expressed as [17]

$$\boldsymbol{X} = \boldsymbol{M}_0 + \boldsymbol{M}_1\alpha + \boldsymbol{M}_2\alpha^2 + \boldsymbol{M}_3\alpha^3 + \cdots = \sum_{k=0}^{q} \boldsymbol{M}_k \alpha^k \tag{5.19}$$

where $\boldsymbol{M}_k$ is the k^{th} moment vector. The expansion is carried out at the DC operating point for the amplifier case, and at the LO frequency for mixers. The CPU cost of obtaining the moments is that of a solution of a system of sparse linear equations. An overview of the moments computation algorithm can be found in section 5.4.

5.3.3 Relation Between IP3 and the Harmonic Balance Moments

In this section, a closed form expression for IP3 as a function of the Harmonic Balance moments will be developed based on the single-tone definitions of IP3 in (5.15) and (5.17). First, the cases of amplifier circuits and mixer circuits will be considered separately, and then an overall framework will be provided at the end.

Amplifier Circuits

Consider an amplifier circuit with an input $v_{in} = \alpha\cos(\omega t)$, with ω being the Radio Frequency. If the circuit is memoryless, the output can be obtained by substituting this input into equation (5.1) and expanding using trigonometric identities, which results in

$$\begin{aligned} X \quad = \quad & \left(k_0 + \frac{1}{2}k_2\alpha^2 + \dots\right) + \\ & \left(k_1\alpha + \frac{3}{4}k_3\alpha^3 + \dots\right)\cos(\omega t) + \\ & \left(\frac{1}{2}k_2\alpha^2 + \dots\right)\cos(2\omega t) + \\ & \left(\frac{1}{4}k_3\alpha^3 + \dots\right)\cos(3\omega t) + \dots \end{aligned} \tag{5.20}$$

The relation in (5.20) can now be compared to that in (5.19), since the solution vector $\boldsymbol{X}$ in (5.19) is essentially the output variable X in (5.20). By equating the same powers of α in these two equations and noting the frequencies, the location of the k_n terms in the moment vectors $\boldsymbol{M}_k$ can be determined and are as follows

$$\underbrace{\begin{vmatrix} \text{DC} \\ \omega \\ 2\omega \\ 3\omega \\ \vdots \end{vmatrix}}_{\text{Frequency}} \begin{matrix} \rightarrow \\ \rightarrow \\ \rightarrow \\ \rightarrow \\ \vdots \end{matrix} \underbrace{\begin{bmatrix} k_0 \\ 0 \\ 0 \\ 0 \\ \vdots \end{bmatrix}}_{\boldsymbol{M}_0} \underbrace{\begin{bmatrix} 0 \\ \boldsymbol{k_1} \\ 0 \\ 0 \\ \vdots \end{bmatrix}}_{\boldsymbol{M}_1} \underbrace{\begin{bmatrix} \frac{1}{2}k_2 \\ 0 \\ \frac{1}{2}k_2 \\ 0 \\ \vdots \end{bmatrix}}_{\boldsymbol{M}_2} \underbrace{\begin{bmatrix} 0 \\ \boldsymbol{\frac{3}{4}k_3} \\ 0 \\ \frac{1}{4}k_3 \\ \vdots \end{bmatrix}}_{\boldsymbol{M}_3} \tag{5.21}$$

Notice that each row of the moment vectors consists of the coefficients of the Taylor series expansion of one of the harmonic amplitudes. For example, the second row contains the Taylor expansion coefficients of the amplitude of the fundamental frequency tone, ω. In this row, we observe that the vector $\boldsymbol{M}_1$ contains the value of k_1 and the vector $\boldsymbol{M}_3$ contains the value of $\frac{3}{4}k_3$. The relation in (5.21) shows the first 3 moment vectors in addition to the zeroth moment vector, with the parameters required for the computation of the third order intercept point according to (5.4) shown in bold.

In the case of systems with memory, a fundamentally similar analysis can be performed.

The additional complexity here comes from the need to represent the output as a Volterra series expansion rather than a power series. To derive the relationship between the moments and the terms required for computing IP3 according to (5.15), consider the system representation as a Volterra series as defined in (5.3), where $H_i[v(t)]$ is the i^{th} Volterra operator and is of the i^{th} order. For this derivation, it is useful to begin by expressing the single-tone input function with an amplitude of α in the following format

$$
\begin{aligned}
v(t) &= \alpha\cos(\omega t) && (5.22)\\
&= \frac{\alpha}{2}e^{j\omega t} + \frac{\alpha}{2}e^{-j\omega t} && (5.23)\\
&= v_a(t) + v_b(t) && (5.24)
\end{aligned}
$$

Substituting (5.22) into (5.3) then results in the following expressions for the first three Volterra operators [3]

$$
\begin{aligned}
H_1[v(t)] &= H_1[v_a] + H_1[v_b] && (5.25)\\
H_2[v(t)] &= H_2[v_a] + H_2[v_b] + H_2\{v_a, v_b\} + H_2\{v_b, v_a\} && (5.26)\\
H_3[v(t)] &= H_3[v_a] + H_3[v_b] + H_3\{v_a, v_a, v_b\} + H_3\{v_a, v_b, v_a\} + H_3\{v_b, v_a, v_a\} + \\
&\quad H_3\{v_b, v_b, v_a\} + H_3\{v_b, v_a, v_b\} + H_3\{v_a, v_b, v_b\} && (5.27)
\end{aligned}
$$

Each of the above operators are then evaluated and expressed using Volterra kernels in the frequency domain via the following expression [3]

$$
H_n\{v_1, \cdots, v_n\} = \int_{-\infty}^{\infty} d\tau_1 \cdots \int_{-\infty}^{\infty} d\tau_n h_n(\tau_1, \cdots, \tau_n) \prod_{r=1}^{n} v_r(t - \tau_r) \quad (5.28)
$$

In these expressions, $h_n(\tau_1, \cdots, \tau_n)$ is the n^{th} order time-domain Volterra kernel and can be assumed to be symmetric without loss of generality. With this being the case, using (5.28) to determine all the terms in (5.25)-(5.27) gives the following results

$$
\begin{aligned}
H_1[v(t)] &= \frac{\alpha}{2}H_1(j\omega)e^{j\omega t} + \frac{\alpha}{2}H_1(-j\omega)e^{-j\omega t} && (5.29)\\
H_2[v(t)] &= \frac{\alpha^2}{4}H_2(j\omega, j\omega)e^{j2\omega t} + \frac{\alpha^2}{4}H_2(-j\omega, -j\omega)e^{-j2\omega t} + 2\left(\frac{\alpha^2}{4}\right)H_2(j\omega, -j\omega) && (5.30)\\
H_3[v(t)] &= \frac{\alpha^3}{8}H_3(j\omega, j\omega, j\omega)e^{j3\omega t} + \frac{\alpha^3}{8}H_3(-j\omega, -j\omega, -j\omega)e^{-j3\omega t} + && (5.31)\\
&\quad 3\left(\frac{\alpha^3}{8}\right)H_3(j\omega, j\omega, -j\omega)e^{j\omega t} + 3\left(\frac{\alpha^3}{8}\right)H_3(j\omega, -j\omega, -j\omega)e^{-j\omega t} && (5.32)\\
& && (5.33)
\end{aligned}
$$

Observing the terms for each Volterra operator reveals that they are all complex conjugates of each other since it is easy to prove that [3]

$$H_n(-j\omega_1, \ldots, -j\omega_n) = H_n^*(j\omega_1, \ldots, j\omega_n) \tag{5.34}$$

Applying this property reduces the final result to the expressions given by

$$
\begin{aligned}
H_1[v(t)] &= \alpha \mathrm{Re}\left(H_1(j\omega)e^{j\omega t}\right) && (5.35)\\
H_2[v(t)] &= \frac{\alpha^2}{2}\mathrm{Re}\left(H_2(j\omega, j\omega)e^{j2\omega t}\right) + \frac{\alpha^2}{2}H_2(j\omega, -j\omega) && (5.36)\\
H_3[v(t)] &= \frac{\alpha^3}{4}\mathrm{Re}\left(H_3(j\omega, j\omega, j\omega)e^{j3\omega t}\right) + \frac{3\alpha^3}{4}\mathrm{Re}\left(H_3(j\omega, j\omega, -j\omega)e^{j\omega t}\right) && (5.37)
\end{aligned}
$$

Substituting (5.35)-(5.37) into (5.3), the following input-output relation is obtained

$$
\begin{aligned}
X &= H_0 + \frac{1}{2}H_2(j\omega, -j\omega)\alpha^2 + \\
&\quad \mathrm{Re}(H_1(j\omega)e^{j\omega t})\alpha + \frac{3}{4}\mathrm{Re}(H_3(j\omega, j\omega, -j\omega)e^{j\omega t})\alpha^3 + \\
&\quad \frac{1}{2}\mathrm{Re}(H_2(j\omega, j\omega)e^{j2\omega t})\alpha^2 + \\
&\quad \frac{1}{4}\mathrm{Re}(H_3(j\omega, j\omega, j\omega)e^{j3\omega t})\alpha^3 + \ldots && (5.38)
\end{aligned}
$$

which can then be re-written as

$$\begin{aligned} X &= \left[H_0 + \frac{1}{2}H_2(j\omega, -j\omega)\alpha^2\right] + \\ &\left[\ |H_1(j\omega)|\,\alpha\right]\cos\big(\omega t + \angle H_1(j\omega)\big) + \\ &\left[\frac{3}{4}\,|H_3(j\omega, j\omega, -j\omega)|\,\alpha^3\right]\cos\big(\omega t + \angle H_3(j\omega, j\omega, -j\omega)\big) + \\ &\left[\frac{1}{2}\,|H_2(j\omega, j\omega)|\,\alpha^2\right]\cos\big(2\omega t + \angle H_2(j\omega, j\omega)\big) + \\ &\left[\frac{1}{4}\,|H_3(j\omega, j\omega, j\omega)|\,\alpha^3\right]\cos\big(3\omega t + \angle H_3(j\omega, j\omega, j\omega)\big) + \ldots \end{aligned} \tag{5.39}$$

By comparing the Volterra Series expression in (5.39) to the expression shown in (5.20), it can be seen that they are very similar in structure. As was the case with memoryless systems, the location of the parameters of (5.39) in the moment vectors can now be deduced and is given by

$$\underbrace{\begin{vmatrix} \text{DC} \\ \omega \\ 2\omega \\ 3\omega \\ \vdots \end{vmatrix}}_{\text{Frequency}} \begin{matrix} \rightarrow \\ \rightarrow \\ \rightarrow \\ \rightarrow \\ \rightarrow \end{matrix} \underbrace{\begin{bmatrix} H_0 \\ 0 \\ 0 \\ 0 \\ \vdots \end{bmatrix}}_{\boldsymbol{M}_0} \underbrace{\begin{bmatrix} 0 \\ \boldsymbol{|H_1(j\omega)|} \\ 0 \\ 0 \\ \vdots \end{bmatrix}}_{\boldsymbol{M}_1} \underbrace{\begin{bmatrix} \frac{1}{2}|H_2(j\omega, j\omega)| \\ 0 \\ \frac{1}{2}|H_2(j\omega, j\omega)| \\ 0 \\ \vdots \end{bmatrix}}_{\boldsymbol{M}_2} \underbrace{\begin{bmatrix} 0 \\ \boldsymbol{\frac{3}{4}|H_3(j\omega, j\omega, -j\omega)|} \\ 0 \\ \frac{1}{4}|H_3(j\omega, j\omega, j\omega)| \\ \vdots \end{bmatrix}}_{\boldsymbol{M}_3} \tag{5.40}$$

The parameters required to compute the value of IP3 according to (5.15) are the entries highlighted in bold.

Mixer Circuits

For the case of mixer circuits, the extra frequency component due to the Local Oscillator must be accounted for in the derivation. A similar derivation to that shown in the previous section is performed to determine the location of the necessary intermodulation distortion terms in the moment vectors. Note that in this case, the computation of the moments is done using only a single RF tone in addition to the local oscillator tone (i.e. two tones total) as opposed to three tones in traditional Harmonic Balance. The moments computation algorithm is therefore similar to the one described in Chapter 4 where the expansion is done around the LO which is considered outside the signal path, which in turn means that the local oscillator amplitude β is embedded inside the moment vectors. After computing the moments, the next step would be to extract the summations of terms needed to compute IP3 according to the formulation given in (5.17) from the moment vectors, before finally proceeding with the computation of IP3.

To derive the link between the moment vectors and the terms required to compute IP3 according to equation (5.17), the case of memoryless systems is first considered to simplify the presentation. The input signal is now defined as $v = \alpha\cos(\omega_1 t) + \beta\cos(\omega_0 t)$, with ω_1 being the single-tone input radio frequency, and ω_0 being the local oscillator frequency. Substituting this expression into (5.1) and expanding using trigonometric identities results in the expression given by

$$\begin{aligned} X \quad = \quad & \left[\left(k_2\beta + \frac{3k_4\beta^3}{2} + \dots\right)\alpha + \left(\frac{3k_4\beta}{2} + \dots\right)\alpha^3\right]\cos((\omega_0 - \omega_1)t) + \\ & \left[\left(k_1\beta + \frac{3}{4}k_3\beta^3 + \dots\right) + \left(\frac{3}{2}k_3\beta + \dots\right)\alpha^2\right]\cos(\omega_0 t) + \\ & \left[\left(k_2\beta + \frac{3k_4\beta^3}{2} + \dots\right)\alpha + \left(\frac{3k_4\beta}{2} + \dots\right)\alpha^3\right]\cos((\omega_0 + \omega_1)t) + \\ & \dots \end{aligned} \tag{5.41}$$

Note that equation (5.41) contains many frequency terms, but only the ones that are relevant for the computation of IP3 are shown. By comparing (5.41) with (5.19), the location of the k_n terms in the system moment vectors $\boldsymbol{M}_k$ can be determined. This is more obvious when the contents of the moments are presented in the following format,

$$
\underbrace{\begin{vmatrix} \vdots \\ \omega_0 - 3\omega_1 \\ \omega_0 - 2\omega_1 \\ \omega_0 - \omega_1 \\ \omega_0 \\ \omega_0 + \omega_1 \\ \omega_0 + 2\omega_1 \\ \omega_0 + 3\omega_1 \\ \vdots \end{vmatrix}}_{\text{Frequency}}
\begin{matrix} \vdots \\ \rightarrow \\ \rightarrow \\ \rightarrow \\ \rightarrow \\ \rightarrow \\ \rightarrow \\ \rightarrow \\ \vdots \end{matrix}
\underbrace{\begin{bmatrix} \vdots \\ 0 \\ 0 \\ 0 \\ k_1\beta + \frac{3}{4}k_3\beta^3 + \dots \\ 0 \\ 0 \\ 0 \\ \vdots \end{bmatrix}}_{\boldsymbol{M}_0}
\underbrace{\begin{bmatrix} \vdots \\ 0 \\ 0 \\ \boldsymbol{k_2\beta + \frac{3}{2}k_4\beta^3 + \dots} \\ 0 \\ \boldsymbol{k_2\beta + \frac{3}{2}k_4\beta^3 + \dots} \\ 0 \\ 0 \\ \vdots \end{bmatrix}}_{\boldsymbol{M}_1}
\underbrace{\begin{bmatrix} \vdots \\ 0 \\ \frac{3}{4}k_3\beta + \dots \\ 0 \\ \frac{3}{2}k_3\beta + \dots \\ 0 \\ \frac{3}{4}k_3\beta + \dots \\ 0 \\ \vdots \end{bmatrix}}_{\boldsymbol{M}_2}
\underbrace{\begin{bmatrix} \vdots \\ \frac{1}{2}k_4\beta + \dots \\ 0 \\ \boldsymbol{\frac{3}{2}k_4\beta + \dots} \\ 0 \\ \boldsymbol{\frac{3}{2}k_4\beta + \dots} \\ 0 \\ \frac{1}{2}k_4\beta + \dots \\ \vdots \end{bmatrix}}_{\boldsymbol{M}_3}
\tag{5.42}
$$

By comparing (5.42) with (5.11), it can be seen that the terms needed for computing IP3 are located in the first and third moment vectors. In fact, we observe that the moments contain the whole summations needed, thereby resulting in accurate values of IP3 for circuits that experience difficulty in convergence of the local oscillator power series. For the more general case of mixer circuits that contain memory elements, the derivation is performed using a Volterra series expansion with the inclusion of the Volterra operators up to the 4th order in the derivation. The Volterra Series representation of a nonlinear system with memory is given by (5.3). The first step is to substitute the expression for an input function with two tones, one being at the RF frequency of interest with amplitude α, and a local oscillator tone with a separate amplitude β, which is given by

$$
\begin{aligned}
v(t) &= \alpha\cos(\omega_1 t) + \beta\cos(\omega_0 t) && (5.43)\\
&= \frac{\alpha}{2}e^{j\omega_1 t} + \frac{\alpha}{2}e^{-j\omega_1 t} + \frac{\beta}{2}e^{j\omega_0 t} + \frac{\beta}{2}e^{-j\omega_0 t} && (5.44)\\
&= v_a(t) + v_b(t) + v_c(t) + v_d(t) && (5.45)
\end{aligned}
$$

into (5.3). The resulting expressions for each Volterra operator are too large to be stated in their entirety. Instead, only the expressions at the frequencies of interest are shown. For the case of an up-conversion mixer with $\omega_0 >> \omega_1$, at the fundamental IF frequency of $\omega_0 + \omega_1$, the distortion terms present will be a result of a second order nonlinearity and a fourth order nonlinearity due to the mixing of the frequencies $\omega_0 + \omega_0 - \omega_0 + \omega_1$ and $\omega_0 + \omega_1 + \omega_1 - \omega_1$. These distortion terms can be represented as

$$\begin{aligned} H_2[v(t)]_{\omega_0+\omega_1} &= 2H_2\{v_a, v_c\} + 2H_2\{v_b, v_d\} &(5.46)\\ H_4[v(t)]_{\omega_0+\omega_1} &= 12H_4\{v_a, v_a, v_b, v_c\} + 12H_4\{v_a, v_b, v_b, v_d\} + \\ &\quad 12H_4\{v_a, v_c, v_c, v_d\} + 12H_4\{v_b, v_c, v_d, v_d\} &(5.47) \end{aligned}$$

Each of the above Volterra operators are then expressed in the frequency domain using Volterra kernels by using the relation in (5.28) to determine all the terms in (5.46), similarly to the case of amplifier circuits. This results in

$$\begin{aligned} H_2\left[v(t)\right]_{\omega_0+\omega_1} &= \alpha\beta \mathrm{Re}\left(H_2(j\omega_0, j\omega_1)e^{j(\omega_0+\omega_1)t}\right) &(5.48)\\ H_4\left[v(t)\right]_{\omega_0+\omega_1} &= \frac{3}{2}\alpha\beta^3 \mathrm{Re}\left(H_4(j\omega_0, j\omega_0, -j\omega_0, j\omega_1)e^{j(\omega_0+\omega_1)t}\right) \\ &\quad + \frac{3}{2}\alpha^3\beta \mathrm{Re}\left(H_4(j\omega_0, j\omega_1, j\omega_1, -j\omega_1)e^{j(\omega_0+\omega_1)t}\right) &(5.49) \end{aligned}$$

By substituting (5.48)–(5.49) and the remaining terms at the other intermodulation and harmonic frequencies into (5.3), then rearranging by grouping similar frequencies together, the following input output relation is obtained

$$\begin{aligned} X = \ &\mathrm{Re}\left[\left(\beta H_2(j\omega_0, -j\omega_1)\alpha + \frac{3\beta^3}{2}H_4(j\omega_0, j\omega_0, -j\omega_0, -j\omega_1)\alpha + \ldots\right)e^{j(\omega_0-\omega_1)t}\right] + \\ &\mathrm{Re}\left[\left(\frac{3\beta}{2}H_4(j\omega_0, j\omega_1, -j\omega_1, -j\omega_1)\alpha^3 + \ldots\right)e^{j(\omega_0-\omega_1)t}\right] + \\ &\mathrm{Re}\left[\left(\beta H_2(j\omega_0, j\omega_1)\alpha + \frac{3\beta^3}{2}H_4(j\omega_0, j\omega_0, -j\omega_0, j\omega_1)\alpha + \ldots\right)e^{j(\omega_0+\omega_1)t}\right] + \\ &\mathrm{Re}\left[\left(\frac{3\beta}{2}H_4(j\omega_0, j\omega_1, j\omega_1, -j\omega_1)\alpha^3 + \ldots\right)e^{j(\omega_0+\omega_1)t}\right] + \ldots \qquad (5.50) \end{aligned}$$

Which can also be expressed in the following format

$$\begin{aligned}
X \;=\; & \left[\left|\beta H_2(j\omega_0,-j\omega_1)+\frac{3\beta^3}{2}H_4(j\omega_0,j\omega_0,-j\omega_0,-j\omega_1)+\ldots\right|\alpha\right]\cos((\omega_0-\omega_1)t+\Theta_1)\\
& +\left[\left|\frac{3\beta}{2}H_4(j\omega_0,j\omega_1,-j\omega_1,-j\omega_1)+\ldots\right|\alpha^3\right]\cos((\omega_0-\omega_1)t+\Theta_2)+\\
& \left[\left|\beta H_2(j\omega_0,j\omega_1)\alpha+\frac{3\beta^3}{2}H_4(j\omega_0,j\omega_0,-j\omega_0,j\omega_1)\alpha+\ldots\right|\alpha\right]\cos((\omega_0+\omega_1)t+\Theta_3)\\
& +\left[\left|\frac{3\beta}{2}H_4(j\omega_0,j\omega_1,j\omega_1,-j\omega_1)+\ldots\right|\alpha^3\right]\cos((\omega_0+\omega_1)t+\Theta_3)+\ldots
\end{aligned} \tag{5.51}$$

The Volterra series expression in (5.50) is similar in structure to the expression shown in (5.41) which implies that the location of the parameters to compute the value of IP3 according to (5.17) are the entries at the fundamental IF frequency locations in the first and third moment vectors. More specifically, in the first moment vector $\boldsymbol{M}_1$, the following summations at the frequencies of $\omega_0 \pm n\omega_1$ are present,

$$\underbrace{\begin{vmatrix}\vdots\\ \omega_0-3\omega_1\\ \omega_0-2\omega_1\\ \omega_0-\omega_1\\ \omega_0\\ \omega_0+\omega_1\\ \omega_0+2\omega_1\\ \omega_0+3\omega_1\\ \vdots\end{vmatrix}}_{\text{Frequency}}
\begin{vmatrix}\vdots\\ \rightarrow\\ \rightarrow\\ \rightarrow\\ \rightarrow\\ \rightarrow\\ \rightarrow\\ \rightarrow\\ \vdots\end{vmatrix}
\underbrace{\begin{bmatrix}\vdots\\ 0\\ 0\\ |\boldsymbol{H_2(j\omega_0,-j\omega_1)\beta+\frac{3}{2}H_4(j\omega_0,j\omega_0,-j\omega_0,-j\omega_1)\beta^3+\ldots}|\\ 0\\ |\boldsymbol{H_2(j\omega_0,j\omega_1)\beta+\frac{3}{2}H_4(j\omega_0,j\omega_0,-j\omega_0,j\omega_1)\beta^3+\ldots}|\\ 0\\ 0\\ \vdots\end{bmatrix}}_{\boldsymbol{M}_1} \tag{5.52}$$

While in the third moment vector $\boldsymbol{M}_3$, the following summations are present at the same frequencies

$$\underbrace{\begin{vmatrix} \vdots \\ \omega_0 - 3\omega_1 \\ \omega_0 - 2\omega_1 \\ \omega_0 - \omega_1 \\ \omega_0 \\ \omega_0 + \omega_1 \\ \omega_0 + 2\omega_1 \\ \omega_0 + 3\omega_1 \\ \vdots \end{vmatrix}}_{\text{Frequency}} \begin{matrix} \vdots \\ \rightarrow \\ \rightarrow \\ \rightarrow \\ \rightarrow \\ \rightarrow \\ \rightarrow \\ \rightarrow \\ \vdots \end{matrix} \underbrace{\begin{bmatrix} \vdots \\ \left|\frac{1}{2}H_4(j\omega_0, -j\omega_1, -j\omega_1, -j\omega_1)\beta + \ldots\right| \\ 0 \\ \boldsymbol{\left|\frac{3}{2}H_4(j\omega_0, j\omega_1, -j\omega_1, -j\omega_1)\beta + \ldots\right|} \\ 0 \\ \boldsymbol{\left|\frac{3}{2}H_4(j\omega_0, j\omega_1, j\omega_1, -j\omega_1)\beta + \ldots\right|} \\ 0 \\ \left|\frac{1}{2}H_4(j\omega_0, j\omega_1, j\omega_1, j\omega_1)\beta + \ldots\right| \\ \vdots \end{bmatrix}}_{\boldsymbol{M}_3} \tag{5.53}$$

As can be seen from (5.52) and (5.53), the moments contain the whole summations of terms necessary for computing IP3, thereby making this method accurate for circuits that experience local oscillator power series convergence issues.

General Formulation for Single-Tone IP3 Computation

The value of the third order intercept point is determined by evaluating the single-tone relations developed in Section 5.3.1. The relations shown in (5.15) and (5.17) can be generalized to obtain the following expression for the input third order intercept point referred to below as $IIP3$

$$IIP3 = \sqrt{\frac{m_{1,1}}{m_{1,3}}} \tag{5.54}$$

The terms $m_{1,1}$ and $m_{1,3}$ represent the entries at the fundamental output frequency in the first and third moment vectors, respectively, as illustrated in Fig. 5.4 for amplifiers and Fig. 5.5 for mixers. In the expressions for mixer circuits, it is important to note that β is the local oscillator amplitude and that the entire summation of series terms (not just the ones shown here) are present.

5.3.4 Summary of the New Algorithm

An overview of the main steps of the new algorithm for computing IP3 using single-tone moments is given in Fig. 5.6. The computation cost of this approach is primarily due to the computation of the moments in step 2 of the algorithm. This amounts to a solution of a linear set of equations

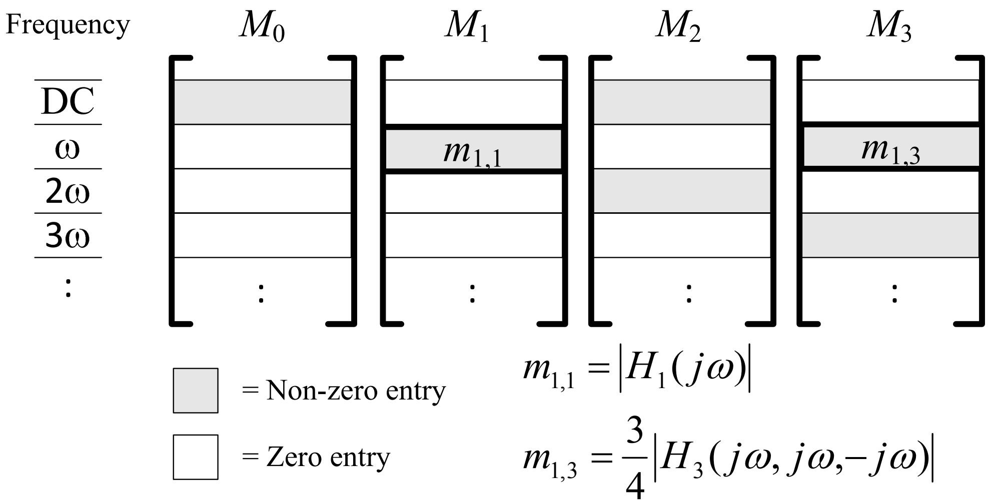

Fig. 5.4 Location of distortion terms in the moments for amplifiers

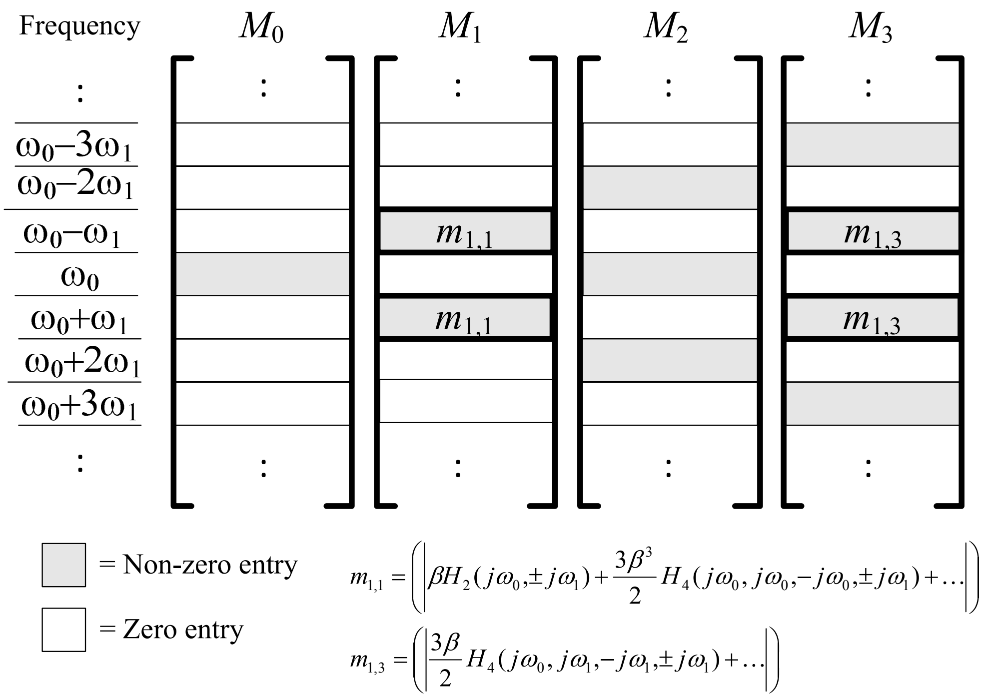

Fig. 5.5 Location of distortion terms in the moments for mixers

which is very sparse and contains a small number of variables since only a single-tone input is needed. The details of the computational cost of obtaining the moments is discussed in section 5.4. Also, it is important to note that, while the new approach does not require the solution of the nonlinear Harmonic Balance equations, it is based on the Harmonic Balance formulation which makes its general steps both topology independent and easy to automate.

1. Set up the system equations in the frequency domain according to the formulation shown in (5.18).
2. Calculate the single RF tone moment vectors $\boldsymbol{M}_k$ as defined in (5.19) by solving the formulations in (5.55) and in (5.57) recursively.
3. Obtain the necessary terms for computing IP3 from the entries in the moment vectors at the locations shown in Fig. 5.4 for amplifiers and in Fig. 5.5 for mixers.
4. Determine the distortion by calculating the third order intercept point according to (5.54).

Fig. 5.6 Summary of the algorithm for computing IP3 using single-tone moments analysis.

5.4 Computational Cost Considerations

For this new approach, the moments algorithm presented in [17] and derived in detail in section 4.3.2 is used to compute the moments of the Harmonic balance equations as defined in (5.19). In this section, a brief overview of the algorithm is presented and insight into the sparsity of the moment computation matrix is provided in order to show the computational efficiency of obtaining the moments as compared to a traditional multi-tone Harmonic Balance simulation.

The moments of a system are defined as the coefficients of the Taylor series expansion of the solution vector $\boldsymbol{X}$ of the system described by (5.18) with respect to the input RF amplitude α. If the solution is expressed using (5.19), then $\boldsymbol{M}_k$ is the k^{th} moment vector. The zeroth moment vector $\boldsymbol{M}_0$, is obtained by finding the solution of the system described by (5.18) with RF amplitude (α) set to zero. The first moment vector $\boldsymbol{M}_1$, is then found by solving the system of equations given by

$$\Phi \boldsymbol{M}_1 = \boldsymbol{B}_{RF} \tag{5.55}$$

where

$$\boldsymbol{\Phi} = \bar{\boldsymbol{G}} + \bar{\boldsymbol{C}} + \left.\frac{\partial \boldsymbol{F}(\boldsymbol{X})}{\partial \boldsymbol{X}}\right|_{(\alpha=0)} \tag{5.56}$$

In this relation, the first moment vector can be obtained using one LU Decomposition to solve (5.55). It is important to note that the matrix $\boldsymbol{\Phi}$ is the sparse moment computation matrix which has the same structure as a Jacobian matrix but contains only DC and LO spectral components. As for the remaining moment vectors $\boldsymbol{M}_n$, these are found by solving the following recursive relation

$$\boldsymbol{\Phi}\boldsymbol{M}_n = -\frac{1}{n}\sum_{j=1}^{n-1}(n-j)\boldsymbol{T}_j\boldsymbol{M}_{n-j} \tag{5.57}$$

The right-hand side of equation (5.57) is calculated using the values of the previous moments ($\boldsymbol{M}_{n-j}$) that have already been obtained, in addition to the values of the moments of the Jacobian ($\boldsymbol{T}_j$). As can be seen from (5.55)–(5.57), the computation of the moment vectors is a solution of a set of linear algebraic equations where the left-hand-side matrix is the same throughout and is therefore very efficient. Furthermore, this left-hand-side matrix is essentially the same as a single tone Harmonic Balance Jacobian evaluated using only DC and LO frequencies, which is a very sparse matrix compared to a typical Harmonic Balance Jacobian.

Finally, it is important to make a note about the effects of numerical tolerance and round-off errors in the moments computation algorithm. It is very important to monitor that the numerical errors in the computation of the moments are low relative to the signal levels in order to have accurate numerical values of the distortion terms using single-tone inputs. Since the moments are computed in a recursive manner (as shown in equation (5.57)), numerical errors grow as subsequent moments are computed. The entries in the moments that are particularly affected are the higher order terms at a specific frequency, including the term $m_{1,3}$. This in turn could result in a large deviation from the expected value of the single-tone IP3. From the experience of testing several numerical examples, circuit topologies which would not converge to small error tolerances in a regular Harmonic Balance simulation, in addition to highly nonlinear circuits were especially susceptible to this problem. In these cases, it is preferable to use the more robust two-tone moments analysis method for computing IP3 described in Section 2.6 and in Chapter 4, which uses the term $m_{3,3}$ instead of $m_{1,3}$ and gives IP3 results that are as accurate as those obtained using Harmonic Balance with a significantly smaller CPU cost.

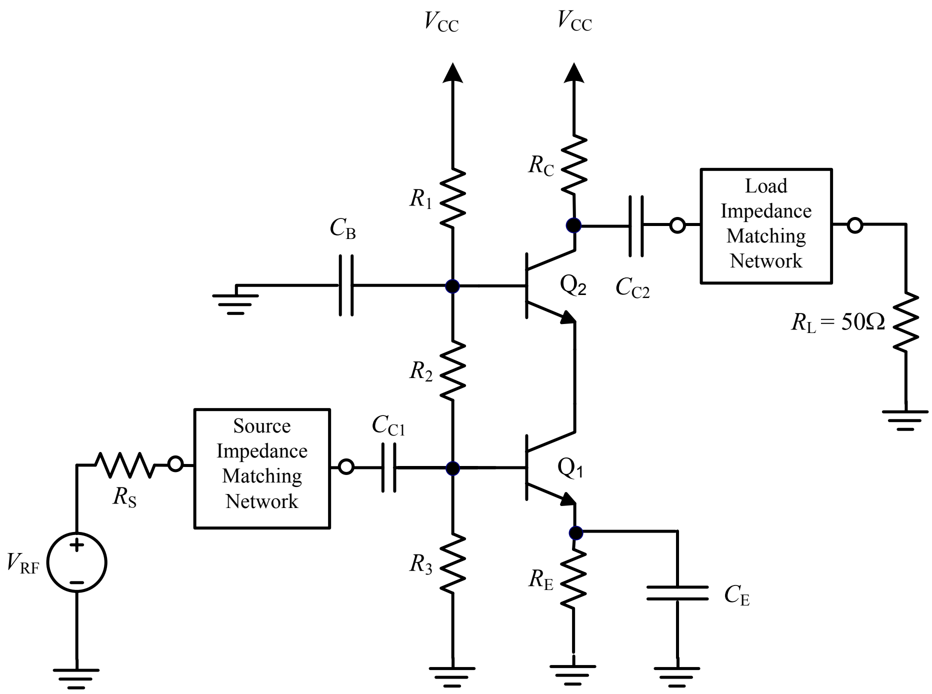

Fig. 5.7 Circuit diagram example 1

5.5 Numerical Examples

In this section, numerical results of simulations performed on two example circuits are shown in order to illustrate the speedup of the single-tone moments approach for computing IP3.

5.5.1 Example 1

Consider the cascode amplifier circuit shown in Fig. 5.7. This amplifier has lumped element input and output matching networks for 50Ω source and load impedances at the standard GSM frequency of 900 MHz. The linear gain of this amplifier is 12.3 dB. In order to test the accuracy and CPU efficiency of the new method, the value of IP3 for the above circuit was computed using three different methods. The first approach was the standard brute force method of multi-tone Harmonic Balance simulation. The second approach was the multi-tone moments based approach presented in Chapter 4 of this thesis. The third approach was the single-tone moments analysis method.

First, using the brute force approach, by applying two -50 dBm input tones at f_1 = 900

MHz and f_2 = 900.1 MHz and performing a standard harmonic balance analysis, the measured lower-side input IP3 was found to be -4.0 dBm and the upper side IP3 was found to be -4.1 dBm. This simulation was run with 10 harmonics, therefore the size of the dense Jacobian which had to be solved was 5083×5083 due to the 10 harmonics of the fundamental tones in addition to the diamond truncation tones [5]. The diagram in Fig. 5.8 shows the sparsity pattern of the Harmonic Balance Jacobian matrix which contains $699,167$ non-zero elements.

The distortion was next analyzed using the multi-tone moments based method. In this method, the same two input frequency tones at f_1 = 900 MHZ and f_2 = 900.1 MHz were applied to the circuit with 10 harmonics. The multi-tone moments were then evaluated and the value of IP3 was computed by extracting the required terms from the moments. In this case, the size of the moments computation matrix was identical to that of the Harmonic Balance Jacobian (5083×5083) since the number of variables was the same. However, the moments computation matrix was significantly more sparse. The computed values of IP3 were also -4.0 dBm and -4.1 dBm for the lower and upper side IP3, respectively.

Finally the distortion was analyzed using the new approach by computing the moments of the system using only a single tone input at $f = 900$MHz, and extracting the required terms at the appropriate frequencies. The size of the sparse moments computation matrix that had to be used was only 483×483. Fig. 5.9 shows the sparsity pattern of the moments computation matrix. As can be seen, this matrix has only $1,784$ non-zero elements. The resulting value of the input third order intercept point was found to be -4.3 dBm. Note that since only a single-input tone is present, there is only a single value for IP3 rather than an upper side IP3 and a lower side IP3. The results obtained are summarized in Table 5.1. As can be seen, the discrepancy between the two approaches was around 0.2 dBm or approximately 5.1% when comparing the value in Volts. It is important to note that this discrepancy occurs due to the approximation in (5.14) and is a matter of definition of IP3 rather than numerical error. Furthermore, as can be seen from the results, the discrepancy between the single tone IP3 and the two tone IP3 is of the same order of magnitude as the discrepancy between the lower-side and upper-side two-tone IP3.

The significant reduction in size and in number of non-zero elements between the Harmonic Balance Jacobian matrix and the Moments computation matrix has resulted in a large reduction in computational cost and therefore a significant speedup between the two approaches. The data in Table 5.2 shows a comparison of the computation times between the single-tone moments method, the two-tone moments method and the Harmonic Balance technique using a prototype MATLAB simulator. The hardware platform on which the simulations were run was a single-core

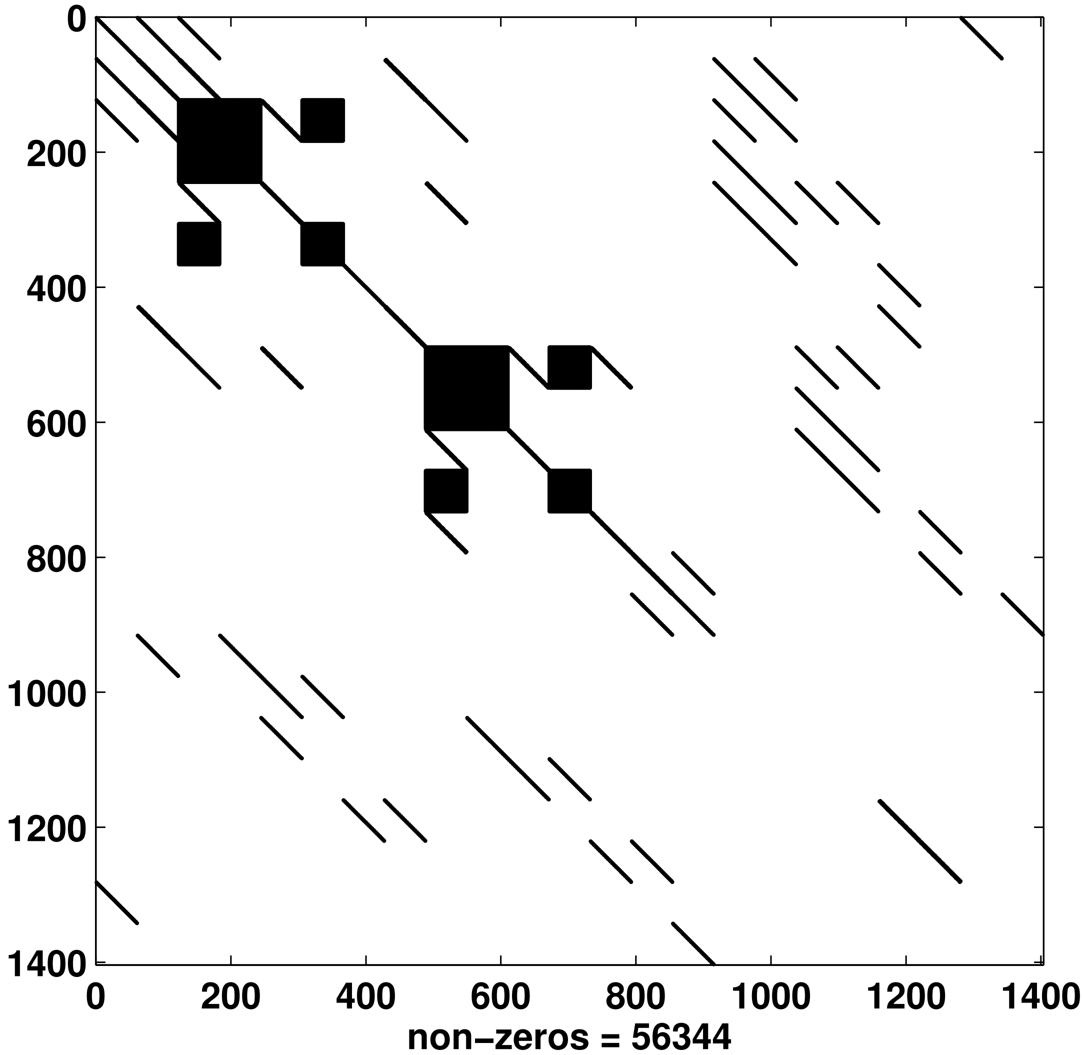

Fig. 5.8 Sparsity pattern of Harmonic Balance Jacobian for the circuit in example 1

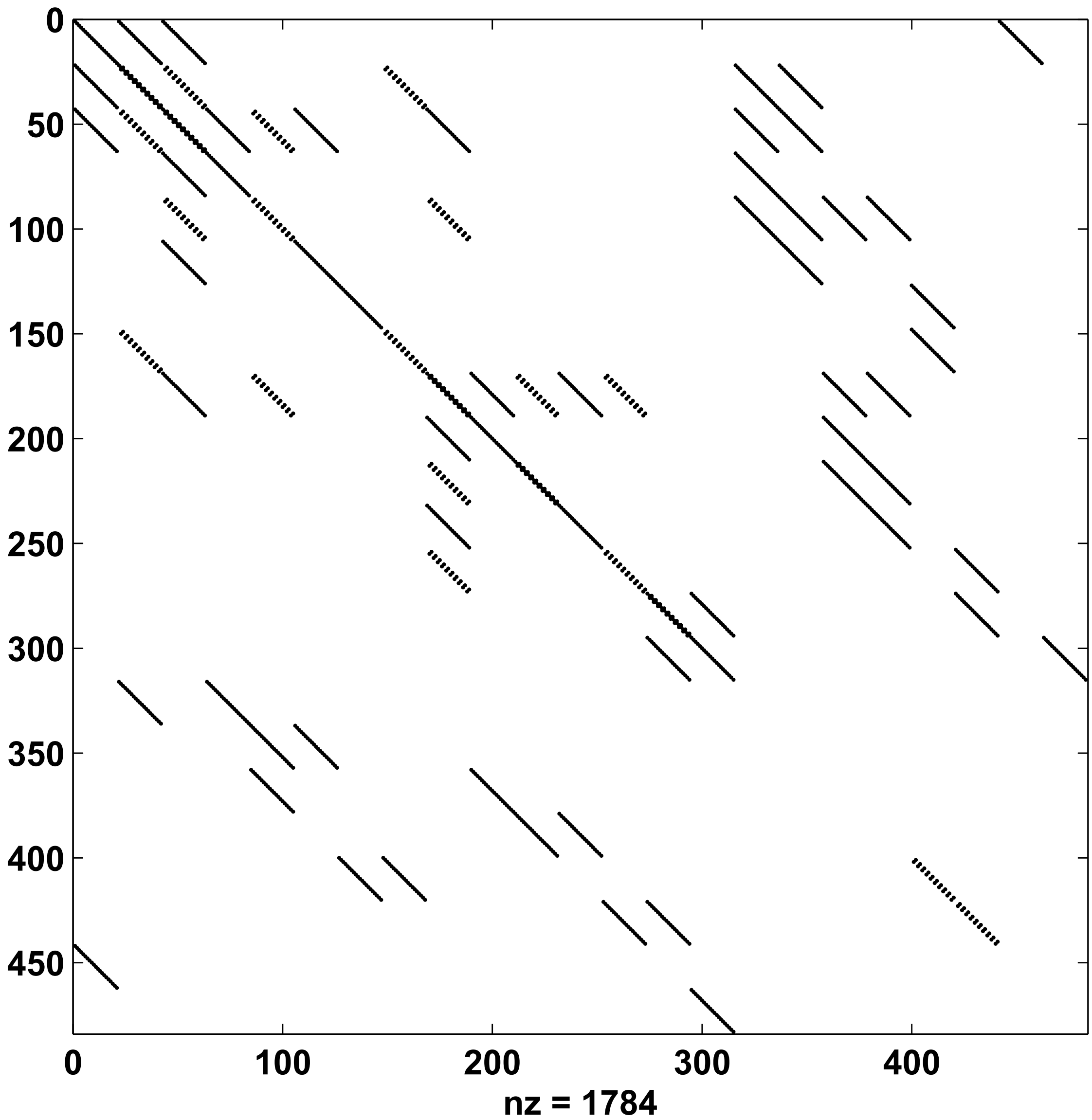

Fig. 5.9 Sparsity pattern of the moments computation matrix for the circuit in example 1

Intel Pentium 4 machine with a clock speed of 3.2 GHz and 3GB of RAM. As can be seen, the speed-up of the new method over the harmonic balance approach was found to be 235 times using 10 harmonics for this example. It is important to note that the number of harmonics required in a simulation depends on the particular circuit, the input power level and the desired accuracy. On the other hand the number of harmonics also affects the CPU cost and the relative advantage of using the new approach. In order to illustrate this fact, the circuit in this example was simulated using a various number of harmonics and the speed-up for each case was computed and reported in Table 5.3.

5.5.2 Example 2

The second example considered is the Gilbert cell bipolar mixer with a local oscillator frequency of 1 GHz shown in Fig. 5.10. The power of the local oscillator signal is -16 dBm. In order to analyze the distortion of this circuit, a similar procedure to that performed in Example 1 is followed. For comparative purposes only, the brute force simulation approach was first used by applying three input tones and performing a full harmonic balance simulation, then measuring IP3 from the output spectrum. The second approach was by finding the value of IP3 from the multi-tone moments that were evaluated also with three input tones according to the method presented in Chapter 4. Finally the value of IP3 was computed from the single-tone moments method with only two input tones total (single RF tone in addition to the local oscillator).

First, using the Harmonic Balance method, the two RF input tone frequencies were f_1 = 99.5 MHz and f_2 = 100.0 MHz, with power levels of -53.5 dBm. The calculated lower-side input IP3 from the steady-state solution was found to be -9.7 dBm, while the upper-side input IP3 was found to be -9.8 dBm. The diagram in Fig. 5.11 shows the sparsity pattern of the Harmonic Balance Jacobian. The size of the Harmonic Balance Jacobian matrix was $18,450 \times 18,450$ and as can be seen from Fig. 5.11, the matrix contains many dense blocks and therefore has $7,271,954$ non-zero entries.

Next, using the multi-tone moments method, and with the same input frequencies and power levels as those used for the Harmonic Balance approach, the calculated lower-side and upper-side input IP3 were also found to be -9.7 dBm and -9.8dBm, respectively. The size of the moments computation matrix was also $18,450 \times 18,450$ since it is of the same structure as the harmonic balance Jacobian while being significantly more sparse.

The distortion was then analyzed using the new approach by computing the moments of the

Table 5.1 Comparison of IP3 values between traditional Harmonic Balance and the single-tone moments method

	Harmonic Balance IIP3 (Lower)	Harmonic Balance IIP3 (Upper)	Single-tone Moments IIP3
Example 1	-4.0 dBm	-4.1 dBm	-4.3 dBm
Example 2	-9.7 dBm	-9.8 dBm	-9.5 dBm

Table 5.2 Comparison of computation times between the single-tone moments method and the Harmonic Balance solution

	Example 1	Example 2
Harmonic Balance	25.94 s	432.16 s
2-tone Moments	1.30 s	4.63 s
Initial Speedup	20 times	93 times
1-tone Moments	0.11 s	1.03 s
Further Speedup	11.8 times	4.5 times
Overall Speedup	235 times	420 times

Table 5.3 The effects of increasing harmonics on speedup of IP3 simulation of example 1 between the single-tone moments method and Harmonic Balance.

Number of Harmonics	Speedup
3	7 times
5	12 times
7	53 times
10	235 times
15	1218 times

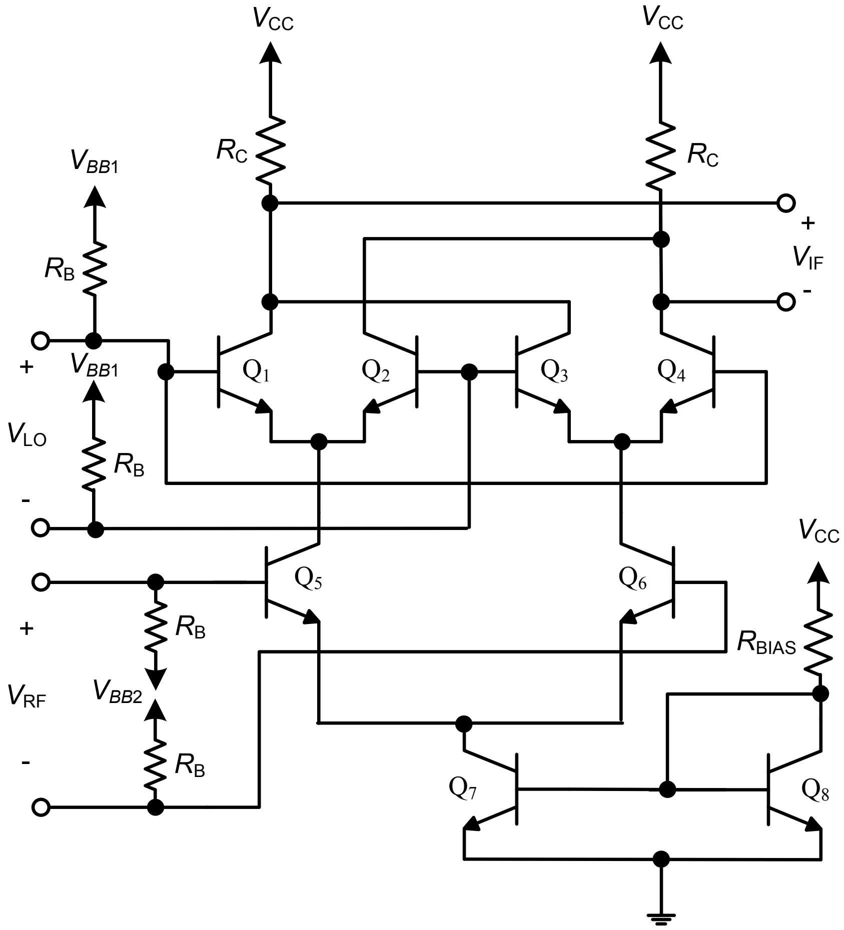

Fig. 5.10 Differential bipolar Gilbert mixer circuit diagram.

system using a single RF input tone at $f = 100$MHz, and extracting the necessary terms at the appropriate frequencies without the need to perform a harmonic balance simulation. The single resulting value of the input IP3 was found to be -9.5 dBm. A summary of the results obtained for this example mixer circuit is given in Table 5.1. Fig. 5.12 shows the sparsity pattern of the moments computation matrix used to find the single-tone moments, which contains only the DC and the local oscillator tones. Since this matrix is significant in size, to clearly illustrate the difference in sparsity between it and the Harmonic Balance Jacobian matrix, Figs. 5.11 and 5.12 contain a close-up of a selection of the blocks within the matrices. The single-tone moments computation matrix is significantly smaller, measuring only $4,050 \times 4,050$. It is also much more sparse, with only $67,788$ non-zero entries. The data in Table 5.4 shows a comparison of the sizes

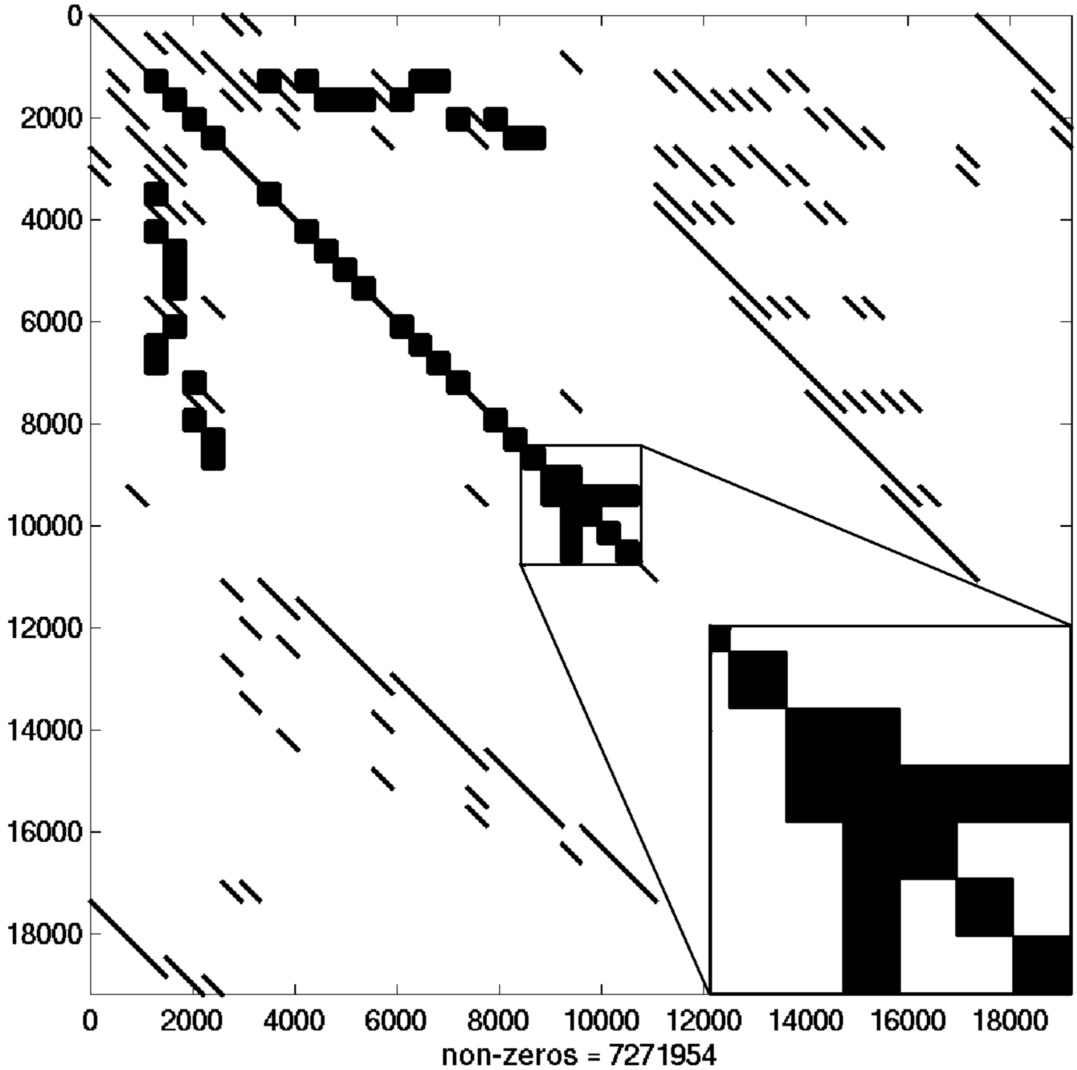

Fig. 5.11 Sparsity pattern of the Harmonic Balance Jacobian for the mixer circuit in example 2

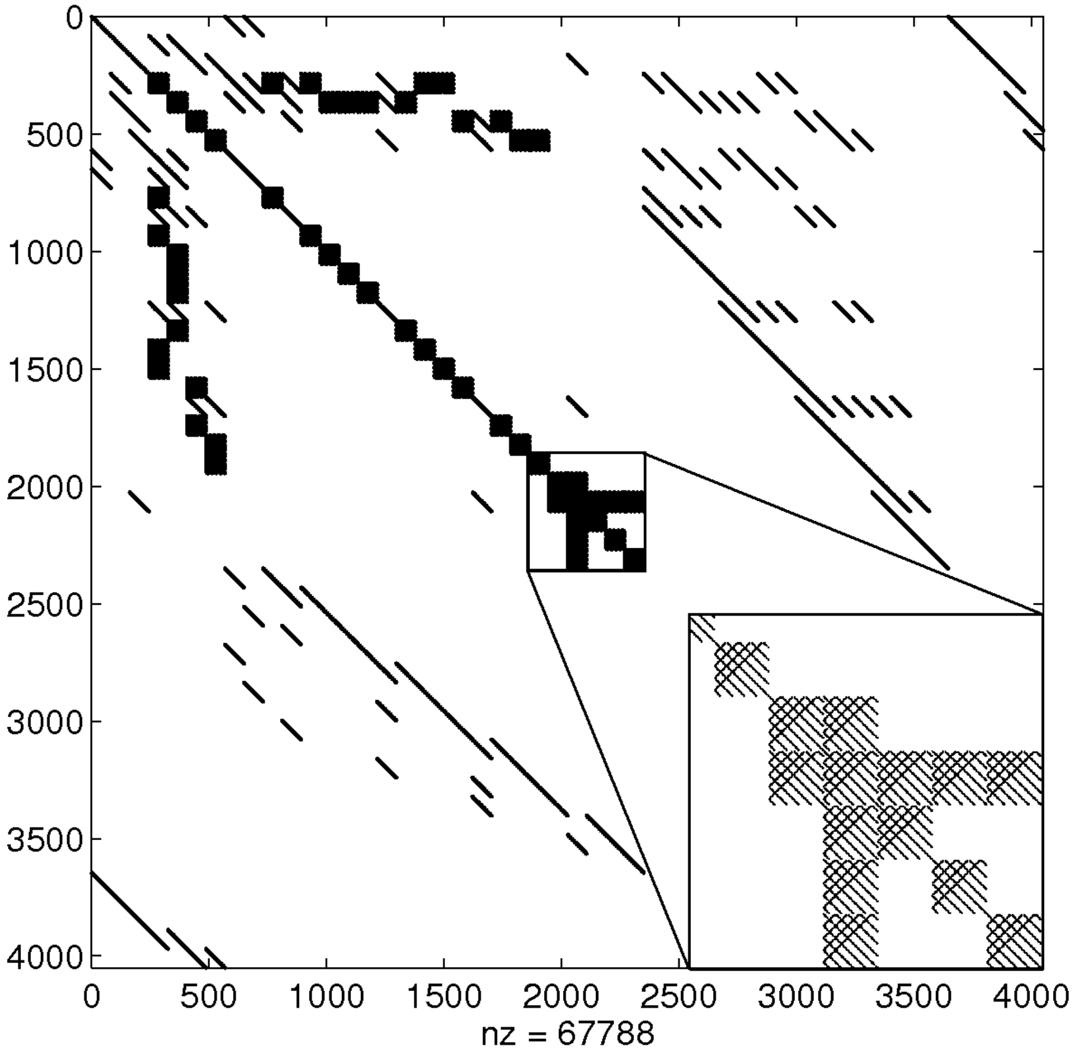

Fig. 5.12 Sparsity pattern of the moments computation matrix for the mixer circuit in example 2

of the moments computation matrices between this approach and the two-tone moments method for both example circuits.

The data in Table 5.2 shows a comparison of the computation times between the single-tone moments method, the two-tone moments method and the Harmonic Balance technique using a prototype MATLAB simulator. The hardware platform on which the simulations were run was a single-core Intel Xeon machine with a clock speed of 3.6 GHz and 4GB of RAM. The speed-up over a harmonic balance simulation was found to be 420 times for this mixer using 4 harmonics. This speed-up is due to two significant reasons. Firstly, the moments are computed using only a single RF tone in the new method (as opposed to two RF tones in the other methods) which significantly reduces the size of the matrices. The second reason is that the Harmonic Balance Jacobian is significantly more dense than the moments computation matrix as was shown earlier.

Table 5.4 Comparison of moments computation matrix sizes between the single-tone and the two-tone moments methods.

	2-tone moments	**1-tone moments**
Example 1	5,083×5,083	483×483
Example 2	18,450×18,450	4,050×4,050

5.6 Conclusion

In this chapter, a new method based on single-tone moment analysis was presented for the computation of the third order intercept point of RF circuits. This method does not require the solution of the Harmonic Balance equations and its computational cost is of the order of a solution of a sparse set of linear equations whose size is the same as the single-tone Harmonic Balance equations. The new method was shown to provide a speed-up that can be orders of magnitude faster than traditional multi-tone Harmonic Balance simulations.

Chapter 6

Efficient Sensitivity Analysis of Nonlinear Intermodulation Distortion

6.1 Introduction

One of the main bottlenecks in the design of RF front ends is the linearity requirement of some of the core blocks such as low noise amplifiers and mixers. Specifically, the effects of the third order nonlinear distortion are of particular importance since they mix back into the passband of the system and lead to many undesirable effects such as gain compression and adjacent channel interference. The key figure of merit for quantifying the third order nonlinear distortion is the third order intercept point (IP3). The computation of IP3 has, however, been a challenging problem due to the multi-tone input requirement which considerably slows down steady-state simulators based on techniques such as the Harmonic Balance method.

In this thesis, a new efficient method for computing the value of IP3 was presented. This method is based on the computation of the Harmonic Balance moments and does not require the solution of the Harmonic Balance equations. This reduced the CPU cost of finding the value of IP3 to that of solving a system of *sparse, linear* equations. However, the moments based approach presented in this thesis does not provide any insight into the sensitivity of IP3 with respect to various circuit parameters. In this chapter, two new approaches for computing the sensitivity of IP3 based on moments analysis are presented [24]–[26]. In the first approach, an analytical relationship is derived between the value of IP3 and the multi-dimensional Harmonic Balance moments [88]–[90]. In the second approach, closed form expressions are derived linking the sensitivity of IP3 to the moments of the adjoint solution [7], [27], [28]. The new approaches benefit from the same CPU cost advantage of the moments based approach while providing the sensitivity of IP3 with respect to circuit parameters. This would provide a critical advantage enabling circuit optimization, design space exploration and design centering. It is to be noted that similarly to the moments based approach for intermodulation distortion analysis, these methods are general and easily automated for any arbitrary circuit topology.

This chapter is organized into two main parts. The first part presents the method for sensitivity analysis using multi-dimensional moments while the second part focuses on the more efficient adjoint sensitivity analysis technique. The multi-dimensional moments section begins with a description of the multi-dimensional Harmonic Balance moments and how to compute them efficiently in section 6.2.1. The method by which sensitivity of IP3 is determined is presented in section 6.2.2. An example is shown in section 6.2.3 to demonstrate the accuracy of the results obtained using the new approach compared to those obtained using perturbation. The moments based adjoint sensitivity approach is presented in sections 6.3–6.8. Finally the conclusion is given in section 6.9.

6.2 Sensitivity Analysis Using Multi-Dimensional Moments

In the multi-dimensional moments approach, an analytical relationship is derived between the value of IP3 and the multi-dimensional Harmonic Balance moments (the moments with respect to the input RF power as well as the design parameters). This allows for the derivation of closed form expressions for the sensitivity of IP3 as a function of these multi-dimensional moments. The CPU cost of the operation is thus reduced to that of finding the moments which is of the same order as solving a system of sparse linear equations.

6.2.1 Computation of the Multi-Dimensional Moments

In order to define the multi-dimensional harmonic balance moments, the general harmonic balance formulation defined in (3.9) is re-written as

$$\bar{\boldsymbol{G}}\boldsymbol{X} + \bar{\boldsymbol{C}}\boldsymbol{X} + \lambda\bar{\boldsymbol{D}}\boldsymbol{X} + \boldsymbol{F}(\boldsymbol{X}) = \boldsymbol{B}_{DC} + \alpha\boldsymbol{B}_{RF}, \tag{6.1}$$

In this relation, λ is the change in the value of a general circuit parameter γ, such that

$$\gamma = \lambda_0 + \lambda \tag{6.2}$$

with λ_0 being the nominal value of the parameter. The matrix $\bar{\boldsymbol{D}}$ shows the location of the parameter in the Harmonic Balance equations.

The multi-dimensional moments of the system are defined as the coefficients of the Taylor Series expansion of the output solution vector $\boldsymbol{X}$ with respect to the input RF amplitude α and the change in the circuit parameter value λ. This can be expressed as

$$\boldsymbol{X} = \sum_{i=0}^{\infty}\sum_{j=0}^{\infty} \boldsymbol{N}_{(i,j)}\alpha^i\lambda^j \tag{6.3}$$

where $\boldsymbol{N}_{(i,j)}$ is the $(i,j)^{th}$ moment vector. Next, the algorithm for computing each of these moments efficiently is presented.

To determine the (0,0) moment vector, the coefficients of $\alpha^0\lambda^0$ on both sides of equation (6.1) are equated, which yields

$$\bar{\boldsymbol{G}}\boldsymbol{N}_{(0,0)} + \bar{\boldsymbol{C}}\boldsymbol{N}_{(0,0)} + \boldsymbol{F}(\boldsymbol{N}_{(0,0)}) = \boldsymbol{B}_{DC} \tag{6.4}$$

Solving this system of equations is basically finding the DC solution of the system from which the value of $\boldsymbol{N}_{(0,0)}$ is obtained. To determine the first order moments $\boldsymbol{N}_{(1,0)}$ and $\boldsymbol{N}_{(0,1)}$, once again powers of $\alpha^1\lambda^0$ and $\alpha^0\lambda^1$, respectively, on both sides of (6.1) are equated, which results in

$$\begin{aligned} \boldsymbol{\Phi}\boldsymbol{N}_{(1,0)} &= \boldsymbol{B}_{RF} &\quad (6.5)\\ \boldsymbol{\Phi}\boldsymbol{N}_{(0,1)} &= -\bar{\boldsymbol{D}}\boldsymbol{N}_{(0,0)} &\quad (6.6)\end{aligned}$$

where

$$\boldsymbol{\Phi} = (\bar{\boldsymbol{G}} + \bar{\boldsymbol{C}} + \boldsymbol{T}_{(0,0)}) \tag{6.7}$$

is the moments computation matrix that has the same structure as a Harmonic Balance Jacobian matrix evaluated at DC and is therefore significantly more sparse than a typical Harmonic Balance Jacobian. This is also the same moments computation matrix that was used in Chapters 4 and 5 to determine the harmonic balance moments for computing IP3. To compute the remaining moments, the following general relation can be solved recursively having already determined the

$\boldsymbol{N}_{(0,0)}$, $\boldsymbol{N}_{(0,1)}$ and $\boldsymbol{N}_{(1,0)}$ vectors,

$$\Phi \boldsymbol{N}_{(p,q)} = \begin{cases} -\dfrac{1}{p}\displaystyle\sum_{j=1}^{p-1}\sum_{k=0}^{q}(p-j)\boldsymbol{T}_{(j,k)}\boldsymbol{N}_{(p-j,q-k)} \\ \qquad -\displaystyle\sum_{i=1}^{q}\boldsymbol{T}_{(0,i)}\boldsymbol{N}_{(p,q-i)}, & (\text{if } q=0) \\ \\ -\dfrac{1}{q}\displaystyle\sum_{j=0}^{p}\sum_{k=1}^{q-1}(q-k)\boldsymbol{T}_{(j,k)}\boldsymbol{N}_{(p-j,q-k)} \\ -\bar{\boldsymbol{D}}\boldsymbol{N}_{(p,q-1)} - \displaystyle\sum_{i=1}^{p}\boldsymbol{T}_{(i,0)}\boldsymbol{N}_{(p-i,q)}, & (\text{if } q\neq 0) \end{cases} \tag{6.8}$$

In (6.7) and (6.8), the matrix $\boldsymbol{T}$ is defined as the partial derivatives of the nonlinear functions with respect to the variables in the circuit. This can be expressed as

$$\boldsymbol{T} = \frac{\partial \boldsymbol{F}(\boldsymbol{X})}{\partial \boldsymbol{X}} = \sum_{i=0}^{p}\sum_{j=0}^{q}\boldsymbol{T}_{(i,j)}\alpha^i\lambda^j \tag{6.9}$$

$$= \begin{bmatrix} \frac{\partial \boldsymbol{F_1}}{\partial \boldsymbol{X_1}} & \cdots & \frac{\partial \boldsymbol{F_1}}{\partial \boldsymbol{X_n}} \\ \vdots & \ddots & \vdots \\ \frac{\partial \boldsymbol{F_n}}{\partial \boldsymbol{X_1}} & \cdots & \frac{\partial \boldsymbol{F_n}}{\partial \boldsymbol{X_n}} \end{bmatrix} \tag{6.10}$$

Each $\frac{\partial \boldsymbol{F_k}}{\partial \boldsymbol{X_k}}$ in the matrix above is a block matrix in itself. To simplify the presentation, only one of these terms, $\boldsymbol{\psi} = \frac{\partial \boldsymbol{F_1}}{\partial \boldsymbol{X_1}}$, is considered. For the case of computing multi-dimensional moments, there is a need to determine $\boldsymbol{T}_{(i,j)}$. More specifically, there is a need to determine the block matrix $\boldsymbol{\psi}_{(i,j)}$, which can be found by evaluating the following relation

$$\boldsymbol{\psi}_{(i,j)} = \boldsymbol{\Gamma}^{-1} \begin{bmatrix} \left(\frac{\partial f_1}{\partial x_1}\right)_{(i,j)}\Big|_{t=t_0} & & 0 \\ & \ddots & \\ 0 & & \left(\frac{\partial f_1}{\partial x_1}\right)_{(i,j)}\Big|_{t=t_q} \end{bmatrix} \boldsymbol{\Gamma} \tag{6.11}$$

The matrix $\boldsymbol{\Gamma}$ is the inverse Fourier Transform matrix and $(t_0, t_1, \ldots, t_n)$ are equally spaced time samples [70]. The parameters $g_{(i,j)} = \left(\frac{\partial f_1}{\partial x_1}\right)_{(i,j)}$ are the partial derivatives of the nonlinear equations in the circuit with respect to one of the variables. For example, for a nonlinear diode current described by the relation $f_1 = I_s(e^{(x_1/V_T)} - 1)$ the following recursive relation can be utilized to evaluate $g_{(i,j)}$

$$g_{(i,j)} = \begin{cases} \dfrac{1}{pV_T}\displaystyle\sum_{j=0}^{p-1}\sum_{k=0}^{q}(p-j)g_{(j,k)}m_{(p-j,q-k)}, & \text{if } q=0 \\ \dfrac{1}{qV_T}\displaystyle\sum_{j=0}^{p}\sum_{k=0}^{q-1}(q-k)g_{(j,k)}m_{(p-j,q-k)}, & \text{if } q\neq 0 \end{cases} \tag{6.12}$$

A list of common nonlinear circuit elements and equations along with the recursive relations to evaluate their derivatives can be found in [17], [18].

6.2.2 Sensitivity of IP3

The objective of the multi-dimensional moments method is to determine the relative sensitivity of IP3 with respect to a parameter γ which is defined as follows

$$S_\gamma^{IP3} = \lambda_0\frac{\partial(IP3)}{\partial\gamma} = \lambda_0\frac{\partial(IP3)}{\partial\lambda} \tag{6.13}$$

since ($\lambda = \gamma - \lambda_0$) as given in (6.2).

In this section, an analytical closed form relation for the relative sensitivity of IP3 as a function of the multi-dimensional harmonic balance moments is presented. The first step is that of expanding the relation given in (6.3) and re-writing it as

$$\begin{aligned} \boldsymbol{X} &= \sum_{i=0}^{p}\sum_{j=0}^{q}\boldsymbol{N}_{(i,j)}\alpha^i\lambda^j \\ &= (\boldsymbol{N}_{(0,0)} + \boldsymbol{N}_{(0,1)}\lambda + \boldsymbol{N}_{(0,2)}\lambda^2 + \ldots) + \\ &\quad (\boldsymbol{N}_{(1,0)} + \boldsymbol{N}_{(1,1)}\lambda + \boldsymbol{N}_{(1,2)}\lambda^2 + \ldots)\alpha + \\ &\quad (\boldsymbol{N}_{(2,0)} + \boldsymbol{N}_{(2,1)}\lambda + \boldsymbol{N}_{(2,2)}\lambda^2 + \ldots)\alpha^2 + \\ &\quad \ldots \end{aligned} \tag{6.14}$$

In order to show the link between the multi-dimensional moments and the value of IP3, it is useful to label the summations that comprise the coefficients of α^n as follows

$$\begin{aligned}
\boldsymbol{M}_0 &= \boldsymbol{N}_{(0,0)} + \boldsymbol{N}_{(0,1)}\lambda + \boldsymbol{N}_{(0,2)}\lambda^2 + \ldots \\
\boldsymbol{M}_1 &= \boldsymbol{N}_{(1,0)} + \boldsymbol{N}_{(1,1)}\lambda + \boldsymbol{N}_{(1,2)}\lambda^2 + \ldots \\
\boldsymbol{M}_2 &= \boldsymbol{N}_{(2,0)} + \boldsymbol{N}_{(2,1)}\lambda + \boldsymbol{N}_{(2,2)}\lambda^2 + \ldots \\
\vdots \quad & \quad \vdots \\
\boldsymbol{M}_n &= \boldsymbol{N}_{(n,0)} + \boldsymbol{N}_{(n,1)}\lambda + \boldsymbol{N}_{(n,2)}\lambda^2 + \ldots
\end{aligned} \tag{6.15}$$

By substituting (6.15) into (6.14), the moments can be expressed using the following relation [17],

$$\begin{aligned}
\boldsymbol{X} &= \boldsymbol{M}_0 + \boldsymbol{M}_1\alpha + \boldsymbol{M}_2\alpha^2 + \boldsymbol{M}_3\alpha^3 + \ldots \\
&= \sum_{k=0}^{q} \boldsymbol{M}_k\alpha^k
\end{aligned} \tag{6.16}$$

This relation expresses the output solution vector $\boldsymbol{X}$ as a Taylor Series expansion of the input RF amplitude α only. The single-dimensional moment vectors $\boldsymbol{M}_n$ of the system are therefore defined as the coefficients of this Taylor series expansion. In sections 2.6 and 4.5, it was shown that the value of the input referred IP3 (IIP3) can be determined from the single-dimensional moments using the following relation

$$IIP3 = \sqrt{\frac{m_{1,1}}{m_{3,3}}} \tag{6.17}$$

The term $m_{1,1}$ represents the entry in the first moment vector at the fundamental frequency of $(\omega_{1,2})$ while the term $m_{3,3}$ represents the entry in the third moment vector at the third order intermodulation frequency (IM3) of $(2\omega_{1,2} - \omega_{2,1})$. For more details on how to obtain the terms $m_{1,1}$ and $m_{3,3}$, please refer to Chapter 4 of this thesis.

To perform a sensitivity analysis using the new approach, the sensitivity of the moments defined in (6.16) to changes in circuit parameters must first be determined. Once this is done, then the sensitivity of IP3 to these changes can be determined. To find the sensitivity of IP3 with respect to the parameter λ, taking the partial derivative of (6.17) results in

$$\frac{\partial}{\partial\lambda}(IIP3) = \frac{\partial}{\partial\lambda}\left(\frac{m_{1,1}}{m_{3,3}}\right)^{\frac{1}{2}} \quad (6.18)$$

$$= \frac{1}{2}\left(\frac{m_{1,1}}{m_{3,3}}\right)^{-\frac{1}{2}} \frac{m_{3,3}\frac{\partial}{\partial\lambda}(m_{1,1}) - m_{1,1}\frac{\partial}{\partial\lambda}(m_{3,3})}{(m_{3,3})^2} \quad (6.19)$$

From these relations, it can be seen that the task of determining the sensitivity of IP3 with respect to a certain circuit parameter λ, is reduced to finding the sensitivity of the first and third moment vectors with respect to that same parameter. With this being the case, the relation in (6.19) now becomes

$$S_{\lambda}^{IIP3} = \frac{\lambda_0}{2}\left(\frac{n^1_{(1,0)}}{n^3_{(3,0)}}\right)^{-\frac{1}{2}} \frac{n^3_{(3,0)}n^1_{(1,1)} - n^1_{(1,0)}n^3_{(3,1)}}{(n^3_{(3,0)})^2} \quad (6.20)$$

In the above relation, $n^1_{(1,0)}$ is the entry in the (0,0) moment vector at the fundamental frequency and $n^3_{(3,0)}$ is the entry in the (3,0) moment vector at the third order intermodulation frequency. Both of these terms are equivalent to $m_{1,1}$ and $m_{3,3}$, respectively, when evaluated at $\gamma = \lambda_0$. The new terms, $n^1_{(1,1)}$ and $n^3_{(3,1)}$ represent the first derivatives of the first and third moment vectors with respect to the parameter γ evaluated at $\gamma = \lambda_0$. These correspond to the entries in the (1,1) moment vector at the fundamental frequency, and in the (3,1) moment vector at the IM3 frequency, respectively. The location of these terms in the moment vectors is more clearly illustrated in Fig. 6.1.

In summary, the new approach presents an efficient way to determine the sensitivity of IP3 from the Harmonic Balance moments of a circuit, without the need for a Harmonic Balance simulation. This therefore adds insight into the main sources of nonlinear distortion to the moments method presented in this thesis, while still being easily automated and general for arbitrary topologies. This method is computationally very cheap since the CPU cost of determining these moments is the solution of a system of linear and sparse algebraic equations. An overview of the main steps of the algorithm is given in Fig. 6.2.

6.2.3 Numerical Example

In this section the value of IP3 and its sensitivity with respect to some parameters are determined for an example amplifier circuit using the multi-dimensional moments method. These results are then compared to those obtained using perturbation to demonstrate the accuracy of the new

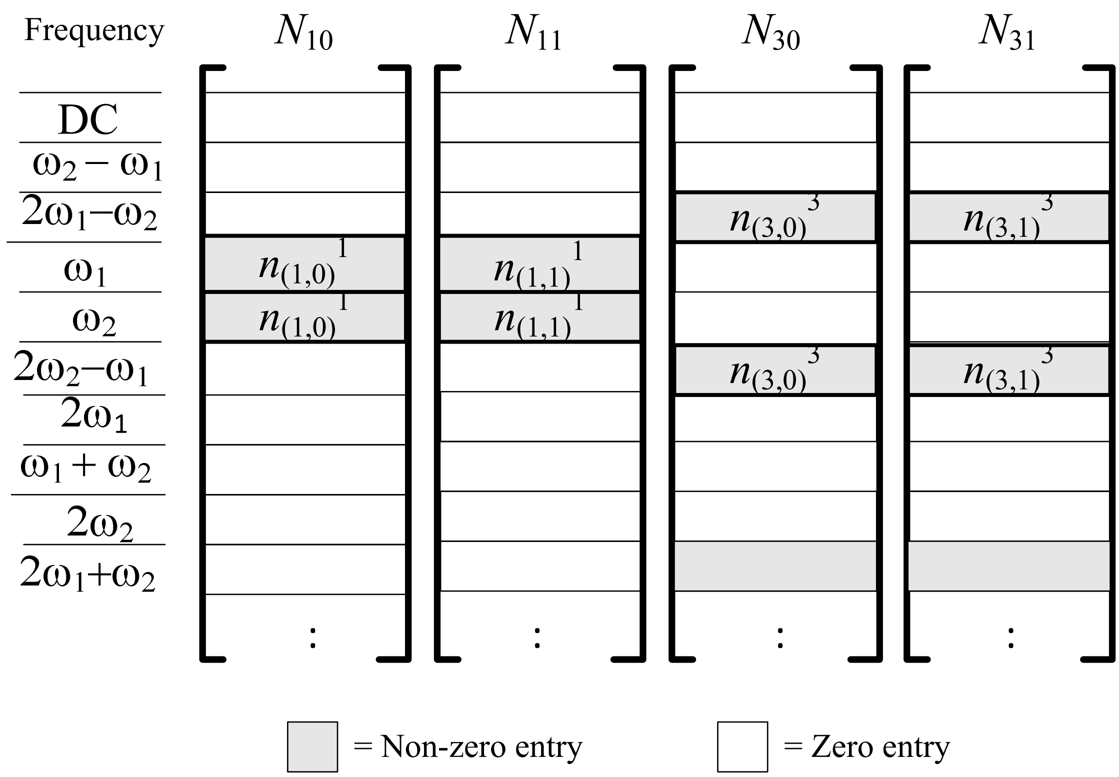

Fig. 6.1 Location of sensitivity terms in the multi-dimensional moment vectors

1. Determine the value of the third order intercept point efficiently using the relation in (6.17).
2. Select which parameter γ needs to be changed by an amount λ, and set-up the modified circuit equations as given by (6.1).
3. Compute the multi-dimensional moments with respect to λ and the RF amplitude α as defined in (6.3) by solving the relations given (6.4)–(6.8).
4. Determine the value of IP3 sensitivity with respect to λ by solving (6.20) using the terms extracted from the moments at the locations illustrated in Fig.6.1.

Fig. 6.2 Summary of the algorithm for computing the sensitivity of IP3 using multi-dimensional moments.

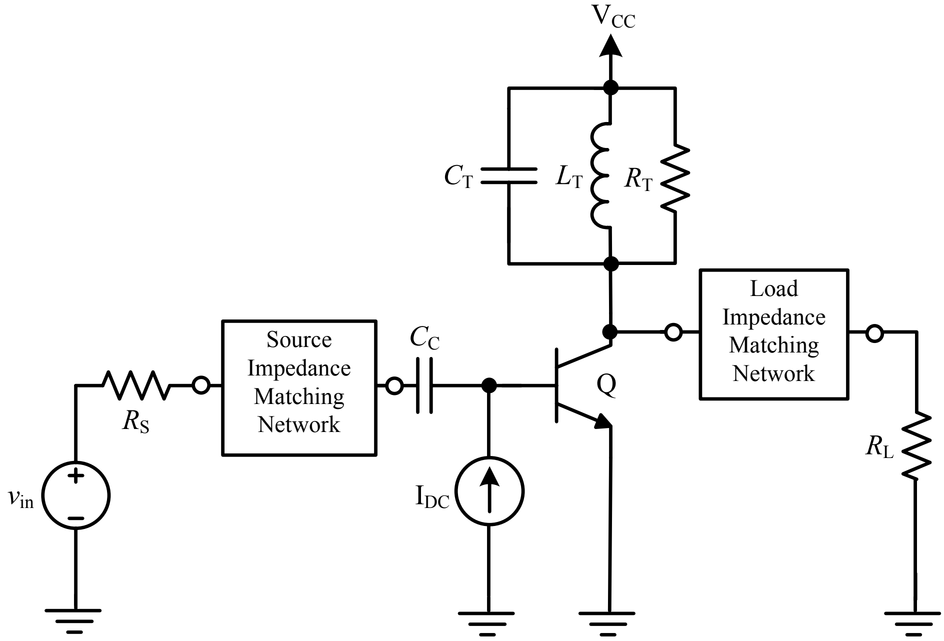

Fig. 6.3 Example circuit diagram

approach. In addition, the CPU cost of obtaining IP3 and its sensitivity using the new approach is compared to the CPU cost of using Harmonic Balance. Typically, the value of IP3 is expressed in dBm in the literature. However, for the sake of sensitivity analysis the results are expressed in Volts as the numbers are more meaningful.

Consider the Low Noise Amplifier circuit shown in Fig. 6.3. The value of IIP3 in this circuit was found to be -12.02 dBm with two input tones at frequencies of $f_1 = 1$ GHz and $f_2 = 1.01$ GHz using the moments computation method. We wish to compute the normalized sensitivities of IP3 with respect to changes in the parameters of R_T and C_T.

To find the sensitivity of IP3 with respect to the resistor R_T, the multi-dimensional moments are first computed, with the matrix $\bar{\boldsymbol{D}}$ in (6.1) being the Harmonic Balance stamp of the resistor. Once these moments are computed, the sensitivity is determined using (6.20). The relative sensitivity found was $7.0864 \times 10^{-4}V$. To compute the sensitivity with respect to the capacitor C_T, the multi-dimensional moments are computed with the matrix $\bar{\boldsymbol{D}}$ being the Harmonic Balance stamp of the capacitor. The relative sensitivity obtained was $6.9464 \times 10^{-4}V$. The results for both circuit parameters are summarized in Table 6.1 where they are also compared to the results obtained using perturbation. As can be seen from the table, the results are very accurate. It is also important to note that the accuracy of the results obtained using the moments approach is independent of step size unlike those obtained using perturbation.

Table 6.1 Normalized sensitivity of IP3 with respect to circuit parameters for the example circuit

	Perturbation Sensitivity	**Moments Method Sensitivity**	**% Error**
R_T	7.0828×10^{-4} V	7.0864×10^{-4} V	0.005%
C_T	6.9459×10^{-4} V	6.9464×10^{-4} V	0.002%

Table 6.2 shows a comparison of the computation times between traditional Harmonic Balance and the multi-dimensional moments method for determining IP3 and its sensitivity with respect to the two parameters R_T and C_T. As can be seen, the moments method presents significant computational speedup. The CPU cost of both the moments approach and the harmonic balance based approach [7] consists of two parts: A fixed cost due to the computation of IP3, and an incremental cost per parameter for computing the sensitivity. In this example the fixed cost for Harmonic balance was 19.58 seconds, and for the moments approach it was 0.94 seconds. For the incremental cost, it was 0.16 seconds/parameter for the moments approach, and 0.01 seconds/parameter for harmonic balance. Note that the small incremental cost for Harmonic Balance (which is due to the use of the adjoint technique [7]) is more than offset by the very large initial fixed cost. The hardware platform on which the simulations were run was a single-core Intel Pentium 4 machine with a clock speed of 3.2 GHz and 3GB of RAM.

Table 6.2 CPU cost comparison of finding IP3 and its sensitivity with respect to 2 parameters for the example circuit

Harmonic Balance	**Multi-Dimensional Moments Method**	**Speed-up**
19.61 seconds	1.26 seconds	15.5 times

6.3 Adjoint Moments Sensitivity Method

In this thesis, an efficient method for computing the value of IP3 was presented based on the computation of the Harmonic Balance moments which reduced the CPU cost to that of solving a system of *sparse, linear* equations. However, this approach did not provide any insight into the sensitivity of IP3 with respect to various circuit parameters. For any sensitivity analysis to be performed, only the brute-force perturbation approach could be employed, which is very inefficient, or the multi-dimensional moments method presented in section 6.2. However, the multi-dimensional moments method also has some key limitations, first in that it is limited to sensitivities of linear parameters, and also the fact that it computes the sensitivity of all variables with respect to one parameter at a time.

In this section, a new approach for computing the sensitivity of IP3 based on the adjoint sensitivity method is presented. The new method computes the sensitivity with respect to all parameters in the general circuit equations including parameters of linear and nonlinear circuit elements. For this approach, closed form expressions for the sensitivity of IP3 as a function of the entries in the adjoint moments for all circuit parameters are developed. The adjoint moments are computed using the same set of *linear* equations used to determine the harmonic balance moments. The new moments method thereby retains the main advantages of the adjoint sensitivity algorithm, namely that of low incremental computation cost and the ability to find the sensitivity of one variable with respect to all the parameters in the system while providing significant speedup over traditional harmonic balance methods. It is to be noted that similarly to the moments based approach for computing IP3, the method is general and easily automated for any arbitrary circuit topology.

The derivation of the moments based adjoint sensitivity algorithm begins with brief overviews of the harmonic balance adjoint formulation and the moments based technique for computing IP3 in sections 6.4 and 6.5 respectively. These sections provide the necessary background information for the method which starts with the adjoint sensitivity derivation using moments in section 6.6. This is followed by the algorithms for the efficient computation of the harmonic balance moments, the moments of the adjoint equation and the moments of the nonlinear vector in section 6.7. Finally, numerical examples are shown in section 6.8 to demonstrate the accuracy of the results obtained as compared to those obtained using the harmonic balance adjoint method.

6.4 Harmonic Balance Adjoint Sensitivity

The adjoint approach has been a classical tool for the efficient and exact sensitivity analysis of circuits. This can be achieved by solving an adjoint system. In this section, the harmonic balance adjoint system formulation for nonlinear circuits with respect to a general circuit parameter λ is presented [7]. This will lay the foundation for the new approach presented in section 6.6, in which the method for obtaining the adjoint solution efficiently using the adjoint moments without the need for a harmonic balance solution will be shown.

It is useful to begin the derivation by expressing the harmonic balance equations in (3.9) as

$$\boldsymbol{A}\left(\lambda\right)\boldsymbol{X}\left(\lambda\right)+\boldsymbol{F}\left(\lambda,\boldsymbol{X}\left(\lambda\right)\right)=\boldsymbol{B} \tag{6.21}$$

where

$$\boldsymbol{A}=\bar{\boldsymbol{G}}+\bar{\boldsymbol{C}} \tag{6.22}$$

is a matrix that represents the linear elements in the circuit. The output variable of interest, X_{out}, can be expressed using a selection vector as

$$X_{out}=\boldsymbol{d}^{T}\boldsymbol{X} \tag{6.23}$$

where $\boldsymbol{d}$ is a selection vector with all entries set to zero except at the location of the variable X_{out} in the general vector of unkowns $\boldsymbol{X}$ where the entry is equal to '1'. The harmonic balance adjoint solution vector $\boldsymbol{X}_a$ for nonlinear circuits is defined using the general relation given by [7]

$$\boldsymbol{J}^{T}\boldsymbol{X}_{a}=-\boldsymbol{d} \tag{6.24}$$

where

$$\boldsymbol{J}=\boldsymbol{A}+\frac{\partial\boldsymbol{F}(\boldsymbol{X})}{\partial\boldsymbol{X}} \tag{6.25}$$

is the harmonic balance Jacobian matrix.

The general expression for the adjoint sensitivity with respect to a general circuit parameter λ can now be written as [7]

$$\frac{\partial X_{out}}{\partial\lambda}=\boldsymbol{X}_{a}^{T}\frac{\partial\boldsymbol{A}}{\partial\lambda}\boldsymbol{X}+\boldsymbol{X}_{a}^{T}\frac{\partial\boldsymbol{F}(\boldsymbol{X})}{\partial\lambda} \tag{6.26}$$

For the case when λ is a parameter that only affects a linear circuit element, only $\boldsymbol{A}$ and $\boldsymbol{X}$ will be functions of λ. Therefore, the relation given in (6.26) can be simplified to

$$\frac{\partial X_{out}}{\partial \lambda} = \boldsymbol{X}_a^T \frac{\partial \boldsymbol{A}}{\partial \lambda} \boldsymbol{X} \tag{6.27}$$

with the matrix $\frac{\partial A}{\partial \lambda}$ being the harmonic balance 'stamp' of the derivative of the circuit element that λ is a parameter of.

In the case when the parameter λ is that of a nonlinear circuit element, only $\boldsymbol{X}$ and $\frac{\partial F(X)}{\partial \lambda}$ will be functions of λ. The general adjoint equation given in (6.26) would then simplify to become

$$\frac{\partial X_{out}}{\partial \lambda} = \boldsymbol{X}_a^T \frac{\partial \boldsymbol{F}(\boldsymbol{X})}{\partial \lambda} \tag{6.28}$$

with the matrix $\frac{\partial F(X)}{\partial \lambda}$ being the sensitivity of the nonlinear vector.

6.5 Moments Based Sensitivity Computation

In this thesis, an efficient method for the computation of IP3 based on the harmonic balance moments was presented. The harmonic balance moments are defined as the Taylor coefficients of the unknown variable $\boldsymbol{X}$ in (3.9) with respect to the input signal amplitude α [17], [18]. The vector $\boldsymbol{X}$ can therefore be written as

$$\begin{aligned} \boldsymbol{X} &= \boldsymbol{M}_0 + \boldsymbol{M}_1\alpha + \boldsymbol{M}_2\alpha^2 + \boldsymbol{M}_3\alpha^3 + \dots \\ &= \sum_{i=0}^{\infty} \boldsymbol{M}_i \alpha^i \end{aligned} \tag{6.29}$$

where $\boldsymbol{M}_k$ is the k^{th} moment vector. In this thesis, a relationship was derived between the above moments and the value of the input referred third order intercept point (IP3) such that

$$\mathrm{IP3} = \sqrt{\frac{m_{1,1}}{m_{3,3}}} \tag{6.30}$$

where $m_{1,1}$ and $m_{3,3}$ are specific entries in the moment vectors $\boldsymbol{M}_1$ and $\boldsymbol{M}_3$, respectively. The locations of $m_{1,1}$ and $m_{3,3}$ for circuits excited with a two-tone input signal at frequencies of ω_1 and ω_2 are shown in Fig. 6.4 for amplifier circuits and in Fig. 6.5 for mixer circuits. Note that the additional frequency tone ω_0 is that of the local oscillator signal in the mixer case. Using this method, the computation of IP3 is reduced to that of finding the harmonic balance moments, which is a much cheaper problem in terms of computational cost than that of solving the harmonic balance equations.

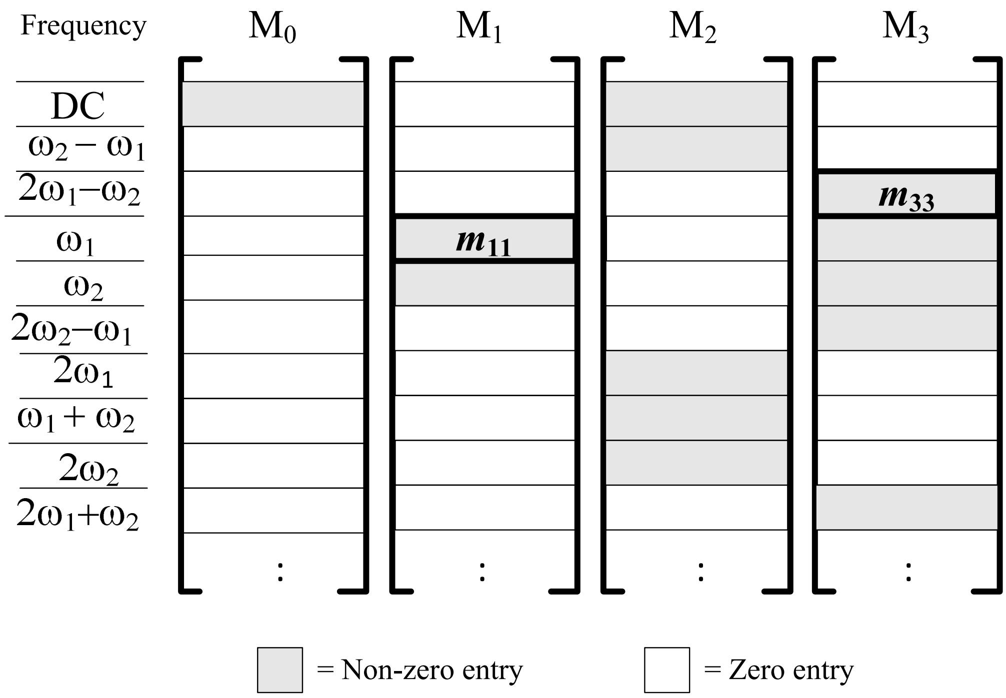

Fig. 6.4 Location of sensitivity terms in the moment vectors for amplifier circuits

Using equation (6.30), the sensitivity of IP3 with respect to λ can be expressed as

$$\frac{\partial}{\partial \lambda}(IP3) = \frac{1}{2}\left(\frac{m_{1,1}}{m_{3,3}}\right)^{-\frac{1}{2}} \frac{m_{3,3}\frac{\partial m_{1,1}}{\partial \lambda} - m_{1,1}\frac{\partial m_{3,3}}{\partial \lambda}}{(m_{3,3})^2} \tag{6.31}$$

The evaluation of the sensitivity therefore requires the terms m_{11} and m_{33} which were also required for obtaining the value of IP3 according to (6.30) and are already available from the computation of IP3. In addition to these terms, now the values of their derivatives with respect to λ ($\frac{\partial m_{1,1}}{\partial \lambda}$ and $\frac{\partial m_{3,3}}{\partial \lambda}$) are also required, the efficient computation of which is the subject of the remainder of this chapter.

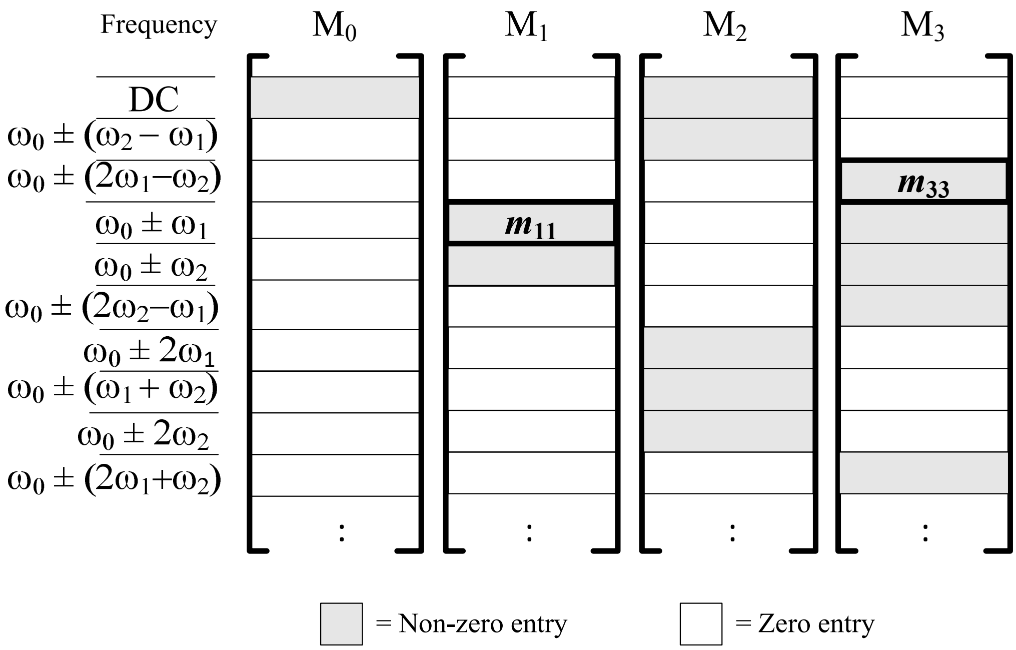

Fig. 6.5 Location of sensitivity terms in the moment vectors for mixer circuits

6.6 Adjoint Sensitivity Derivation Using Moments

In this method, a sensitivity analysis algorithm is derived that is applicable to the moments based method and shares the same properties as the adjoint algorithm, namely those of low incremental computation cost to the original algorithm and the ability to determine the sensitivity of one variable with respect to all the circuit parameters. This is accomplished by the efficient computation of the adjoint moment vectors.

In the previous section, the problem of computing the sensitivity of IP3 was reduced to that of finding the derivatives with respect to λ of the terms $m_{1,1}$ and $m_{3,3}$. In this section the derivation of an efficient adjoint based approach for computing these derivatives is presented. We start by recalling the definition of the harmonic balance moments

$$\boldsymbol{X} = \boldsymbol{M}_0 + \boldsymbol{M}_1\alpha + \boldsymbol{M}_2\alpha^2 + \boldsymbol{M}_3\alpha^3 + \ldots \tag{6.32}$$

As illustrated in Fig. 6.4 and Fig. 6.5, the terms $m_{1,1}$ and $m_{3,3}$ can be written as

$$m_{11} = \boldsymbol{d}_1^T \boldsymbol{M}_1 \tag{6.33}$$

$$m_{33} = \boldsymbol{d}_3^T \boldsymbol{M}_3 \tag{6.34}$$

where $\boldsymbol{d}_1$ and $\boldsymbol{d}_3$ are selection vectors. Note that m_{11} and m_{33} appear in the Taylor expansions of $\boldsymbol{X}_{o1}$ and $\boldsymbol{X}_{o3}$ defined as

$$\boldsymbol{X}_{o1} = \boldsymbol{d}_1^T \boldsymbol{X} = m_{1,0} + m_{1,1}\alpha + m_{1,2}\alpha^2 + m_{1,3}\alpha^3 + \ldots \tag{6.35}$$

$$\boldsymbol{X}_{o3} = \boldsymbol{d}_3^T \boldsymbol{X} = m_{3,0} + m_{31}\alpha + m_{3,2}\alpha^2 + m_{3,3}\alpha^3 + \ldots \tag{6.36}$$

The derivatives of $\boldsymbol{X}_{o1}$ and $\boldsymbol{X}_{o3}$ with respect to λ can now be written as

$$\frac{\partial X_{o1}}{\partial \lambda} = \frac{\partial m_{1,0}}{\partial \lambda} + \boldsymbol{\frac{\partial m_{1,1}}{\partial \lambda}}\alpha + \frac{\partial m_{1,2}}{\partial \lambda}\alpha^2 + \frac{\partial m_{1,3}}{\partial \lambda}\alpha^3 + \ldots \tag{6.37}$$

$$\frac{\partial X_{o3}}{\partial \lambda} = \frac{\partial m_{3,0}}{\partial \lambda} + \frac{\partial m_{3,1}}{\partial \lambda}\alpha + \frac{\partial m_{3,2}}{\partial \lambda}\alpha^2 + \boldsymbol{\frac{\partial m_{3,3}}{\partial \lambda}}\alpha^3 + \ldots \tag{6.38}$$

From these equations, it can be deduced that the terms $\frac{\partial m_{1,1}}{\partial \lambda}$ and $\frac{\partial m_{3,3}}{\partial \lambda}$ required in (6.19) are the first and third moments of the expansions of $\frac{\partial X_{o1}}{\partial \lambda}$ and $\frac{\partial X_{o3}}{\partial \lambda}$, respectively. In order to compute these moments, the first step is to use the adjoint sensitivity expression in (6.26) to write

$$\frac{\partial X_{o1}}{\partial \lambda} = \boldsymbol{X}_{a1}^T \frac{\partial \boldsymbol{A}}{\partial \lambda}\boldsymbol{X} + \boldsymbol{X}_{a1}^T \frac{\partial \boldsymbol{F}(\boldsymbol{X})}{\partial \lambda} \tag{6.39}$$

$$\frac{\partial X_{o3}}{\partial \lambda} = \boldsymbol{X}_{a3}^T \frac{\partial \boldsymbol{A}}{\partial \lambda}\boldsymbol{X} + \boldsymbol{X}_{a3}^T \frac{\partial \boldsymbol{F}(\boldsymbol{X})}{\partial \lambda} \tag{6.40}$$

where $\boldsymbol{X}_{a1}$ and $\boldsymbol{X}_{a3}$ are the solutions of the Adjoint equations

$$\boldsymbol{J}^T \boldsymbol{X}_{a1} = -\boldsymbol{d}_1 \tag{6.41}$$

$$\boldsymbol{J}^T \boldsymbol{X}_{a3} = -\boldsymbol{d}_3 \tag{6.42}$$

From (6.39) and (6.40) it can be seen that the moments of $\frac{\partial X_{o1}}{\partial \lambda}$ and $\frac{\partial X_{o3}}{\partial \lambda}$ can be expressed in terms of the moments of $\boldsymbol{X}$, $\boldsymbol{X}_{a1}$, $\boldsymbol{X}_{a3}$ and $\frac{\partial F(X)}{\partial \lambda}$. The evaluation of these moments is the focus of the next two subsections. First, the case of λ being a parameter of a linear element is presented followed by the case of λ being a parameter of a nonlinear element.

6.6.1 Linear Parameter Sensitivity

For the case of λ being a parameter of a linear element, equations (6.39) and (6.40) can be simplified to

$$\frac{\partial X_{o1}}{\partial \lambda} = \boldsymbol{X}_{a1}^T \frac{\partial \boldsymbol{A}}{\partial \lambda} \boldsymbol{X} \tag{6.43}$$

$$\frac{\partial X_{o3}}{\partial \lambda} = \boldsymbol{X}_{a3}^T \frac{\partial \boldsymbol{A}}{\partial \lambda} \boldsymbol{X} \tag{6.44}$$

with $\boldsymbol{X}_{a1}$ and $\boldsymbol{X}_{a3}$ being the solutions of the adjoint equations shown in (6.41) and (6.42). The adjoint moment vectors are defined as the Taylor series coefficients of the expansion of the adjoint solution vector $\boldsymbol{X}_a$, defined in (6.24), with respect to the signal amplitude voltage α. The expansions of $\boldsymbol{X}_{a1}$ and $\boldsymbol{X}_{a3}$ can therefore be expressed as

$$\begin{aligned} \boldsymbol{X}_{a1} &= \boldsymbol{M}_{a10} + \boldsymbol{M}_{a11}\alpha + \boldsymbol{M}_{a12}\alpha^2 + \boldsymbol{M}_{a13}\alpha^3 + \ldots \\ &= \sum_{i=0}^{\infty} \boldsymbol{M}_{a1i}\alpha^i \end{aligned} \tag{6.45}$$

$$\begin{aligned} \boldsymbol{X}_{a3} &= \boldsymbol{M}_{a30} + \boldsymbol{M}_{a31}\alpha + \boldsymbol{M}_{a32}\alpha^2 + \boldsymbol{M}_{a33}\alpha^3 + \ldots \\ &= \sum_{i=0}^{\infty} \boldsymbol{M}_{a3i}\alpha^i \end{aligned} \tag{6.46}$$

where $\boldsymbol{M}_{a1k}$ is the k^{th} adjoint moment vector of $\boldsymbol{X}_{a1}$ and $\boldsymbol{M}_{a3k}$ is the k^{th} adjoint moment vector of $\boldsymbol{X}_{a3}$. By substituting (6.29), (6.37) and (6.45) in (6.43), and also substituting (6.29), (6.38) and (6.46) in (6.44), the final expressions in terms of the moments are obtained. Then, by equating powers of α and α^3 on both sides of the resulting expressions, the following relations are obtained

$$\frac{\partial m_{1,1}}{\partial \lambda} = \boldsymbol{M}_{a10}^T \left(\frac{\partial \boldsymbol{A}}{\partial \lambda}\right) \boldsymbol{M}_1 + \boldsymbol{M}_{a11}^T \left(\frac{\partial \boldsymbol{A}}{\partial \lambda}\right) \boldsymbol{M}_0 \tag{6.47}$$

$$\begin{aligned} \frac{\partial m_{3,3}}{\partial \lambda} &= \boldsymbol{M}_{a30}^T \left(\frac{\partial \boldsymbol{A}}{\partial \lambda}\right) \boldsymbol{M}_3 + \boldsymbol{M}_{a31}^T \left(\frac{\partial \boldsymbol{A}}{\partial \lambda}\right) \boldsymbol{M}_2 + \\ &\quad \boldsymbol{M}_{a32}^T \left(\frac{\partial \boldsymbol{A}}{\partial \lambda}\right) \boldsymbol{M}_1 + \boldsymbol{M}_{a33}^T \left(\frac{\partial \boldsymbol{A}}{\partial \lambda}\right) \boldsymbol{M}_0 \end{aligned} \tag{6.48}$$

It is important to note that the matrix $\frac{\partial A}{\partial \lambda}$ contains only the harmonic balance 'stamp' of the derivative of the element that λ is a parameter of, and is therefore an extremely sparse matrix with at most four non-zero block entries [9]. In fact the computations above can be further simplified based on the type of element that λ is a parameter of without the need for $\frac{\partial A}{\partial \lambda}$. For example, in the case of a linear resistor of nominal value R_0 that is connected between indexes i and j, (6.47) and (6.48) become

$$\begin{aligned}
\frac{\partial m_{1,1}}{\partial \lambda} = \quad & -\frac{1}{{R_0}^2}\left[\left(\boldsymbol{M}^T_{a10,i} - \boldsymbol{M}^T_{a10,j}\right)\left(\boldsymbol{M}_{1,i} - \boldsymbol{M}_{1,j}\right)\right. \\
& \left. + \left(\boldsymbol{M}^T_{a11,i} - \boldsymbol{M}^T_{a11,j}\right)\left(\boldsymbol{M}_{0,i} - \boldsymbol{M}_{0,j}\right)\right] \qquad (6.49) \\
\frac{\partial m_{3,3}}{\partial \lambda} = \quad & -\frac{1}{{R_0}^2}\left[\left(\boldsymbol{M}^T_{a30,i} - \boldsymbol{M}^T_{a30,j}\right)\left(\boldsymbol{M}_{3,i} - \boldsymbol{M}_{3,j}\right)\right. \\
& + \left(\boldsymbol{M}^T_{a31,i} - \boldsymbol{M}^T_{a31,j}\right)\left(\boldsymbol{M}_{2,i} - \boldsymbol{M}_{2,j}\right) \\
& + \left(\boldsymbol{M}^T_{a32,i} - \boldsymbol{M}^T_{a32,j}\right)\left(\boldsymbol{M}_{1,i} - \boldsymbol{M}_{1,j}\right) \\
& \left. + \left(\boldsymbol{M}^T_{a33,i} - \boldsymbol{M}^T_{a33,j}\right)\left(\boldsymbol{M}_{0,i} - \boldsymbol{M}_{0,j}\right)\right] \qquad (6.50)
\end{aligned}$$

6.6.2 Nonlinear Parameter Sensitivity

For the case of λ being a parameter of a nonlinear element, equations (6.39) and (6.40) can be simplified to

$$\frac{\partial X_{o1}}{\partial \lambda} = \boldsymbol{X}^T_{a1}\frac{\partial \boldsymbol{F}(\boldsymbol{X})}{\partial \lambda} \qquad (6.51)$$

$$\frac{\partial X_{o3}}{\partial \lambda} = \boldsymbol{X}^T_{a3}\frac{\partial \boldsymbol{F}(\boldsymbol{X})}{\partial \lambda} \qquad (6.52)$$

For this case, we also need to define and compute the moments of the derivative of $\boldsymbol{F}(\boldsymbol{X})$ with respect to λ. This is given by

$$\begin{aligned}
\frac{\partial \boldsymbol{F}(\boldsymbol{X})}{\partial \lambda} = \boldsymbol{G}(\boldsymbol{X}) \quad &= \quad \boldsymbol{G}_0 + \boldsymbol{G}_1\alpha + \boldsymbol{G}_2\alpha^2 + \boldsymbol{G}_3\alpha^3 + \ldots \\
&= \quad \sum_{k=0}^{\infty} \boldsymbol{G}_k\alpha^k \qquad (6.53)
\end{aligned}$$

where $\boldsymbol{G}_k$ is the k^{th} moment of $\frac{\partial F(X)}{\partial \lambda}$. By substituting (6.37), (6.45) and (6.53) into (6.51) and also (6.38), (6.46) and (6.53) into (6.52), then equating powers of α and α^3 on both sides of the resulting expressions, we obtain

$$\frac{\partial m_{1,1}}{\partial \lambda} = \boldsymbol{M}_{a10}^T \boldsymbol{G}_1 + \boldsymbol{M}_{a11}^T \boldsymbol{G}_0 \tag{6.54}$$

$$\begin{aligned} \frac{\partial m_{3,3}}{\partial \lambda} &= \boldsymbol{M}_{a30}^T \boldsymbol{G}_3 + \boldsymbol{M}_{a31}^T \boldsymbol{G}_2 + \\ &\quad \boldsymbol{M}_{a32}^T \boldsymbol{G}_1 + \boldsymbol{M}_{a33}^T \boldsymbol{G}_0 \end{aligned} \tag{6.55}$$

What remains now is to show how the computation of all the moments ($\boldsymbol{M}_k$, $\boldsymbol{M}_{a1k}$, $\boldsymbol{M}_{a3k}$ and $\boldsymbol{G}_k$) in (6.49), (6.50) and in (6.54),(6.55) can be achieved with very low computation cost. This is the focus of section 6.7.

6.6.3 Extension to IP3 Sensitivity Using Single-tone Moments

It was shown in Chapter 5 that it is possible to determine the value of IP3 using only single-tone moments analysis [22], [23], thereby considerably reducing the size of the system of equations which leads to significant CPU cost savings. In this case, it was shown that the value of IP3 can be obtained from the single-tone moments expansion by evaluating the expression given by (5.54) and repeated here as

$$IIP3 = \sqrt{\frac{m_{1,1}}{m_{1,3}}} \tag{6.56}$$

It is possible to determine the sensitivity of IP3 when only single-tone inputs are used by applying a logical extension of the adjoint moments method presented in this section. More specifically, the term $m_{3,3}$ in equations (6.30)-(6.55) is replaced by $m_{1,3}$ and by using the selection vector $\boldsymbol{d}_1$ instead of $\boldsymbol{d}_3$. The remainder of the algorithm remains essentially the same, including all the moments computation algorithms presented in the next section.

6.7 Moments Computation Algorithms

In the previous sections, simple closed form relationships were derived for computing IP3 and its sensitivity as a function of the harmonic balance moments and the adjoint moments. The bulk of the computation cost is thus spent on computing the moments. In this section, the moments computation algorithms are presented and their efficiencies as compared to traditional harmonic balance simulations are discussed. In section 6.7.1 the traditional harmonic balance moments computation is reviewed, followed by the adjoint moments and the moments of the nonlinear vector in sections 6.7.2 and 6.7.3.

6.7.1 Computation of the Harmonic Balance Moments

In this section, the moments algorithm presented in section 4.3 for computing the harmonic balance moments $\boldsymbol{M}_k$ defined in (6.29) is briefly reviewed.

The zeroth moment vector $\boldsymbol{M}_0$ is obtained by finding the solution of the system described by the Harmonic Balance formulation given in (3.9) with the RF signal amplitude α set to zero. For the remaining moments, the nonlinear harmonic balance Jacobian is expressed as a Taylor series expansion with respect to α as given by

$$\frac{\partial \boldsymbol{F}(\boldsymbol{X})}{\partial \boldsymbol{X}} = \sum_{i=0}^{\infty} \boldsymbol{T}_i \alpha^i \tag{6.57}$$

Substituting (6.29) and (6.57) into (3.9), then equating powers of α on both sides of the resulting expression allows for the computation of the remaining moment vectors $\boldsymbol{M}_n$. The system of equations that need to be solved are given by

$$\begin{aligned} \boldsymbol{\Phi} \boldsymbol{M}_1 &= \boldsymbol{B}_{RF} && (6.58) \\ \boldsymbol{\Phi} \boldsymbol{M}_n &= -\frac{1}{n} \sum_{j=1}^{n-1} (n-j) \boldsymbol{T}_j \boldsymbol{M}_{n-j}, \quad n \geq 2 && (6.59) \end{aligned}$$

with,

$$\boldsymbol{\Phi} = \boldsymbol{A} + \left. \frac{\partial \boldsymbol{F}(\boldsymbol{X})}{\partial \boldsymbol{X}} \right|_{(\alpha=0)} \tag{6.60}$$

It is important to note that the matrix $\boldsymbol{\Phi}$ has the same structure as a Jacobian matrix but with only the DC and local oscillator components present, which makes it very sparse. The first moment vector ($\boldsymbol{M}_1$) is obtained by using one LU Decomposition to solve (6.58). As for the remaining moment vectors $\boldsymbol{M}_n$, these are found by recursively solving (6.59). As can be seen from (6.58) and (6.59), the computation of the moment vectors is a solution of a set of linear algebraic equations where the left-hand-side matrix is the same throughout and is therefore very efficient.

6.7.2 Computation of the Adjoint Moments

The adjoint moment vectors $\boldsymbol{M}_{ak}$ are defined as the Taylor series coefficients of the expansion of the adjoint solution vector $\boldsymbol{X}_a$ in (6.24) with respect to the signal amplitude voltage α. By substituting the general form of the adjoint moments given in (6.45)-(6.46) and the moments of the Jacobian matrix given in (6.57) into the definition of the adjoint vector shown in (6.24), the following relation is obtained

$$\left(\boldsymbol{A}+\sum_{i=0}^{\infty}\boldsymbol{T}_i\alpha^i\right)^T\left(\sum_{i=0}^{\infty}\boldsymbol{M}_{ai}\alpha^i\right)=-\boldsymbol{d} \tag{6.61}$$

Equating powers of α on both sides of (6.61) then results in the following set of equations that can be solved sequentially to obtain the adjoint moments.

$$\boldsymbol{\Phi}^T\boldsymbol{M}_{a0} = -\boldsymbol{d} \tag{6.62}$$

$$\boldsymbol{\Phi}^T\boldsymbol{M}_{a1} = -\boldsymbol{T}_1^T\boldsymbol{M}_{a0} \tag{6.63}$$

$$\boldsymbol{\Phi}^T\boldsymbol{M}_{a2} = -\boldsymbol{T}_1^T\boldsymbol{M}_{a1}-\boldsymbol{T}_2^T\boldsymbol{M}_{a0} \tag{6.64}$$

$$\boldsymbol{\Phi}^T\boldsymbol{M}_{a3} = -\boldsymbol{T}_1^T\boldsymbol{M}_{a2}-\boldsymbol{T}_2^T\boldsymbol{M}_{a1}-\boldsymbol{T}_3^T\boldsymbol{M}_{a0} \tag{6.65}$$

Notice that in these relations, the adjoint moments computation matrix

$$\boldsymbol{\Phi}=\boldsymbol{A}+\boldsymbol{T}_0 \tag{6.66}$$

is the same sparse moments computation matrix that was used to determine the original moments in (6.58) and (6.59) for computing IP3. This means that no additional LU decompositions are required to find the adjoint moments. Furthermore, the matrices $\boldsymbol{T}_i$ are also available from the original computation of IP3. The computation of the adjoint moments is therefore very efficient. To determine the two sets of adjoint moment vectors $\boldsymbol{M}_{a1k}$ and $\boldsymbol{M}_{a3k}$, equations (6.62)–(6.65) are solved twice, the first time using $\boldsymbol{d}_1$ and the second time with $\boldsymbol{d}_3$.

6.7.3 Computation of the Nonlinear Vector Moments

In this section, the algorithm for computing the moments of $\frac{\partial F(X)}{\partial \lambda}$ defined in (6.53) is presented. To simplify the presentation, we will discuss this algorithm for one of the nonlinear entries in $\boldsymbol{F}(\boldsymbol{X})$. The extension to the whole vector is trivial. Consider an entry in $\boldsymbol{F}(\boldsymbol{X})$ corresponding to a simple diode current equation

$$f(x) = I_s(e^{(x/V_T)} - 1) \tag{6.67}$$

Suppose we would like to compute the sensitivity of this function with respect to the saturation current I_s. In this case, $\lambda = I_s$ and $g(x)$ would be defined as

$$g(x) = \frac{\partial f}{\partial I_s} = (e^{(x/V_T)} - 1) \tag{6.68}$$

The first step toward computing $\boldsymbol{G}_k$ is to express (6.68) as a Taylor series expansion with respect to the radio frequency voltage amplitude α as follows

$$g(x) = g_0 + g_1\alpha + g_2\alpha^2 + g_3\alpha^3 + \ldots \tag{6.69}$$

From this relation, we can then deduce the following expressions

$$\begin{aligned} g_0 &= g(x)|_{\alpha=0} && (6.70)\\ g_1 &= \left.\frac{\partial g}{\partial \alpha}\right|_{\alpha=0} && (6.71)\\ 2g_2 &= \left.\frac{\partial^2 g}{\partial \alpha^2}\right|_{\alpha=0} && (6.72)\\ 6g_3 &= \left.\frac{\partial^3 g}{\partial \alpha^3}\right|_{\alpha=0} && (6.73) \end{aligned}$$

The derivatives $\frac{\partial^n g}{\partial \alpha^n}$ can be expressed analytically as

$$\begin{aligned} \frac{\partial g}{\partial \alpha} &= \frac{\partial g}{\partial x}\frac{\partial x}{\partial \alpha} && (6.74)\\ \frac{\partial^2 g}{\partial \alpha^2} &= \frac{\partial g}{\partial x}\frac{\partial^2 x}{\partial \alpha^2} + \frac{\partial}{\partial \alpha}\left(\frac{\partial g}{\partial x}\right)\frac{\partial x}{\partial \alpha} && (6.75)\\ &= \frac{\partial g}{\partial x}\frac{\partial^2 x}{\partial \alpha^2} + \frac{\partial^2 g}{\partial x^2}\left[\frac{\partial x}{\partial \alpha}\right]^2 && (6.76)\\ \frac{\partial^3 g}{\partial \alpha^3} &= \frac{\partial g}{\partial x}\frac{\partial^3 x}{\partial \alpha^3} + 3\frac{\partial^2 g}{\partial x^2}\frac{\partial x}{\partial \alpha}\frac{\partial^2 x}{\partial \alpha^2} + \frac{\partial^3 g}{\partial x^3}\left[\frac{\partial x}{\partial \alpha}\right]^3 && (6.77) \end{aligned}$$

In these relations, $\frac{\partial^n x}{\partial \alpha^n}$ are the moments of the solution vector as defined in (6.29) and are already available from the computation of IP3 itself. As for the derivatives of the function $g(x)$ with respect to x ($\frac{\partial^n g}{\partial x^n}$), the expressions are determined analytically. For example, for the diode current equation in (6.68), the derivatives with respect to x would be

$$\frac{\partial g}{\partial x} = \frac{e^{(x/V_T)}}{V_T} \tag{6.78}$$

$$\frac{\partial^2 g}{\partial x^2} = \frac{e^{(x/V_T)}}{(V_T)^2} \tag{6.79}$$

$$\frac{\partial^3 g}{\partial x^3} = \frac{e^{(x/V_T)}}{(V_T)^3} \tag{6.80}$$

The $\boldsymbol{G}_k$ terms in (6.53) are the frequency domain versions of g_k in (6.70)–(6.73). To obtain $\boldsymbol{G}_k$ we need to express each of the relations in (6.74)–(6.77) in the frequency domain which we do so with the aid of the Fourier Transform matrix $\boldsymbol{\Gamma}$ [70].

$$\boldsymbol{G}_0 = \boldsymbol{\Gamma}^{-1} \begin{bmatrix} g(x)|_{\alpha=0} & & \\ & \ddots & \\ & & g(x)|_{\alpha=0} \end{bmatrix} \tag{6.81}$$

$$\boldsymbol{G}_1 = \boldsymbol{\Gamma}^{-1} \begin{bmatrix} \frac{\partial g}{\partial x}|_{\alpha=0} & & \\ & \ddots & \\ & & \frac{\partial g}{\partial x}|_{\alpha=0} \end{bmatrix} \boldsymbol{m}_1 \tag{6.82}$$

$$\boldsymbol{G}_2 = \boldsymbol{\Gamma}^{-1} \begin{bmatrix} \frac{\partial g}{\partial x}|_{\alpha=0} & & \\ & \ddots & \\ & & \frac{\partial g}{\partial x}|_{\alpha=0} \end{bmatrix} 2\boldsymbol{m}_2 + \boldsymbol{\Gamma}^{-1} \begin{bmatrix} \frac{\partial^2 g}{\partial x^2}|_{\alpha=0} & & \\ & \ddots & \\ & & \frac{\partial^2 g}{\partial x^2}|_{\alpha=0} \end{bmatrix} \boldsymbol{m}_1^2 \tag{6.83}$$

$$\begin{aligned} \boldsymbol{G}_3 = {} & \boldsymbol{\Gamma}^{-1} \begin{bmatrix} \frac{\partial g}{\partial x}|_{\alpha=0} & & \\ & \ddots & \\ & & \frac{\partial g}{\partial x}|_{\alpha=0} \end{bmatrix} 6\boldsymbol{m}_3 + 3\boldsymbol{\Gamma}^{-1} \begin{bmatrix} \frac{\partial g}{\partial x}|_{\alpha=0} & & \\ & \ddots & \\ & & \frac{\partial g}{\partial x}|_{\alpha=0} \end{bmatrix} \boldsymbol{m}_1 2\boldsymbol{m}_2 + \\ & \boldsymbol{\Gamma}^{-1} \begin{bmatrix} \frac{\partial g}{\partial x}|_{\alpha=0} & & \\ & \ddots & \\ & & \frac{\partial g}{\partial x}|_{\alpha=0} \end{bmatrix} \boldsymbol{m}_1^3 \end{aligned} \tag{6.84}$$

In these relations, the vectors $\boldsymbol{m}_k$ are the time domain versions of the Harmonic Balance moment vectors are therefore defined as

$$\boldsymbol{m}_k = \boldsymbol{\Gamma}^{-1}\boldsymbol{M}_k \tag{6.85}$$

For the more general case of multi-node circuits with multi-variable nonlinearities, a fundamentally similar analysis to that of the single-node circuits is performed. The resulting derivations and expressions of the partial derivatives are too long and redundant to be stated in their entirety. Essentially, the analytical expression for the first derivative $\frac{\partial g}{\partial \alpha}$ is given by

$$\frac{\partial g}{\partial \alpha} = \frac{\partial g}{\partial x_1}\frac{\partial x_1}{\partial \alpha} + \frac{\partial g}{\partial x_2}\frac{\partial x_2}{\partial \alpha} + \cdots + \frac{\partial g}{\partial x_n}\frac{\partial x_n}{\partial \alpha} \tag{6.86}$$

The higher order derivatives are then deduced from this relationship by following a similar approach as that of the one variable case. It is important to note that while the derivation of this method might seem complex, this only needs to be done once, and the rest of the complexity is shielded from the user at the implementation stage. Fig. 6.6 provides a summary of the new moments based adjoint algorithm in pseudo-code format.

1. Set up the general harmonic balance equations of the circuit according to the formulation shown in (6.21).
2. Calculate the moment vectors $\boldsymbol{M}_k$ as defined in (6.29) by solving the formulations in (6.58) and in (6.59) recursively.
3. Obtain the terms $m_{1,1}$ and $m_{3,3}$ from the entries in the moment vectors at the locations shown in Fig. 6.4 for amplifiers and in Fig. 6.5 for mixers.
4. Calculate the Adjoint moment vectors $\boldsymbol{M}_{ak}$ as defined in (6.45) by solving the formulations in (6.62)–(6.65) recursively.
5. For every parameter λ, perform the following
(a) If λ is a parameter of a nonlinear element, compute the moments G_k as defined in (6.53) by solving the formulations in (6.81)–(6.82).
(b) Obtain the terms $\frac{\partial m_{1,1}}{\partial \lambda}$ and $\frac{\partial m_{3,3}}{\partial \lambda}$ by evaluating (6.47) and (6.48) if λ represents a linear element, or (6.54) and (6.55) if λ represents a nonlinear element.
(c) Determine the value of the IP3 sensitivity according to (6.19).

Fig. 6.6 Summary of the algorithm for the adjoint sensitivity analysis of nonlinear distortion in RF circuits.

6.8 Numerical Examples

In this section, the new algorithm is applied to several common example Radio Frequency circuit topologies. The results are then compared with those obtained using the harmonic balance adjoint sensitivity technique in order to demonstrate the accuracy and speed-up of the new approach.

6.8.1 Circuit Descriptions

The example circuits tested are a common emitter low noise amplifier, a differential amplifier, a singly balanced mixer and a doubly balanced Gilbert/Jones mixer circuit. All of these circuit topologies are implemented using Bipolar Junction transistors. For each of these circuits, we wish to compute the relative sensitivities of the third order intercept point with respect to changes in the values of both linear and nonlinear parameters. In all cases, the linear parameter selected was the collector resistance of the RF input transistor, while the nonlinear parameter selected was the saturation current of the collector-base pn junction of the transistor.

The first example circuit tested is a standard common emitter type amplifier. This circuit is quite linear in nature and the value of the input referred third order intercept point in this circuit was found to be 20.2 dBm using the moments computation method with two input tones at frequencies of $f_1 = 100$ MHz and $f_2 = 100.1$ MHz. For the differential amplifier circuit, the two input frequency tones were $f_1 = 1000$ MHz and $f_2 = 1001$ MHz and the resulting input IP3 was found to be -7.24 dBm.

As for the mixer circuits, in both cases we used up-conversion mixers with the local oscillator frequency being $f_{LO} = 1$ GHz and the RF signal frequencies were $f_1 = 100$ MHz and $f_2 = 100.1$ MHz. The value of the input referred IP3 was -3.4dBm for the singly balanced mixer, and 13.77 dBm for the doubly balanced Jones mixer.

6.8.2 Methodology and Results

To compute the adjoint moments sensitivity with respect to the linear resistance, first the adjoint moments are computed using the relations given in (6.62)–(6.65). Once these moments are computed, the sensitivity expressions are determined using (6.47) and (6.48) with the matrix $\frac{\partial A}{\partial \lambda}$ being the harmonic balance stamp of the resistor. The sensitivity of the third order intercept point is then computed by evaluating (6.19). The same procedure is applied to all of the example circuits. The results obtained are all summarized in Table 6.3.

Table 6.3 Comparison of relative sensitivities of IP3 with respect to a linear and nonlinear parameter for the example circuits.

Type of Circuit	Sensitivity parameter	Harmonic Balance Sensitivity	Moments Method Sensitivity	% Error
Common Emitter Amplifier	Linear	8.601×10^{-1}	8.604×10^{-1}	0.035%
	Nonlinear	2.180×10^{-3}	2.179×10^{-3}	0.046%
Differential Amplifier	Linear	-2.354×10^{-4}	-2.354×10^{-4}	0.004%
	Nonlinear	-4.1526×10^{-13}	-4.1533×10^{-13}	0.017%
Singly Balanced Mixer	Linear	3.1040×10^{-2}	3.1146×10^{-2}	0.340%
	Nonlinear	-1.375×10^{-13}	-1.402×10^{-13}	1.925%
Doubly Balanced Mixer	Linear	2.840×10^{-2}	2.816×10^{-2}	0.816%
	Nonlinear	-1.860×10^{-15}	-1.891×10^{-15}	1.640%

Table 6.4 CPU cost comparison of finding the adjoint sensitivity of IP3 for the example circuits

Type of Circuit	Harmonic Balance CPU time (s)	Moments Method CPU time (s)	Speed-up
Common Emitter Amplifier	0.81	0.31	2.6 times
Differential Amplifier	6.03	0.52	11.7 times
Singly Balanced Mixer	21.63	2.59	8.4 times
Doubly Balanced Mixer	41.66	3.34	12.4 times

To compute the IP3 sensitivity with respect to the nonlinear parameter, the additional step that needs to be taken is computing the moments of the nonlinear vector sensitivity, $\boldsymbol{G}_k$. Once these moments are computed, the values of $\frac{\partial m_{1,1}}{\partial \lambda}$ and $\frac{\partial m_{3,3}}{\partial \lambda}$ are obtained by solving (6.54) and (6.55). The relative sensitivity obtained was 0.002 V for the common emitter topology. The same procedure is applied to all of the example circuits and the results for both circuit parameters are summarized in Table 6.3 where they are also compared to the results obtained using the harmonic balance adjoint sensitivity approach. As can be seen from the table, the results are very accurate.

6.8.3 Computation Cost Analysis

A comparison of the computation times between traditional harmonic balance and the new moments method for determining the sensitivity of IP3 using the adjoint approach is shown in Table 6.4. These computation times are obtained using a prototype MATLAB simulator on a local workstation powered by a single-core Intel Xeon processor with a clock speed of 3.6 GHz and 4GB of RAM. As can be seen, the moments method presents a significant speedup in the computation time needed to determine the relative IP3 sensitivity.

It is also important to note that both the harmonic balance approach and the moments method cannot be taken independently. In the case of harmonic balance we must first compute the value of IP3 from a standard harmonic balance simulation in order to obtain the harmonic balance Jacobian that is needed for computing the sensitivity. In the case of the moments approach, we also need to obtain IP3 using the moments based method in order to have access to the moments computation matrix. With this being the case, it is more meaningful to combine the computation times for computing both the nominal value of IP3 and its sensitivity using both approaches, which will give us an idea of the speedup for the overall simulation. Therefore when the computation times shown in Table 6.4 are coupled with the time of the original moments technique for obtaining IP3 as described in Chapter 4, the result is a very efficient technique for finding both IP3 and its sensitivity with an overall speedup shown in Table 6.5 over harmonic balance. It is important to note that the computational cost of the overall algorithm is very low since the moments computation matrix is the same for determining both the original harmonic balance moments and also the adjoint moments. In addition, this matrix is very sparse since it is the harmonic balance Jacobian matrix evaluated with the amplitude of the radio frequency tones set to zero (i.e. $\alpha = 0$). For both the moments method and the harmonic balance method, the computation time for finding the sensitivity with respect to additional circuit parameters was

Table 6.5 Computation cost comparison of finding both IP3 and its adjoint sensitivity for the example circuits

Type of Circuit	Type of Computation	Harmonic Balance CPU time (s)	Moments Method CPU time (s)	Speed-up
Common Emitter Amplifier	IP3	8.78	1.22	7.2 times
	Sensitivity	0.81	0.31	2.6 times
	Total	9.59	1.53	**6.3 times**
Differential Amplifier	IP3	44.67	3.45	13.0 times
	Sensitivity	6.03	0.52	11.7 times
	Total	50.7	3.97	**12.7 times**
Singly Balanced Mixer	IP3	118.43	4.01	29.5 times
	Sensitivity	21.63	2.59	8.4 times
	Total	140.06	6.60	**21.2 times**
Doubly Balanced Mixer	IP3	158.91	5.08	31.3 times
	Sensitivity	41.66	3.34	12.4 times
	Total	200.57	8.42	**23.8 times**

Table 6.6 Computation cost comparison of finding both IP3 and its adjoint sensitivity using single-tone moments analysis

Type of Circuit	Type of Computation	Harmonic Balance time (s)	1-tone Moments Method time (s)	Speed-up
Differential Amplifier	IP3	44.67	0.34	129.8 times
	Sensitivity	6.03	0.03	201 times
	Total	50.7	0.37	**137.0 times**
Singly Balanced Mixer	IP3	118.43	0.43	275 times
	Sensitivity	21.63	0.21	103 times
	Total	140.06	0.64	**218 times**

negligible, which is a property of the adjoint method.

Additional savings in computation times can be achieved when single-tone moments analysis is used to compute IP3 and its sensitivity. To illustrate this point, the sensitivity of IP3 obtained from a single-tone moments analysis was determined for the common emitter amplifier and the singly-balanced mixer circuits. The CPU time and the overall speedups for computing both IP3 and its sensitivity is shown in Table 6.6

6.9 Conclusion

In this chapter, two new methods were presented for the efficient sensitivity analysis of third order nonlinear distortion using moments analysis. The first approach was based on computing the moments expansion with respect to a sensitivity parameter and the second approach was based on the adjoint moments analysis. These approaches complement the moments based method for computing IP3 presented in Chapters 4 and 5 by providing insight into the sources of distortion while still remaining significantly more efficient than traditional simulation approaches for computing IP3 based on Harmonic Balance. The sensitivity obtained using the moments approach was as accurate as the Harmonic Balance adjoint sensitivity method.

Chapter 7

Summary and Future Work

7.1 Summary

In this thesis, a new simulation method for measuring nonlinear intermodulation distortion and its sensitivity at the output of a non-linear system based on the calculation of the system moments was presented. It has been demonstrated that by using the new algorithms to compute IP3 and its sensitivity from the moments, distortion analysis of RF circuits becomes significantly more efficient. The new method is also very flexible and works for many types of systems.

1. The first contribution presented was an efficient moments based technique for computing the value of IP3 in mixer circuits. The main advantages that the new method exhibits over the Harmonic Balance method are summarized as follows:

    - The moments computation matrix $\boldsymbol{\Phi}$ used to obtain the moment vectors from the expanded set of MNA equations is very sparse as it is evaluated with the RF amplitude set to zero. This is in contrast to the Harmonic Balance Jacobian matrix which is dense.
    - The moments computation matrix that is used is also static and does not change throughout the algorithm. For this reason, it needs to be computed, stored and inverted only once. The Harmonic Balance Jacobian matrix changes at each iteration of the solution, which could be a significant number of times. This means it has to be computed and manipulated at each iteration, which when you also consider its dense structure, leads to increased CPU cost.

- The new method is essentially equivalent to numerically computing the summation of necessary Volterra Series terms for analyzing intermodulation distortion. This avoids the need to perform complex analytical manipulations to compute the Volterra kernels. It also provides accurate results for circuits that experience LO convergence issues.

 The speedup obtained on a double-balanced Gilbert cell mixer was found to be 40 times. When the method in this contribution is combined with the moments based approach for computing IP3 in amplifier circuits [57], an overall framework for the computation of IP3 using moments analysis in general RF circuits is now available.

2. The second method presented was a new approach for the fast computation of IP3 using single-tone inputs. This method shares the same properties as the moments based technique for computing IP3 but with the added advantage of significantly reduced circuit equations due to the presence of only single-tone RF signal inputs instead of the traditional multi-tone inputs for computing IP3. This is made possible by the separation of the third order nonlinear response that causes gain compression at the fundamental frequency from the desired linear response through access to the closed form expressions for each component. The significantly reduced size of the systems of equations leads to further speed-ups in computation time over traditional multi-tone steady-state simulation methods, with computation times that were orders of magnitude faster. This is especially the case in mixer circuits where only two frequency tones are required (the single-tone RF input in addition to the LO) as opposed to the traditional 3 input tones.

3. The third contribution of this thesis consists of new techniques for the sensitivity analysis of intermodulation distortion. This was accomplished using two methods, the first through finding the multi-dimensional moments expansion of the solution, and the second through finding the moments of the adjoint solution which is a more efficient and practical approach. In the first approach, closed form expressions linking the IP3 sensitivity terms to the expansion of the Harmonic balance moments with respect to the input amplitude in addition to a sensitivity parameter were developed. The method was fully automated and very efficient when the sensitivity of only a few parameters was required.

 In the adjoint approach, a general adjoint moments method for computing the sensitivity of IP3 that covers all parameters in the general circuit equations including parameters of linear and nonlinear circuit elements was presented. Closed form expressions for the sensitivity of IP3 as a function of the entries in the adjoint moments for all circuit parameters were developed. The adjoint moments are computed using the same set of linear equations used to determine the harmonic balance moments. The new method for sensitivity analysis thereby retains the main advantages of the adjoint sensitivity algorithm, namely that of low incremental computation cost and the ability to find the sensitivity of one variable with respect to all the parameters in the system while providing significant speedup over traditional harmonic balance methods. The new algorithm was tested on a number of different circuit topologies including LNAs and mixers and retained the same speedup of the original moments approach for finding IP3 but now with added option of finding its sensitivity.

7.2 Future Work

1. Benchmarking results with other IP3 computation methods: To verify the accuracy and speed-up of the new methods presented in this thesis, the numerical results of the simulations were compared with those of brute-force Harmonic Balance. There are several other methods for computing IP3 that are available in the literature, as shown in [30]-[38] and as described in Sections 2.5 and 2.6. These include using periodic steady-state and periodic AC analysis (PSS/PAC) for fast IP3 computation, distortion analysis using simplified Newton, linear centric distortion analysis methods and weakly nonlinear circuit reduction methods, among others. All of these methods present a speed-up in computation time for computing IP3 over brute-force harmonic balance simulations, with some methods achieving this at the expense of accuracy. Implementing these alternative IP3 computation techniques in the same circuit simulator environment and on the same hardware platform as that of the moments technique would provide the basis for a 1:1 comparison between the methods and would further verify the effectiveness of the new moments based method.

2. Improvements to the Harmonic Balance method: In the implementation of the brute-force Harmonic Balance method, Newton iteration combined with the FFT and IFFT algorithms were used to solve the system of nonlinear algebraic equations to find the steady-state solution of the nonlinear circuits. In practice, several variations on the solution algorithm can be implemented to try and improve the convergence and CPU cost of the Harmonic Balance method as described in Section 3.6. Some algorithms use direct approaches to

solve the nonlinear equations while others use different iterative methods in the place of Newton iteration. Some modifications are also aimed at improving convergence through the use of preconditioners or relaxation methods, for example. However, the improvement in computation time by using these modifications is not guaranteed for all types of circuit topologies. Nevertheless, a comparison of the speed-ups obtained when using moments analysis as opposed to using modified Harmonic Balance techniques would be important for the completeness of the results.

3. Parallel algorithms for the Moments based computation of intermodulation distortion: In this thesis, new methods for the efficient computation of the value of IP3 and its sensitivity in RF circuits based on the system moments were presented. The presented algorithms however, are serial in nature. The trend in microprocessors design has shifted from increasing clock speed to increasing the number of cores. Existing simulation algorithms can no longer rely on increased clock speed to offset the slowdown due to increased complexity. Changing the algorithms presented in thesis to run on emerging parallel processing platforms will allow the algorithm to scale in tandem with new processor technology.

4. Intermodulation Distortion Analysis of RF Microsystems: Integrating microelectronics with circuits of different energy domains such as RF MEMS based oscillators [91], [92] has led to dramatically increased circuit complexities. In addition, designers are increasingly being faced with having to use components that are characterized by measurements or extensive numerical simulations, but for which a circuit model is not readily available in the CAD tools. For these reasons, there is a strong demand for efficient EDA tools that can handle complex RF microsystems in an efficient, accurate and cost effective manner.

5. Use of the Moments computation algorithm for other applications of Volterra series: The moments computation algorithm used in this thesis was shown to be essentially equivalent to the numerical computation of the Volterra kernels. The algorithm was used to compute IP3 since an important use of Volterra series in RF circuits is in the analysis of nonlinear distortion. However, there are also many other important applications of Volterra series. One of the most important applications is in the fields of medicine (biomedical engineering) and biology, especially neuroscience [93]–[95]. An interesting extension of this research work would be trying to numerically compute the Volterra kernels to model nonlinear effects in biomedical applications and target some of the bottlenecks in the simulation and

modeling of biomedical system devices and behavior.

References

[1] B. Razavi, *RF Microelectronics*. New Jersey: Prentice-Hall, 1998.

[2] F. Yuan and A. Opal, "Distortion analysis of periodically switched nonlinear circuits using time-varying Volterra series," *IEEE Transactions on Circuits and Systems-I*, vol. 48, pp. 726–738, 2001.

[3] P. Wambacq and W. Sansen, *Distortion Analysis of Analog Integrated Circuits*. The Netherlands: Kluwer Academic Publishers, 1998.

[4] P. Li and L. T. Pileggi, "Efficient per-nonlinearity distortion analysis for analog and rf circuits," *IEEE Transactions on Computer Aided Design of Integrated Circuits and Systems*, vol. 10, pp. 1297–1309, 2003.

[5] K. S. Kundert, J. K. White, and A. Sangiovanni-Vincentelli, *Steady-State Methods for Simulating Analog and Microwave Circuits*. Boston: Kluwer Academic, 1990.

[6] J. Rogers and C. Plett, *Radio Frequency Integrated Circuit Design*. Norwood, MA: Artech House, Inc., 2003.

[7] J. W. Bandler, Q. J. Zhang, and R. M. Biernacki, "A unified theory for frequency-domain simulation and sensitivity analysis of linear and nonlinear circuits," *IEEE Transactions on Microwave Theory and Techniques*, vol. 36, pp. 1661–1669, Dec. 1988.

[8] Nokia, "Nokia n97 technical specifications," in *Nokia N97 Operations Manual*, pp. 1324–1327, 2009.

[9] J. Vlach and K. Singhal, *Computer Methods for Circuit Analysis and Design*. New York: Van Norstrand Reinolds, 1983.

[10] R. Kumar, D. Taggart, and A. Mathur, "Detailed analysis of the impact of the distortion due to nonlinear amplifiers on BER performance," in *IEEE Aerospace Conference*, pp. 1–11, 2009.

[11] T. J. Aprille, Jr. and T. N. Trick, "Steady-state analysis of nonlinear circuits with periodic inputs," *Proceedings IEEE*, vol. 60, pp. 108–114, Jan. 1972.

[12] K. Kundert and A. Sangiovanni-Vincentelli, “Simulation of nonlinear circuits in the frequency domain,” *IEEE Transactions on Computer-Aided Design*, vol. 5, pp. 521–535, Oct. 1986.

[13] M. S. Nakhla and J. Vlach, “A piecewise harmonic-balance technique for determination of periodic response of nonlinear systems,” *IEEE Transactions on Circuits and Systems*, vol. 23, pp. 85–91, Feb. 1976.

[14] Y. Hu, X. Duan, and K. Mayaram, “A comparison of time-domain and harmonic balance steady-state analyses for coupled device and circuit simulation,” in *NEWCAS*, pp. 93–96, 2004.

[15] K. Mayaram, D. C. Lee, S. Moinian, D. Rich, and J. Roychowdhury, “Overview of computer-aided analysis tools for RFIC simulation: Algorithms, features, and limitations,” in *Proceedings IEEE Custom Integrated Circuits Conference*, pp. 505–512, 1997.

[16] S. Maas, *Nonlinear Microwave and RF Circuits*. Upper Saddle River, NJ: Artech House Publishers, 2003.

[17] E. Gad, R. Khazaka, M. Nakhla, and R. Griffith, “A circuit reduction technique for finding the steady-state solution of nonlinear circuits,” *IEEE Transactions on Microwave Theory and Techniques*, vol. 48, pp. 2389–2396, Dec. 2000.

[18] R. Griffith and M. Nakhla, “A new high order absolutely stable explicit numerical integration algorithm for the time domain simulation of nonlinear circuits,” in *Proceedings ACM International Conference on Computer Aided Design*, pp. 504–509, 1997.

[19] D. Tannir and R. Khazaka, “Moments based computation of intermodulation distortion in RF circuits,” *IEEE Transactions on Microwave Theory and Techniques*, vol. 55, pp. 2135–2146, Oct. 2007.

[20] D. Tannir and R. Khazaka, “Moments based computation of intermodulation distortion in mixer circuits,” in *Proceedings IEEE MTT-S International Microwave Symposium*, pp. 95–98, 2007.

[21] C. W. Ho, A. E. Ruehli, and P. A. Brennan, “The modified nodal approach to network analysis,” *IEEE Transactions on Circuits and Systems*, vol. 22, pp. 504–509, June 1975.

[22] D. Tannir and R. Khazaka, “Computation of intermodulation distortion in RF circuits using single-tone moments analysis,” *IEEE Transactions on Computer Aided Design of Integrated Circuits and Systems (Accepted for Future Publication)*, 2010.

[23] D. Tannir and R. Khazaka, “Computation of IP3 using single-tone moments analysis,” in *Proceedings Design Automation and Test in Europe (DATE) Conference*, pp. 718–723, 2009.

[24] D. Tannir and R. Khazaka, “Efficient sensitivity analysis of nonlinear distortion in RF amplifier circuits,” in *Proceedings Northeast Workshop Circuits and Systems (Submitted)*, 2010.

[25] D. Tannir and R. Khazaka, “Adjoint sensitivity analysis of nonlinear distortion in RF circuits,” in *Proceedings IEEE Custom Integrated Circuits Conference*, pp. 633–636, 2009.

[26] D. Tannir and R. Khazaka, “Adjoint sensitivity analysis of nonlinear distortion in radio frequency circuits,” *IEEE Transactions on Microwave Theory and Techniques (Submitted)*, 2010.

[27] S. W. Director and R. A. Rohrer, “The generalized adjoint network and network sensitivities,” *IEEE Transactions on Circuit Theory*, vol. CT–16, pp. 318–323, Dec. 1969.

[28] L. O. Chua and P. M. Lin, *Computer-Aided Analysis of Electronic Circuits*. Englewood Cliffs, NJ: Prentice-Hall, 1975.

[29] T. H. Lee, *The Design of CMOS Radio-Frequency Integrated Circuits*. New York, NY: Cambridge University Press, 2004.

[30] K. Kundert, “Introduction to RF simulation and its application,” *IEEE Journal of Solid-State Circuits*, vol. 34, pp. 1298–1319, 1999.

[31] J. Ortega and W. Rheinboldt, *Iterative Solution of Nonlinear Equations in Several Variables*. New York: Academic, 1970.

[32] S. C. Chapra and R. P. Canale, *Numerical Methods for Engineers*. New York, NY: McGraw-Hill, 2005.

[33] M. M. Gourary, S. G. Rusakov, S. L. Ulyanov, M. M. Zharov, and B. J. Mulvaney, “Applying harmonic Newton method for distortion analysis of electronic circuits,” in *European Microwave Conference*, pp. 233–236, 2004.

[34] M. M. Gourary, S. G. Rusakov, S. L. Ulyanov, M. M. Zharov, K. Gullapalli, and B. J. Mulvaney, “New computational technique for periodic distortion analysis of communication circuits,” in *International Microwave Symposium*, pp. 941–944, 2004.

[35] R. Telicheveski, K. Kundert, and J. White, “Receiver characterization using periodic small-signal analysis,” in *Proceedings IEEE Custom Integrated Circuits Conference*, pp. 449–452, 1996.

[36] P. Li and L. T. Pileggi, “Nonlinear distortion analysis via linear-centric models,” in *Asia South Pacific Design Automation Conference*, pp. 897–903, 2003.

[37] P. Li, *Analysis and Macromodeling Continuum for Analog and RF ICs*. PhD dissertation thesis, Carnegie Mellon University, Pittsburg PA, USA, 2003.

[38] P. Li and L. T. Pileggi, “A linear-centric modeling approach to harmonic balance analysis,” in *Design Automation Test Europe Conference*, pp. 634–639, 2002.

[39] N. Dong and J. Roychowdhury, “General-purpose nonlinear model-order reduction using piecewise-polynomial representations,” *IEEE Transactions on Computer-Aided Design of Integrated Circuits and Systems*, vol. 27, pp. 249–264, Feb. 2000.

[40] P. Li and L. T. Pileggi, “NORM: compact model order reduction of weakly nonlinear systems,” in *Proceedings Design Automation Conference*, pp. 472–477, 2003.

[41] J. Roychowdhury, “Reduced-order modeling of time-varying systems,” *IEEE Transactions on Circuits and Systems II*, vol. 46, pp. 1273–1288, Oct. 1999.

[42] P. Li and L. T. Pileggi, “Compact reduced-order modeling of weakly nonlinear analog and RF circuits,” *IEEE Transactions on Computer-Aided Design of Integrated Circuits and Systems*, vol. 23, pp. 184–203, Feb. 2005.

[43] W. Dong and P. Li, “Hierarchical harmonic-balance methods for frequency-domain analog-circuit analysis,” *IEEE Transactions on Computer Aided Design of Integrated Circuits and Systems*, vol. 26, pp. 2089–2101, Dec. 2007.

[44] W. Dong and P. Li, “A parallel harmonic-balance approach to steady-state and envelope-following simulation of driven and autonomous circuits,” *IEEE Transactions on Computer Aided Design of Integrated Circuits and Systems*, vol. 28, pp. 490–501, Apr. 2009.

[45] V. Rizzoli, E. Montanari, D. Masotti, A. Lipparini, and F. Mastri, “Domain-decomposition harmonic balance with block-wise constant spectrum,” in *Proceedings IEEE MTT-S International Microwave Symposium*, pp. 860–863, 2006.

[46] S. Narayanan, “Transistor distortion analysis using Volterra series representation,” *The bell systems technical J.*, vol. 46, pp. 991–1024, May/June 1967.

[47] S. Narayanan, “Application of Volterra series to intermodulation distortion analysis of transistor feedback amplifiers,” *IEEE Transactions on Circuit Theory*, vol. 17, pp. 518–527, Nov. 1970.

[48] P. Wambacq, G. G. E. Gielen, P. R. Kinget, and W. Sansen, “High frequency distortion analysis of analog integrated circuits,” *Circuits and Systems II: Analog and Digital Signal Processing*, vol. 46, 1999.

[49] M. Youssef, E. Chong, and K. Phang, “Distortion analysis using signal flow graphs and Volterra series,” in *IEEE International Symposium on Micro-NanoMechatronics and Human Science*, pp. 84–89, 2003.

[50] I. Sarkas, D. Mavridis, and G. Papadopoulos, “Large and small signal distortion analysis using modified Volterra series,” in *Proceedings Norchip Conference*, pp. 63–66, 2006.

[51] I. Sarkas, D. Mavridis, M. Papamichail, and G. Papadopoulos, “Volterra analysis using chebyshev series,” in *Proceedings International Symposium Circuits and Systems*, pp. 1931–1934, 2007.

[52] M. T. Terrovitis and R. Meyer, “Intermodulation distortion in current-commutating cmos mixers,” *IEEE Journal of Solid-State Circuits*, vol. 35, pp. 1461–1473, Oct. 2000.

[53] G. Zhu and A. Opal, “Sensitivity analysis of nonlinear circuits using Volterra series,” in *Proceedings International Symposium Circuits and Systems*, pp. 5035–5038, 2006.

[54] G. Zhu and A. Opal, “Efficient Volterra series based sensitivity analysis of mildly nonlinear circuits,” in *Midwest Symposium on Circuits and Systems*, pp. 722–725, 2007.

[55] M. Schetzen, “Multilinear theory of nonlinear networks,” *Journal of the Franklin Institute*, vol. 320, no. 5, pp. 221–247, 1985.

[56] D. Tannir and R. Khazaka, “Efficient nonlinear distortion analysis of RF circuits,” in *Proceedings Design Automation and Test in Europe (DATE) Conference*, pp. 1–6, 2007.

[57] D. Tannir, *Efficient Nonlinear Distortion Analysis of RF Circuits*. Masters thesis, McGill University, Montreal QC, Canada, August 2006.

[58] S. Skelboe, “Computation of the periodic steady-state response of nonlinear networks by extrapolation methods,” *IEEE Transactions on Circuits and Systems*, vol. 27, pp. 161–175, Mar. 1980.

[59] G. W. Roberts and A. S. Sedra, *SPICE*. New York, NY: Oxford University Press, 1997.

[60] M. S. Nakhla and F. H. Branin, “Determining the periodic response of nonlinear systems by a gradient method,” *International Journal Circuit Theory Applications*, vol. 5, pp. 225–273, July 1977.

[61] P. K. Gunupudi, M. S. Nakhla, and R. Achar, “Efficient simulation of high-speed distributed interconnects using krylov-subspace techniques,” in *Proceedings IEEE Conf. on Electrical Performance of Electronic Packaging*, Oct. 1998.

[62] K. Kundert, “Simulation methods for RF integrated circuits,” in *Proceedings ACM International Conference on Computer Aided Design*, pp. 752–765, 1997.

[63] K. S. Kundert and A. Sangiovanni-Vincentelli, “Finding the steady-state response of analog and microwave circuits,” in *Custom Integrated Circuits Conference*, pp. 6.1/1–6.1/7, 1988.

[64] V. Rizzoli, A. Lipparini, and E. Marazi, "A general-purpose program for nonlinear microwave circuit design," *IEEE Transactions on Microwave Theory and Techniques*, vol. 31, pp. 762–769, 1983.

[65] V. Rizzoli and A. Neri, "State of the art and present trends in nonlinear microwave CAD techniques," *IEEE Transactions on Microwave Theory and Techniques*, vol. 36, pp. 343–365, Feb. 1988.

[66] M. Ma, *Model Order Reduction for Efficient Simulation and Modeling of Interconnect Networks*. PhD dissertation thesis, McGill University, Montreal QC, Canada, 2007.

[67] R. Khazaka, *Projection Based Techniques for the Simulation of RF Circuits and High Speed Interconnects*. PhD dissertation thesis, Carleton University, Ottawa ON, Canada, 2002.

[68] M. Vouvakis, K. Zhao, and J.-F. Lee, "Modeling large almost periodic structures using a non-overlapping domain decomposition method," in *Antennas and Propagation Society International Symposium*, pp. 343–346, 2004.

[69] V. Rizzoli, F. Mastri, F. Sgallari, and G. Spaletta, "Harmonic-balance simulation of strongly nonlinear very large-size microwave circuits by inexact newton methods," in *Proceedings IEEE MTT-S International Microwave Symposium*, pp. 1357–1360, 1996.

[70] S. K. Mitra, *Digital Signal Processing: A Computer-Based Approach*. New York, NY: McGraw-Hill Science/Engineering/Math, 2005.

[71] S. Egami, "Nonlinar, linear analysis and computer-aided design of resistive mixers," *IEEE Transactions on Microwave Theory and Techniques*, vol. 22, pp. 270–275, Mar. 1973.

[72] P. Pai, E. Gad, R. Khazaka, R. Achar, and M. Nakhla, "Parametric circuit reduction for steady-state simulation with multi-tone inputs," in *Proceedings IEEE MTT-S International Microwave Symposium*, 2004.

[73] A. R. Kerr, "A technique for determining the local oscillator waveforms in a microwave mixer," *IEEE Transactions on Microwave Theory and Techniques*, pp. 828–831, Oct. 1975.

[74] R. G. Hicks and P. J. Khan, "Numerical analysis of nonlinear solid-state device excitation in microwave circuits," *IEEE Transactions on Microwave Theory and Techniques*, vol. 30, pp. 251–259, Mar. 1982.

[75] R. C. Melville, L. Trajković, S.-C. Fang, and L. T. Watson, "Artificial parameter homotopy methods for the DC operating point problem," *IEEE Transactions on Computer-Aided Design*, vol. 12, pp. 861–877, June 1993.

[76] K. S. Chao and R. Saeks, "Continuation methods in circuit analysis," *Proceedings IEEE*, vol. 65, pp. 1187–1194, 1977.

[77] S. L. Richter and R. A. DeCarlo, "Continuation methods: theory and applications," *IEEE Transactions on Circuits and Systems*, vol. 30, pp. 347–352, 1983.

[78] R. C. Melville, P. Feldmann, and J. Roychowdhury, "Efficient multi-tone distortion analysis of analog integrated circuits," in *Proceedings IEEE Custom Integrated Circuits Conference*, pp. 241–244, 1995.

[79] P. Feldmann, B. Melville, and D. Long, "Efficient frequency domain analysis of large nonlinear analog circuits," in *Proceedings IEEE Custom Integrated Circuits Conference*, pp. 461–464, 1996.

[80] D. Long, R. Melville, K. Ashby, and B. Horton, "Full-chip harmonic balance," in *Proceedings IEEE Custom Integrated Circuits Conference*, pp. 379–382, 1997.

[81] A. Mehrotra and A. Somani, "A robust and efficient harmonic balance (HB) using direct solution of HB jacobian," in *Proceedings Design Automation Conference*, pp. 370–375, 2009.

[82] A. Ushida and L. O. Chua, "Frequency-domain analysis of nonlinear circuits driven by multi-tone signals," *IEEE Transactions on Circuits and Systems*, vol. 31, pp. 766–778, Sept. 1984.

[83] K. S. Kundert, G. B. Sorkin, and A. Sangiovanni-Vincentelli, "Applying harmonic balance to almost-periodic circuits," *IEEE Transactions on Microwave Theory and Techniques*, vol. 36, pp. 366–378, Feb. 1988.

[84] A. Ushida, L. O. Chua, and T. Sugawara, "A substitution algorithm for solving nonlinear circuits with multi-frequency components," *International Journal Circuit Theory Applications*, vol. 15, pp. 327–355, 1987.

[85] R. J. Gilmore and F. J. Rosenbaum, "Modeling of nonlinear distortion in GaAs MESFETs," in *Proceedings IEEE MTT-S International Microwave Symposium*, pp. 430–431, May 1984.

[86] B. Gilbert, "A precise four-quadrant multiplier with subnanosecond response," *IEEE Journal of Solid-State Circuits*, vol. 3, no. 4, pp. 365–373, 1968.

[87] D. M. Pozar, *Microwave Engineering*. Hoboken, NJ: John Wiley & Sons, Inc., 2005.

[88] P. Gunupudi, R. Khazaka, and M. S. Nakhla, "Analysis of transmission line circuits using multi-dimensional model reduction techniques," *IEEE Trans. on Packaging*, vol. 25, pp. 174–180, May 2002.

[89] P. Gunupudi, R. Khazaka, and M. S. Nakhla, "Analysis of transmission line circuits using multi-dimensional model reduction techniques," in *Proceedings IEEE Conf. on Electrical Performance of Electronic Packaging*, pp. 43–46, Oct. 2001.

[90] P. Gunupudi, , and M. S. Nakhla, “Multi-dimensional model reduction of VLSI interconnects,” in *Proceedings IEEE Custom Integrated Circuits Conference*, pp. 499–502, May 2000.

[91] F. Nabki, K. Allidina, F. Ahmad, P. Cicek, and M. El-Gamal, “A highly integrated 1.8 ghz frequency synthesizer based on a mems resonator,” *IEEE Journal of Solid-State Circuits*, vol. 44, no. 8, pp. 2154–2168, 2009.

[92] F. Nabki and M. El-Gamal, “Modeling and simulation of micro electromechanical (mem) beam resonator-based oscillators,” in *Proceedings International Symposium Circuits and Systems*, pp. 1324–1327, 2008.

[93] G. D. Mitsis, M. Markakis, and V. Marmarelis, “Nonlinear modeling of the dynamic effects of infused insulin on glucose: Comparison of compartmental with Volterra models,” *IEEE Transactions on Biomedical Engineering*, vol. 56, no. 10, pp. 2347–2357, 2009.

[94] M. Asyali and M. Juusola, “Use of Meixner functions in estimation of Volterra kernels of nonlinear systems with delay,” *IEEE Transactions on Biomedical Engineering*, vol. 52, no. 2, pp. 229–237, 2005.

[95] A. Dimoka, S. Courellis, G. Gholmieh, V. Marmarelis, and T. Berger, “Modeling the nonlinear properties of the in vitro hippocampal perforant path-dentate system using multi-electrode array technology,” *IEEE Transactions on Biomedical Engineering*, vol. 55, no. 2, pp. 693–702, 2008.